Impact of Cascadia Subduction Zone Earthquakes on Coastal Bridges in Washington State

Brianna Hansen

A thesis

submitted in partial fulfillment of the

requirements for the degree of

Master of Science

University of Washington

2025

Committee:

Jeffrey W. Berman

Marc O. Eberhard

Brett Maurer

Program Authorized to Offer Degree:

Civil and Environmental Engineering

University of Washington

Abstract

Impact of Cascadia Subduction Zone Earthquakes on Coastal Bridges in Washington State

Brianna Hansen

Chairs of the Supervisory Committee:
Jeffrey W. Berman and Marc O. Eberhard
Civil and Environmental Engineering

The Cascadia Subduction Zone in the Pacific Northwest means is likely to generate a magnitude 9 earthquake in the future. A set of 30 synthetic (physics-based) ground motions were created by researchers from the University of Washington and United States Geological Survey. Using an existing velocity model of the region and assuming a surface shear wave velocity of 600 m/s. This research uses the simulated ground motions as input into regional-scale bridge damage analyses. To account for the variation of near-surface soil conditions across the Pacific Northwest, amplification factors for each site class were generated for 10 locations in the Washington State. To apply the amplification factors to other locations, the medians and dispersions of the amplification factors of all 10 locations for all soil profiles were computed for each class. In the area specifically of interest, Gray's Harbor and Pacific counties, the most common bridge type is a prestressed concrete girder bridge. Four bridge categories were identified including prestressed simply supported concrete bridges built before 1990, prestressed simply supported bridges built on or after 1990, prestressed continuous concrete bridges built on

or after 1990, and movable bridges, which were included because of their unique vulnerability and importance in the region. Fragility curves, which can be used to determine the likely damage state of a bridge given a ground motion intensity, were assigned for each bridge category. The selected fragility curves came from a variety of sources including from HAZUS as developed by FEMA and from research literature. Given the different realizations for ground motions, the variability in amplification factors, and the various fragility curves, a parametric study was completed using at first a single bridge. Then a regional case study was completed for all 483 bridges in Gray's Harbor and Pacific counties. In the regional case study two different sets of ground motions were used, as well as two site classes and associated amplification factor variability, and three sets of fragility relationships; creating 12 unique cases that included variation in damage predictions due to each component of the analysis. From both of these studies it was concluded that the variation among the possible fragility curves most affect the estimated damage state of the bridges. An important factor in assessing the impact of the ground motions on the region was the number of single span bridges, because these are far less likely to be damaged during an earthquake than multi-span bridges. The bridge inventory in the southern half of Gray's Harbor and Pacific counties were found to be more vulnerable to the given M9 ground motions than the bridges in the northern half.

TABLE OF CONTENTS

LIST OF FIGURES

LIST OF TABLES

ACKNOWLEDGEMENTS

This thesis certainly wouldn't be possible without my advisors Marc and Jeff who have supported and encouraged me throughout the whole process. When I first joined the project, it was very overwhelming and I had no idea where to start, but Marc and Jeff were very patient with me as I began to figure things out. I'm so thankful they saw the vision with this project, even though at times I wasn't sure what the end picture would be. I'm grateful for all the times they made themselves available for me and were flexible with their schedules so that they could meet with me.

I'm also grateful for all the past researchers who have contributed to this overall project before me. I'm so grateful to have such a strong foundation on which to build and expand my own research. Especially the generation of the M9 ground motions by alex grant, Arthur Frankel, and Erin Wirth, the ground motions have been an integral piece in my work. The authors of various fragility relationships whose work is referenced and cited in this thesis, have also made a big contribution to my work.

I also have to thank the CoPes Hub or Cascadia Coastlines and Peoples Hazards Research Hub for providing me with the funding to this project. It felt good to be a part of a group with such a worthy goal. I hope my project can help contribute to helping the people along the Washington coast be safe and prepared in the face of a natural disaster.

I also want to thank Jinyan Zhao at UC Berkley who is one of the developers for R2D, a program which I used. I sent countless emails asking him questions about the program and sending him files so he could figure out where I went wrong. He was always so responsive and

patient with me, and I never got the impression that I was burdensome to him. The work I did with R2D would not be possible without him, and I mean that quite literally.

Of course, I have to thank my friends and family for always being big supporters and believers of me. My parents helped me move all of my stuff here and have always been encouraging of my education. The friends I have made in my cohort have been absolutely incredible and they are the best. Classes would have been a lot harder without them and my time here wouldn't be as memorable without them. I'm excited for all of our upcoming opportunities and I will miss them.

Last but not least, I have to express my gratitude for my fiancé Nate, he is my biggest supporter and has seen me through the ups and downs of grad school and life even while being long distance. His encouragement and belief in me kept me going especially when life got a little hectic. Thank you for always listening to me rant or talk about my homework assignments even when you have no idea what any of it means. I'm so grateful for your unconditional love and for loving me through all seasons of life.

Chapter 1: INTRODUCTION

1.1 MOTIVATION

The Pacific Northwest has unique geologic and tectonic features that bring inherent risk to the region and its inhabitants. It lies on the boundary between the North American tectonic plate and the Juan de Fuca plate, which is sandwiched between the North American plate and the Pacific plate. As seen in Figure 1.1, this situation creates a subduction zone where one of the plates (the Juan de Fuca plate) is forced under the other (the North American plate). The subduction zone can generate a megathrust earthquake, which as the name implies is an earthquake of enormous magnitude, and can create a subsequent tsunami as uplift occurs under the ocean. Unfortunately, there are no recorded data that documents how a Cascadia Subduction Zone earthquake would impact the region.

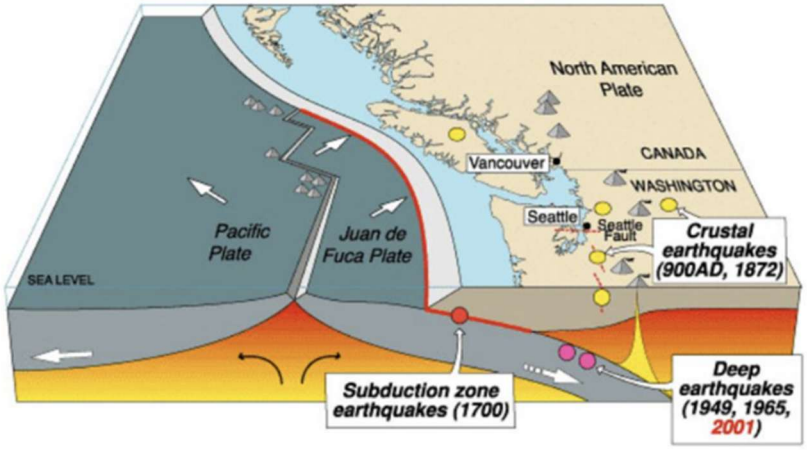

Source	Affected area	Max. Size	Recurrence
Subduction Zone	W.WA, OR, CA	M 9	500-600 yr
Deep Juan de Fuca plate	W.WA, OR,	M 7+	30-50 yr
Crustal faults	WA, OR, CA	M 7+	Hundreds of yr?

Figure 1.1 Cascadia Subduction Zone (USGS 2017)

The region closest to the subduction zone, which in Washington state is the Olympic Peninsula and the coast of Washington, is susceptible to the higher intensity ground motions during a magnitude 9 earthquake. The transportation network in this region is important because there are many rural communities along the coast that are not well interconnected. For example, Figure 1.2 shows the major transportation network for along the coast from roughly Queets, WA to Tokeland, WA. The figure shows that the small cities from Taholah, WA to Ocean Shores, WA along the coast only have one road that connects each of the cities and by which residents can get to Aberdeen, WA where the nearest hospital is located. The primary concern would be to know if people in these communities still have access to emergency services after an M9 earthquake. It is also important to know if bridges that connect these communities are still operational in the event that people need to evacuate inland due to an incoming tsunami.

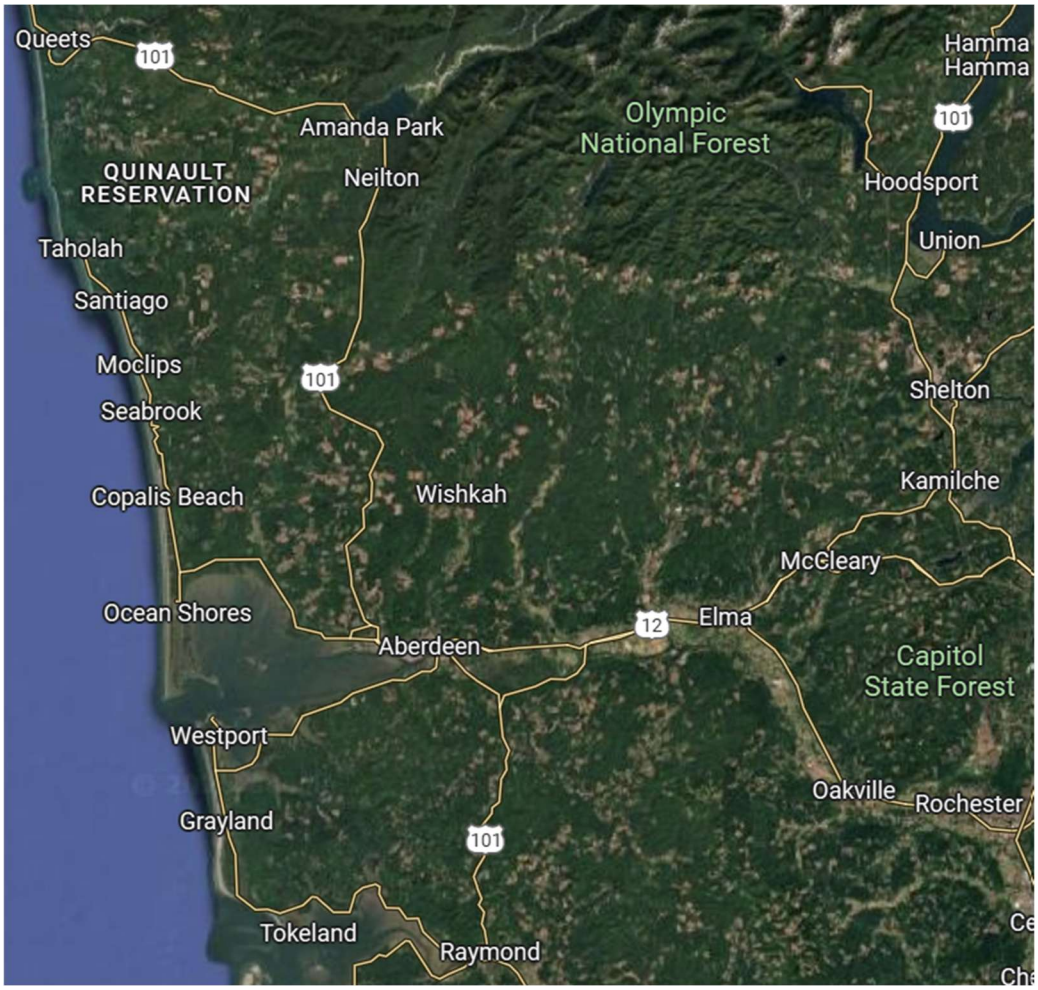

Figure 1.2 Transportation Network Along Washington Coastline from Queets, WA to Tokeland, WA (Google 2025)

1.2 RESEARCH GOALS

A more in depth understanding of how a M9 Cascadia Subduction Zone earthquake impacts the bridges along the coast of Washington is needed. To do this, this thesis focused on three sensitivities identified in Figure 1.3, which are also identified in the next section as areas of previous research. Bridge Type is grouped with Fragility Curve because for this research the bridge type informs what fragility curve is paired with it. All three parameters contribute to the

level of predicted damage a bridge could experience. The goal of this thesis is to evaluate the uncertainties within each parameter, the contributions of these uncertainties to predicted bridge damage, and to uncover trends in bridge damage that might exist in Gray's Harbor and Pacific counties, and for the common types of bridges found there.

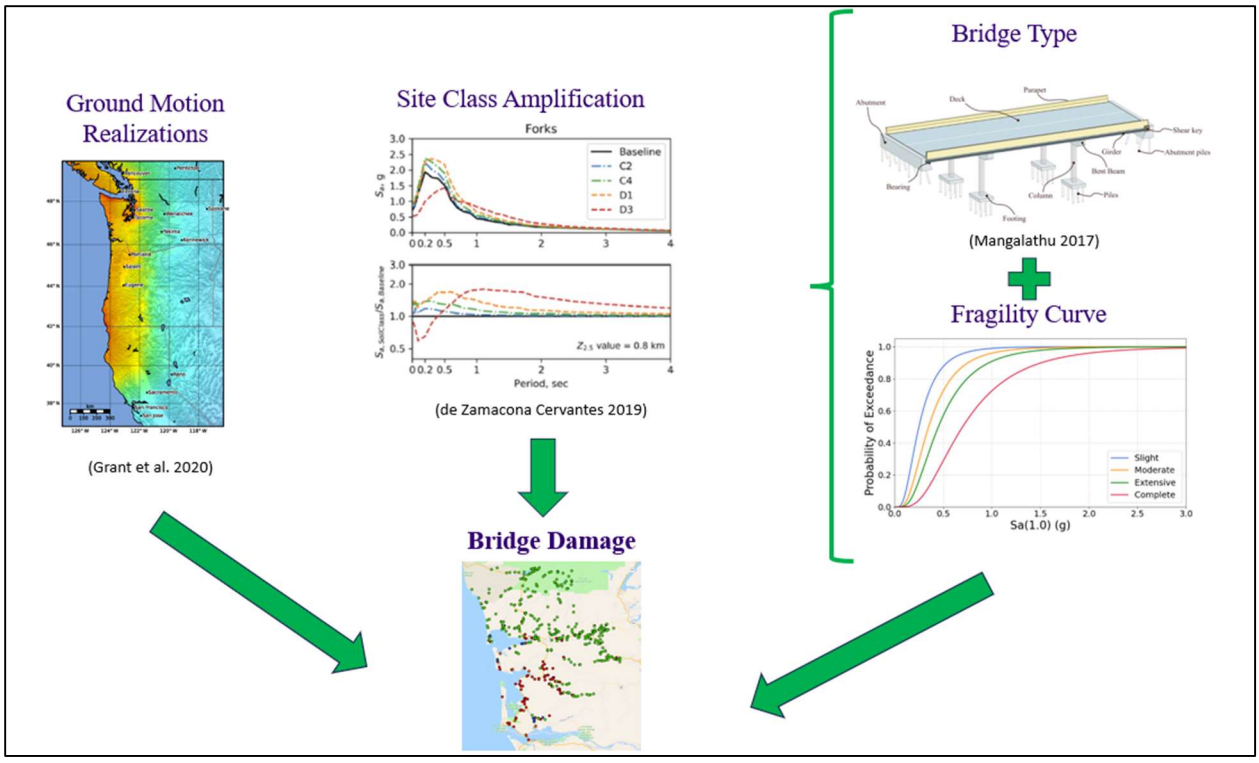

Figure 1.3 Three Sensitivities that Contribute to Predicted Bridge Damage

1.3 PREVIOUS RESEARCH

1.3.1 M9 Ground Motions

Because there are no recorded data of an M9 earthquake in the Pacific Northwest, 30 sets of synthetic physics-based M9 ground motions were simulated for the Cascadia Subduction Zone (Frankel et al. 2018a). Figure 1.2 shows the shaking intensity and median value of peak ground

acceleration (PGA) for a M9 Cascadia Subduction Zone earthquake. According to this figure, moderate to heavy damage can be expected along the coast.

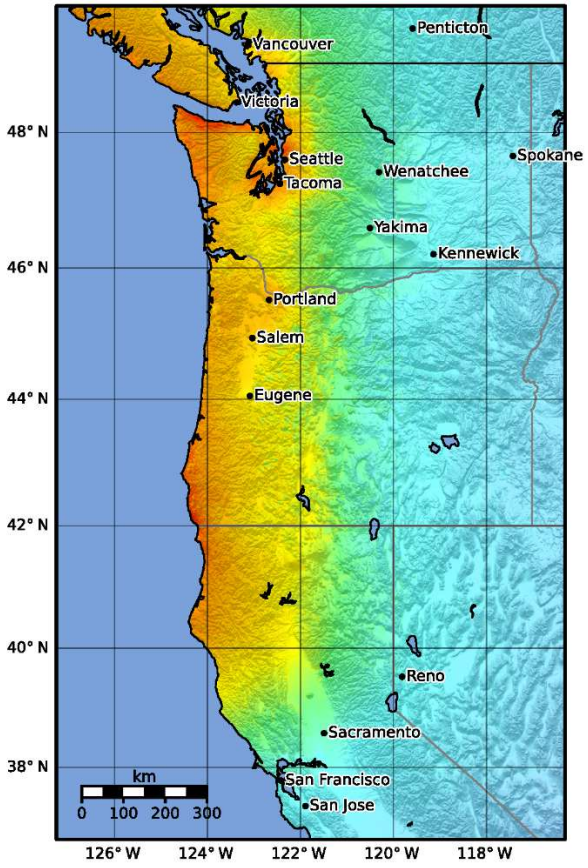

SHAKING	Not felt	Weak	Light	Moderate	Strong	Very strong	Severe	Violent	Extreme
DAMAGE	None	None	None	Very light	Light	Moderate	Moderate/heavy	Heavy	Very heavy
PGA (%g)	<0.0464	0.297	2.76	6.2	11.5	21.5	40.1	74.7	>139
PGV (cm/s)	<0.0215	0.135	1.41	4.65	9.64	20	41.4	85.8	>178
INTENSITY	I	II-III	IV	V	VI	VII	VIII	IX	X+

Scale based on Worden *et al.* (2012)

Figure 1.3 Shake Map of the Median Value of PGA for a M9 CSZ Earthquake (Grant et al. 2020)

1.3.2 Site Class Amplification

To better understand the impact of soil site class with a M9 earthquake, site adjusted ground motions were generated for 10 locations by Grant et al. (2020). These locations correspond to locations near and far from the coast, and within and outside of sedimentary

basins. It was assumed that the lessons from those ten locations could be extrapolated to other locations.

1.3.3 Fragility Curves

To predict the damage a structure might experience in a M9 earthquake, fragility curves can be used. Fragility curves usually come in a set, with one curve representing a damage state. Given an intensity measure from a ground motion, the likelihood of each damage state can then be estimated. Fragility curves are also usually specific to a structure type. Various organizations and researchers have developed fragility curves for specific bridge types.

1.4 SCOPE OF WORK

This thesis focused specifically on Gray's Harbor and Pacific counties in the Olympic Peninsula area. While still rural, these two counties contain the majority of the population along the Washington coast. The bridges considered in this research were identified from the National Bridge Inventory (NBI) database, which documents all publicly owned bridges and is maintained by the Federal Highway Administration (Federal Highway Administration 2024). The outline of the thesis is as follows:

1. Chapter 2 reviews the M9 ground motions and its 30 realizations. It also identifies the variations of the ground motion intensities among the realizations and between adjacent grid points.
2. For each site class, Chapter 3 develops relationships to characterize intensity-based amplification factors for several intensity measures.
3. Chapter 4 discusses the bridge types found in Gray's Harbor and Pacific counties, as well as corresponding fragility curves that can be applied.

4. Chapter 5 describes a series of parametric bridge studies, in which the ground motion realizations used, the site amplification factors, and the bridge/fragility type were all varied one at a time at a single location.
5. Chapter 6 describes a set of regional case studies in R2D (SimCenter 2024) where all bridges in Gray's Harbor and Pacific counties are considered. The ground motion, site class amplification and fragility relationship set were all varied to create a total of 12 case studies.
6. Chapter 7 summarizes the thesis and its findings. It also recommends future work that can be done building off of the information acquired from this study.

Chapter 2. M9 GROUND MOTIONS BASELINE

2.1 DESCRIPTION OF GROUND MOTIONS

As described in Frankel et al. (2018a), broadband synthetic seismograms for magnitude 9 earthquakes on the Cascadia Subduction Zone were created by United States Geological Survey (USGS) and University of Washington researchers. The seismograms were computed using 3D physics-based simulations and stochastic synthetics for the low and high frequency components, respectively, and will be referenced as the M9 ground motions herein. Thirty realizations were completed with ground acceleration versus time available on several different grid layouts throughout the Pacific Northwest. These are made available at Frankel et al. (2018b). Additional work by Marafi (2018) developed acceleration response spectra from the synthetic seismograms. Each grid point within a grid layout has a latitude and longitude coordinate and for each realization they have East-West (x) and North-South (y) ground motions (acceleration versus time) and corresponding computed response spectra that are from the surface of the seismological model. For Grids A, C, D, and E shown in Figure 2.1, the grid points are spaced one kilometer apart and cover the Puget Sound, Portland, Vancouver BC, and Victoria, BC areas, respectively. Grid B covers all the Pacific Northwest and grid points are spaced 20 kilometers apart. Because this research is focused on the Olympic Peninsula, the ground motions involved will come from Grid B, the least dense grid. Fortunately, the R2D application can make up for this gap using either a nearest neighbor approximation or other interpolation schemes. As the name “nearest neighbor” implies, R2D takes samples of the spectral acceleration values from the nearest grid points and weights the values according to the grid point’s distance from the point of interest. For this research the peak ground acceleration (PGA), and spectral accelerations for

periods of 0.3 seconds, 1.0 second and 2.0 seconds will be extracted from the M9 ground motion data. These are the relevant accelerations needed for the fragility curves that will be used and are described in Chapter 4.

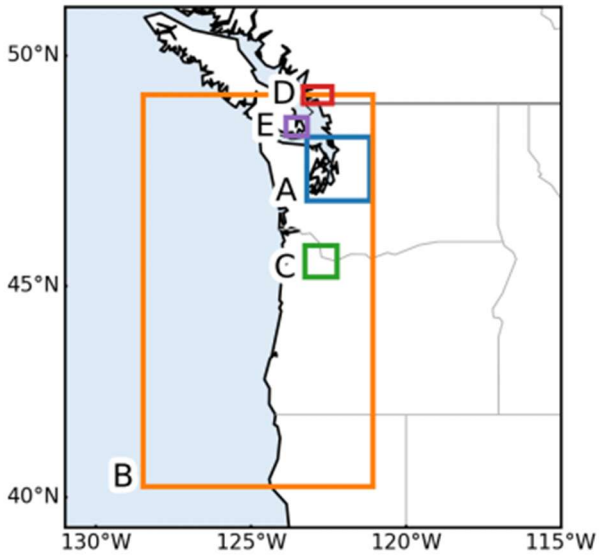

Figure 2.1 Schematic of Grids Where M9 Ground Motions are Available at Different Resolutions (Frankel et al. 2018a)

2.2 VARIABILITY IN THE 30 REALIZATIONS

As outlined in Frankel et al. (2018a), the thirty M9 realizations were generated using different rupture characteristics that were sampled using a logic tree approach. The result is that even at a single grid point the ground motion can vary greatly between each realization. Figure 2.2 shows baseline (i.e., rock site) acceleration response spectra for each realization for the locations of Forks, Graham, Port Angeles and Seattle. The response spectra shown are calculated by taking the geometric mean of the response spectra for the North-South and East-West ground

motion components. The line in bold represents the geometrics mean of all 30 realizations. The figure shows that there is considerable variability between realization and geographically within each realization. It also shows that the variability appears larger closer to the subduction zone (Forks and Port Angeles) and in locations with deep sedimentary basins (Seattle). Note that the thirty realizations are labelled here consistently with how they are labelled in Frankel et al. (2018b): Csz002, Csz003, Csz004, Csz005, Csz006, Csz007, Csz008, Csz009, Csz010, Csz011, Csz012, Csz013, Csz014, Csz017, Csz018, Csz019, Csz020, Csz021, Csz022, Csz023, Csz024, Csz025, Csz026, Csz027, Csz028, Csz029, Csz030, Csz031, Csz032, Csz033.

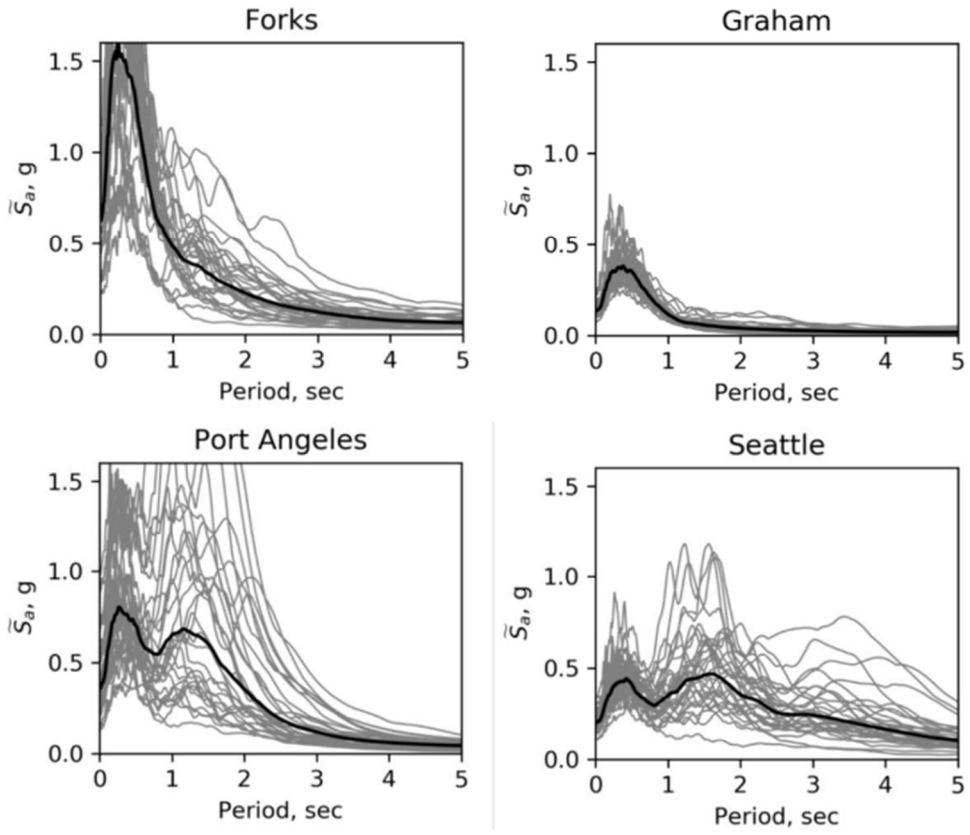

Figure 2.2 Acceleration Response Spectra for Baseline M9 Ground Motion (de Zamacona Cervantes 2019)

The variability in ground motion intensity between realizations at a particular point can also be seen in Figure 2.3, which gives the spectral accelerations at 0.3, 1.0, and 2.0 second periods for a location near Aberdeen, WA that will be denoted as the Reference Point herein (Latitude: 47.07787, Longitude: -123.94112). Again, the intensities shown are calculated by taking the geometric mean of the North-South and East-West horizontal components. The peak ground acceleration value is calculated by taking the maximum absolute value of the time history motion at the Reference Point. Note that Reference Point is a point in Grib B shown in Figure 2.1.

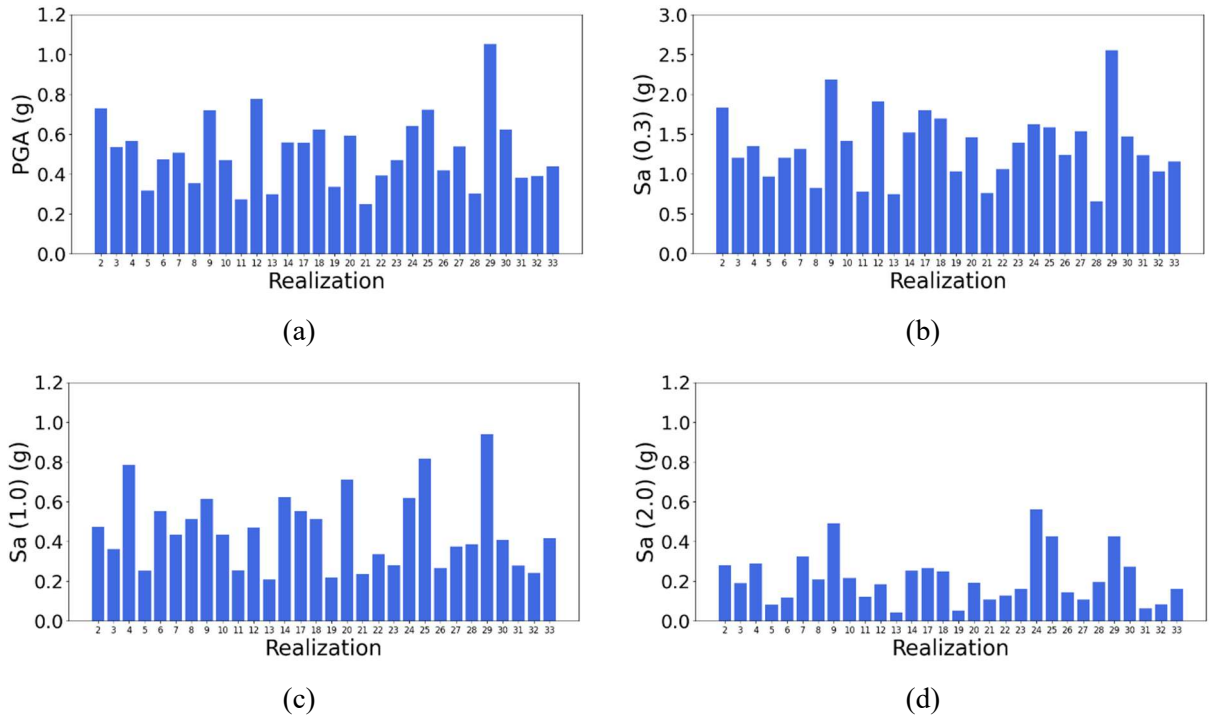

Figure 2.3 Ground Motion Intensities at the Reference Point near Aberdeen, WA (a) PGA, (b) S_a(0.3 sec), (c) S_a(1.0 sec), (d) S_a(2.0 sec)

While general trends can be observed, such as that Realization Csz029 causes large intensities at the Reference Point for all of the considered intensity measures, the variability

across realizations is clear. For example, the spectral acceleration at 0.3 seconds ranges from 0.654g to 2.548g. Table 2.1 characterizes the dispersion by giving the 14th percentile, median, and 86th percentile values for each intensity measure shown above at the Reference Point. As shown, the spectral acceleration at 2.0 second period has the lowest dispersion. A more detailed table showing all of the intensity measure values for each realization at the Reference Point can be found in Table A.1 in Appendix A.

Table 2.1 Variability in Ground Motion Intensity Measures Between Realizations at the Reference Point

Percentile	**PGA** (g)	**S_a (0.3)** (g)	**S_a (1.0)** (g)	**S_a (2.0)** (g)
14th	0.317	0.835	0.254	0.087
50th	0.489	1.333	0.425	0.192
86th	0.715	1.790	0.624	0.322

To study the spatial variability of the ground motion intensity measures near the Reference Point, specific realizations were chosen that approximately correlate to the 14th, 50th, and 86th percentile intensity measure values at the Reference Point and are shown in Table 2.2. The same intensity measures for those specific realizations are then compared at four other adjacent grid points. The surrounding grid points were chosen as the four points nearest to the Reference Point in the north, south, east, and west directions along Grid B. They will be referred to as North, South, East and West Points here after. Figure 2.4 shows visually where the points are located in relation to each other and Table 2.3 gives all of the latitude and longitude coordinates.

Table 2.2 Ground Motion Realizations Corresponding to a Specific Intensity Measure Percentiles at the Reference Point

Percentile	**Realizations**			
	PGA	S_a (0.3)	S_a (1.0)	S_a (2.0)
14th	Csz005	Csz008	Csz005	Csz032
50th	Csz007	Csz004	Csz007	Csz020
86th	Csz009	Csz017	Csz014	Csz007

Figure 2.4 Ground Motion Grid B on the Olympic Peninsula with the Reference Point Shown in Orange, and the North, South, East, and West Points shown in Yellow

Table 2.3 Geographical Coordinates of the Reference Point and its Surrounding Points

Point	Latitude	Longitude
Reference	47.07787	-123.94112
North	47.25707	-123.94112
South	46.89865	-123.94112
East	47.07787	-123.70563
West	47.07787	-124.17660

Figures 2.5 and 2.6 shows the intensity measures for the points along the same longitudinal line in the North-South direction, and the points along the same latitude line in the East-West direction, respectively. The y-axis intensity measure values shown are for the specific realizations identified in Table 2.2 that correspond to the 14^{th}, 50^{th}, and 86^{th}, percentile intensity measure values at the Reference Point, which are the horizontal axis labels. Because ground motions propagate from the fault which lies to the west of the points, there is a strong correlation of the intensities going from larger to smaller as the points move from west to east. In the North-South direction there is no discernable correlation (i.e. the North Point has the largest S_a at 0.3 sec period for the 86^{th} percentile realization but not the 50^{th} percentile realization).

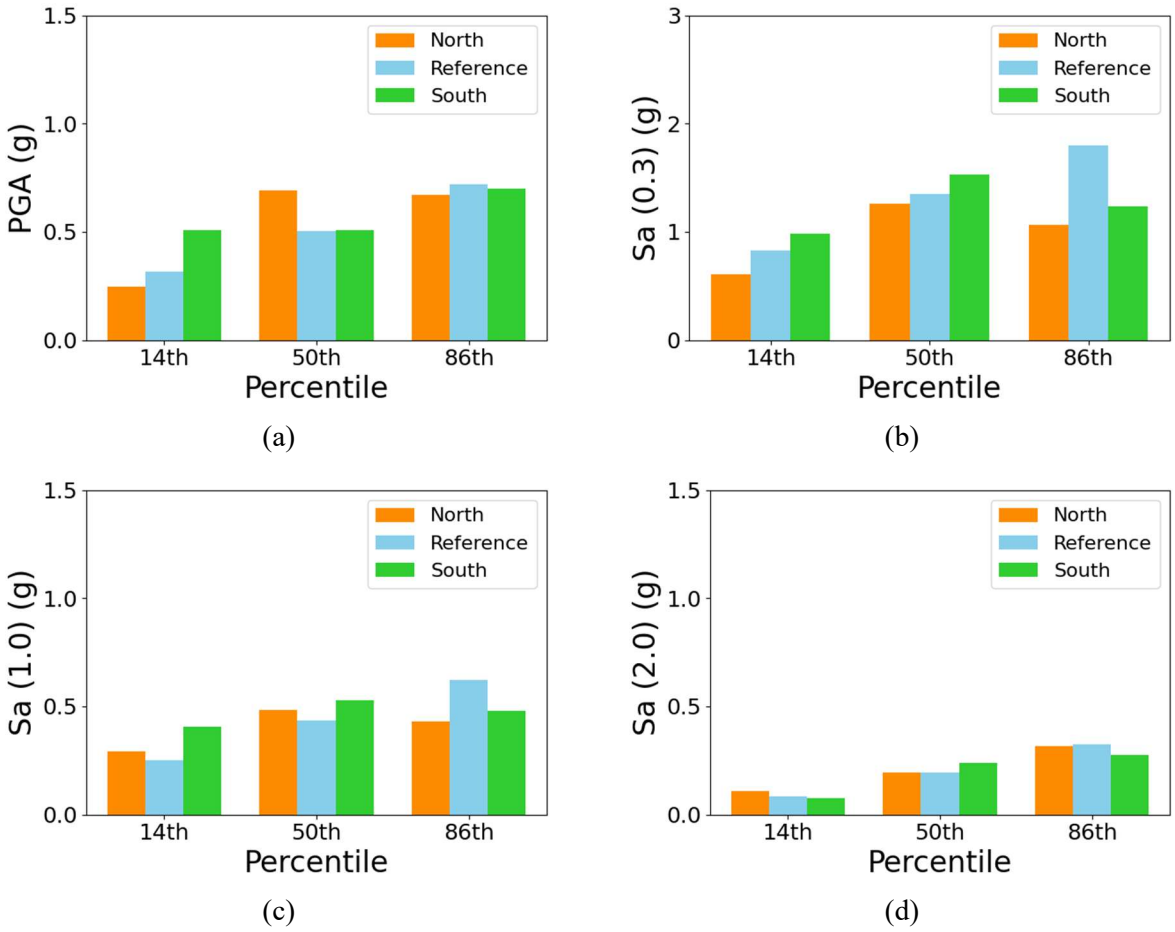

Figure 2.5 Comparison of Ground Motion Intensities in the North-South Direction for Specific Realizations (a) PGA, (b) S_a(0.3 sec), (c) S_a(1.0 sec), (d) S_a(2.0 sec)

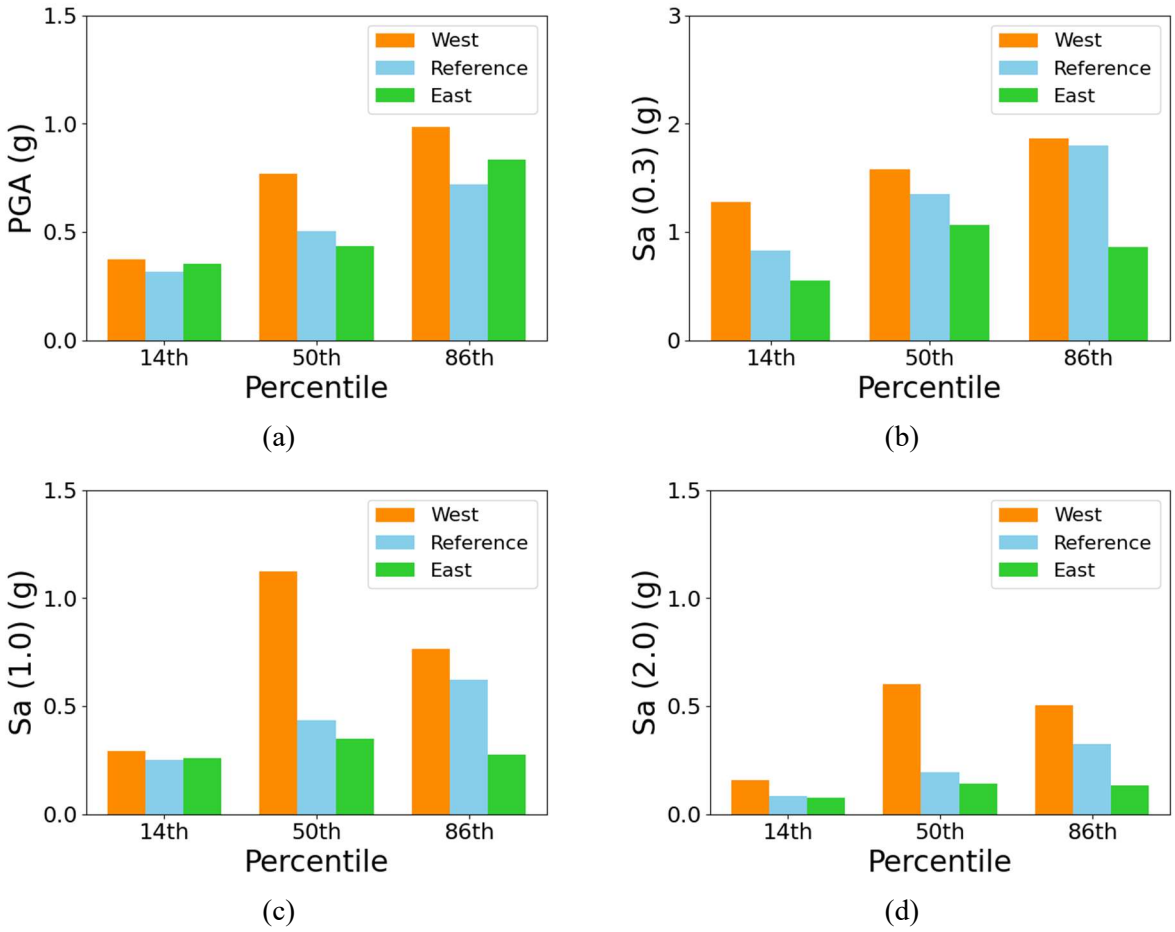

Figure 2.6 Comparison of Ground Motion Intensities in the East-West Direction for Specific Realizations (a) PGA, (b) S_a(0.3 sec), (c) S_a(1.0 sec), (d) S_a(2.0 sec)

A more detailed table of each of the four surrounding grid points that provides the four intensity measure values for all 30 realizations can also be found in Appendix A (Tables A.2 – A.5). Tables giving the 14th percentile, median, and 86th percentile values from the 30 realizations for each intensity measure for each of the four surrounding grid points can be found in the Appendix as well (Tables A.6 – A.9).

Figure 2.7 compares the ratios of each intensity measure at the surrounding grid points over the value at the Reference Point for the specific realization in Table 2.2. From this it can be

observed that the intensity measures for the West Point are all larger than those for the Reference Point resulting in a ratio always greater than one. The intensity measures at the East Point are often smaller than those at the Reference Point resulting in ratios less than 1.

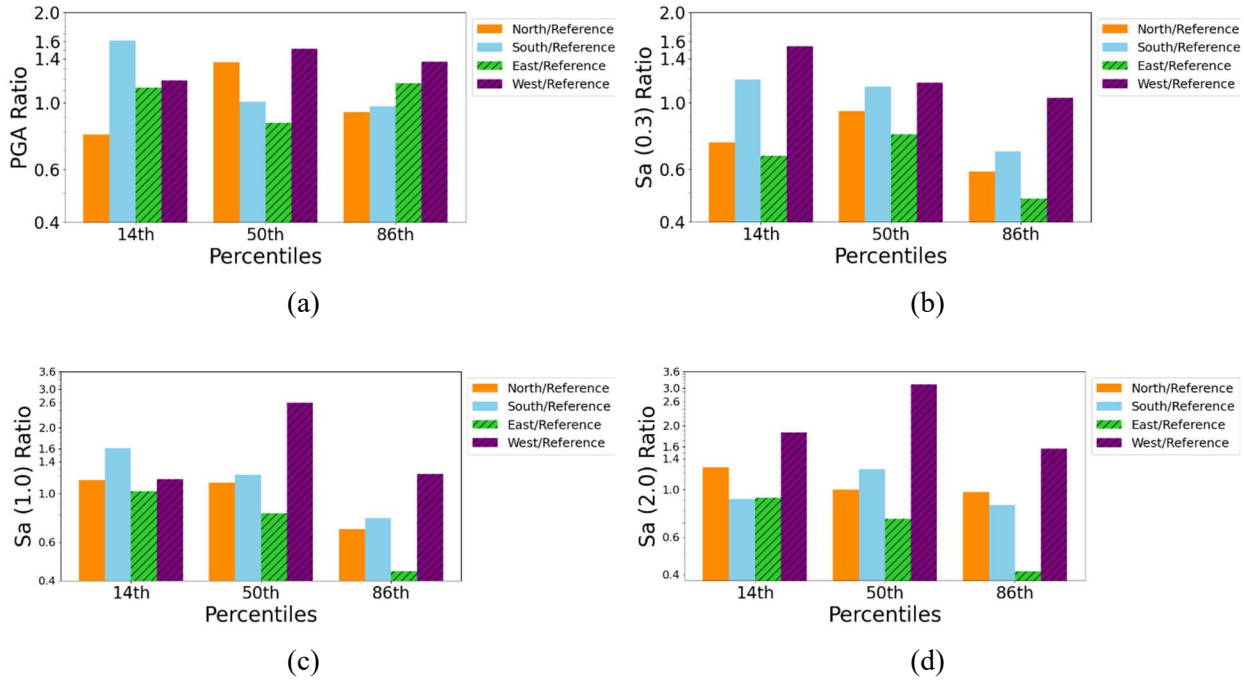

Figure 2.7 Ratios of North, South, East, West Points to the Reference Point at Ground Motion Values of PGA, S_a(0.3 sec), S_a(1.0 sec), and S_a(2.0 sec)

Chapter 3. SOIL SITE CLASSES

3.1 SITE ADJUSTED GROUND MOTIONS

The M9 baseline ground motions were developed for a minimum shear wave velocity at the surface of 600 m/s, which corresponds to a soft rock or stiff soil site (Marafi 2018). Near-surface geotechnical conditions were not considered in the physics-based ground motion simulation. In the Pacific Northwest, soil site classes generally range from B – F (Palmer et al. 2007).

To account for local soil conditions, site adjusted ground motions were generated at the following ten locations, by Grant et al. (2020): Forks, Ocean Shores, Port Angeles, Olympia, Port Townsend, Vancouver, Tacoma, Seattle, Everett, and Graham. A database of soil profiles for the Pacific Northwest collected and analyzed by Ahdi et al. (2017), were used to generate the site-adjusted ground motions. Profiles within that database for Site Class C and D soils were used and those were subdivided into the subcategories of C1, C2, C3, C4, D1, D2, and D3. A total of 444 profiles were used across the Site Class C and D subcategories. Grant et al. used equivalent linear site response analysis for each realization at each of the ten locations and for each soil profile, to generate a new set of ground motions that are soil-adjusted.

The impact of site response on the spectral accelerations for the soil-adjusted ground motions relative to the original ground motions can be characterized by an amplification factor that is unique for each city, sub-site class, structural period, soil profile and realization. It is referred to as the amplification factor because for most cases it amplifies the original spectral acceleration, in some cases though there is a slight reduction. Variability in site amplification is expected to be large as each soil profile within each site class subcategory was significantly

different and the baseline ground motions were highly variable. The variation of the soil amplification factors can be seen in Figure 3.1 for simulated ground shaking in Forks, WA where the x-axis represents peak ground acceleration of the baseline ground motion. A column of data points represents a realization and the variance along the y-axis is due to linear site response analysis for the different soil profiles.

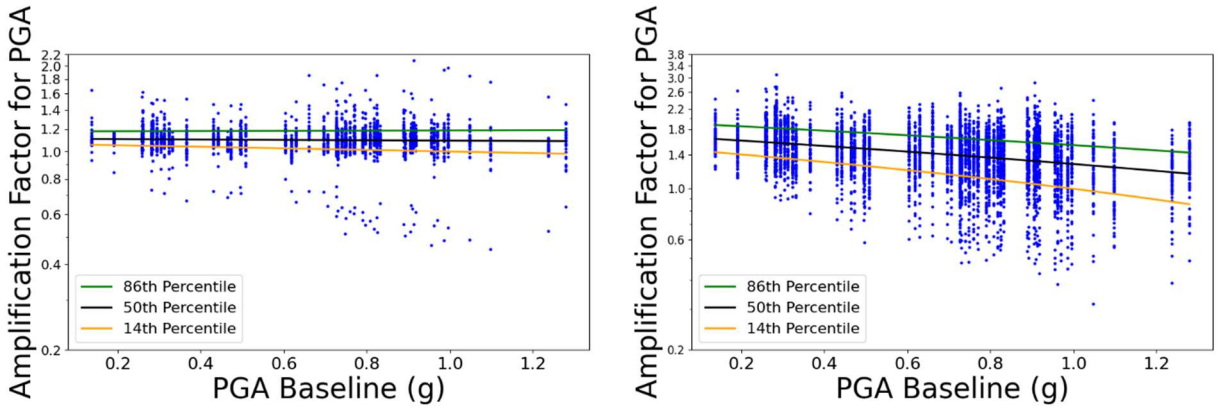

(a) Site Class C2 (b) Site Class D1

Figure 3.1 Soil Amplification Factor Dispersion for Ground Motions in Forks, WA

3.2 QUANTIFYING SOIL AMPLIFICATION AS A FUNCTION OF BASELINE GROUND MOTION INTENSITY

The area of interest for the current study is Gray's Harbor County and Pacific County, WA, not only the 10 locations for which local site response analysis was conducted by Grant et al. (2020). Therefore, the impact of local site response needed to be quantified in a generalized way that can then be used for the study area here. To do this, soil amplification factors were computed for various intensity measures using the results from Grant et al. (2020). The selected intensity measures correspond to those that are important for the bridge fragility analyses discussed later and include: PGA, and spectral accelerations for 0.3 seconds, 1.0

second, and 2.0 seconds structural periods. It is known that the amplification factors should vary with intensity and Grant et al. (2020) identified the amplification factors for different intensity measures as a function of PGA of the baseline ground motion. Such data is also in Cervantes (2019). In Figures 3.2 and 3.3 this can be seen in the graphs on the left side, where for the ground motions for Forks, WA the amplification of each intensity measure is plotted against the baseline ground motion for of PGA. The figures show fitted lines representing the 14^{th}, 50^{th}, and 86^{th} percentile amplification values which are described further below.

In order to potentially reduce the amplification factor variability for use in the bridge analyses later in this thesis, the amplification factors are also computed and plotted as a function of the other intensity measures for the baseline ground motion (i.e. the spectral acceleration at periods of 0.3, 1.0, and 2.0 seconds). In particular the amplification factors were quantified for a given intensity measure as a function of that same intensity measure for the baseline motions. This data is plotted in the graphs on the right side of Figures 3.2 and 3.3. The plots again show fitted lines at the 14^{th}, 50^{th}, and 86^{th} percentiles that are described below and can be used to generate specific values of the amplification factor. Figure 3.2 shows the amplification factors vs the baseline motions for the Forks, WA location for Site Class C2 soil profiles, and Figure 3.3 shows the same graphs but for Site Class D1 soil profiles.

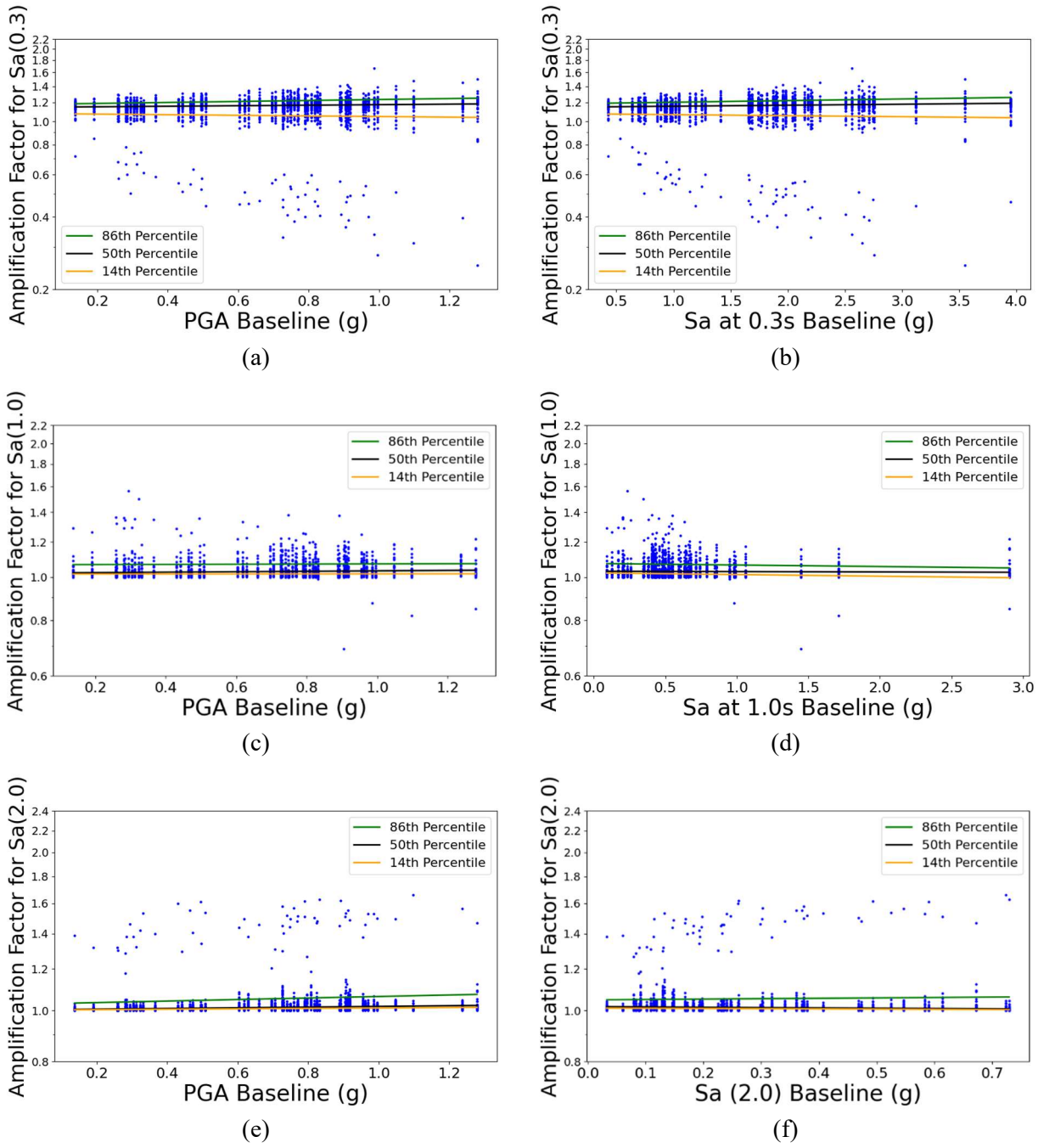

Figure 3.2 Soil Amplification Factors for Different Intensity Measures versus Baseline Ground Motion PGA (a, c, e) or Spectral Accelerations (b, d, f) for Forks, WA ground motions and Site Class C2 Profiles

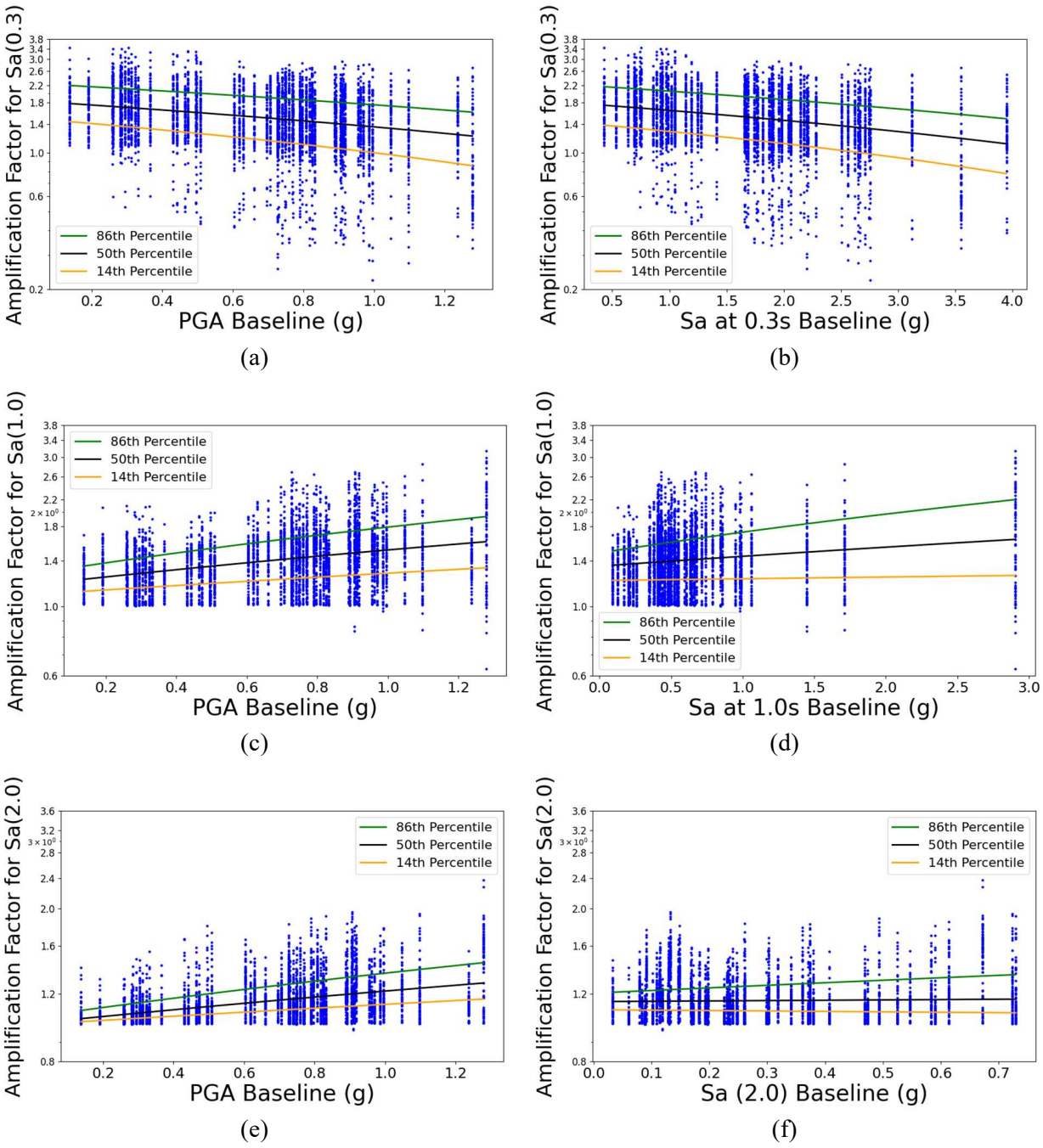

Figure 3.3 Soil Amplification Factors for Different Intensity Measures versus Baseline Ground Motion PGA (a, c, e) or Spectral Accelerations (b, d, f) for Forks, WA ground motions and Site Class D1 Profiles

Despite having some outliers, the fitted lines for Site Class C2 are pretty close together, but for D1 they are further apart indicating more dispersion in the amplification factors for that

site class. Tables 3.1 and 3.2 gives the coefficients A and B of the equation for the fitted lines given the format $y = Ax + B$, where x is the baseline ground motion and y is the amplification factor. As shown, when comparing the lines for specific percentiles, the B parameter is similar regardless of whether PGA of the baseline ground motion is used as the x-axis or the same spectral acceleration intensity measure is used as the x-axis and is identical in many cases. The biggest difference occurs for Site Class D1 for spectral acceleration at 1.0 and 2.0 seconds. The parameter A is more dependent on which intensity measure is used as the x-axis. While using the PGA baseline to quantify amplification or using the same S_a baseline yields comparable results, ultimately casting the amplification factors for the intensity measure as functions of that intensity measure for the baseline ground motion was determined to provide a better fit, especially on a larger scale when combining data for all 10 locations.

Table 3.1 Values for the Equation of the Fitted Lines in Figure 3.2 for Site Class C2 Soil Amplification in Forks, WA

Intensity Measure	**PGA of Baseline as x-axis**						**Same S_a of Baseline as x-axis**					
	14th		50th		86th		14th		50th		86th	
	A	B	A	B	A	B	A	B	A	B	A	B
PGA	-0.07	1.06	-0.02	1.11	0.01	1.18	-0.07	1.06	-0.02	1.11	0.01	1.18
S_a (0.3)	-0.03	1.08	0.03	1.14	0.06	1.18	-0.01	1.08	0.01	1.15	0.02	1.18
S_a (1.0)	0.001	1.02	0.01	1.02	0.001	1.07	-0.01	1.02	-0.001	1.03	-0.01	1.07
S_a (2.0)	0.01	1.00	0.02	1.00	0.04	1.03	-0.01	1.01	-0.01	1.02	0.02	1.05

Table 3.2 Values for the Equation of the Fitted Lines in Figure 3.3 for Site Class D1 Soil Amplification in Forks, WA

Intensity Measure	**PGA of Baseline as x-axis**						**Same S_a of Baseline as x-axis**					
	14th		50th		86th		14th		50th		86th	
	A	B	A	B	A	B	A	B	A	B	A	B
PGA	-0.51	1.50	-0.42	1.69	-0.40	1.93	-0.51	1.50	-0.42	1.69	-0.40	1.93
S_a (0.3)	-0.51	1.51	-0.50	1.85	-0.52	2.27	-0.17	1.45	-0.18	1.82	-0.19	2.25
S_a (1.0)	0.19	1.09	0.34	1.17	0.52	1.27	0.02	1.21	0.10	1.35	0.25	1.48
S_a (2.0)	0.13	1.00	0.22	1.00	0.32	1.04	-0.03	1.09	0.02	1.15	0.19	1.21

3.3 ADJUSTMENTS TO LINEAR REGRESSIONS FOR SOIL AMPLIFICATION FACTORS

Since the fitted lines for the 14th, 50th, and 86th percentiles are not perfectly parallel, there is a possibility that when trying to amplify the M9 ground motions used in the regional analyses later in this thesis there could be an acceleration large enough that the linearly regressed fitted lines eventually intersect, falsely implying for example that the 86th percentile amplification is less than the 50th percentile amplification. To avoid this possibility the least squares error method was used to create modified regressed values for the 14th and 86th percentile based off the equation of the line for the 50th percentile, ensuring that they do not cross. Table 3.3 shows the parameters of the equation of the fitted line for the 50th percentile and its regression values for the 14th and 86th percentile for Forks, Seattle, and Vancouver for Site Class C2 and D1. These locations were chosen because they represent the three basic geographical conditions: near the coast, inland but on a basin, and inland and not on a basin. The regression values are labeled as Z and are applied in the format $y = Z(Ax + B)$ for the 86th and 14th percentile new lines.

Table 3.3 Values for the Parameters of the 50th Percentile Line and the Regressed Values of Z for the 14th and 86th Percentile Lines for Each Intensity Measure

Intensity Measure	**Locations**	**Site Class C2**				**Site Class D1**			
		50th		14th	86th	50th		14th	86th
		A	B	Z	Z	A	B	Z	Z
PGA	Forks	-0.02	1.11	0.92	1.09	-0.42	1.69	0.80	1.21
	Seattle	-0.18	1.09	0.98	1.03	-1.10	1.61	0.91	1.12
	Vancouver	-0.10	1.10	0.96	1.05	-0.82	1.70	0.9	1.13
$S_a(0.3)$	Forks	0.01	1.15	0.90	1.05	-0.18	1.82	0.75	1.29
	Seattle	0.04	1.11	0.93	1.04	-0.01	1.62	0.80	1.22
	Vancouver	0.001	1.14	0.93	1.04	-0.27	1.82	0.80	1.25
$S_a(1.0)$	Forks	-0.001	1.03	0.98	1.03	0.10	1.35	0.82	1.25
	Seattle	-0.01	1.02	0.99	1.03	0.01	1.15	0.93	1.14
	Vancouver	-0.001	1.02	0.99	1.04	0.03	1.19	0.91	1.15
$S_a(2.0)$	Forks	-0.01	1.02	0.99	1.04	0.02	1.15	0.93	1.10
	Seattle	0.001	1.00	1.00	1.04	0.02	1.04	0.97	1.09
	Vancouver	-0.01	1.01	0.99	1.04	0.05	1.07	0.95	1.12

Within a single site class across the three locations, it can be observed that the 50th percentile lines are nearly the same, although there is definitely more variation for Site Class D1. Most regression (Z) values between the three locations in a single site class and percentile are close in value and at most 0.11 in difference, again with the most variation coming from site class D1. Because of this, it can be justified to combine all the data from each city to create a fitted line for each site class with the understanding that this results in larger variability for amplification factors for sub categories of Site Class D.

Figures 3.4 and 3.5 show the new regressed Z factored lines at the 86th percentile and 14th percentile with the original 14th, 50th, and 86th percentile fitted lines at Forks, WA for Site Class C2 and Site Class D1, respectively. While the corresponding 14th and 86th percentile lines are similar there is some discrepancy, with more difference coming from Site Class D1. This is expected due to the larger variation in this site class. Note that while necessary, these Z factored lines introduce more uncertainty when calculating amplification factor at the 86th and 14th percentile for a specific site class.

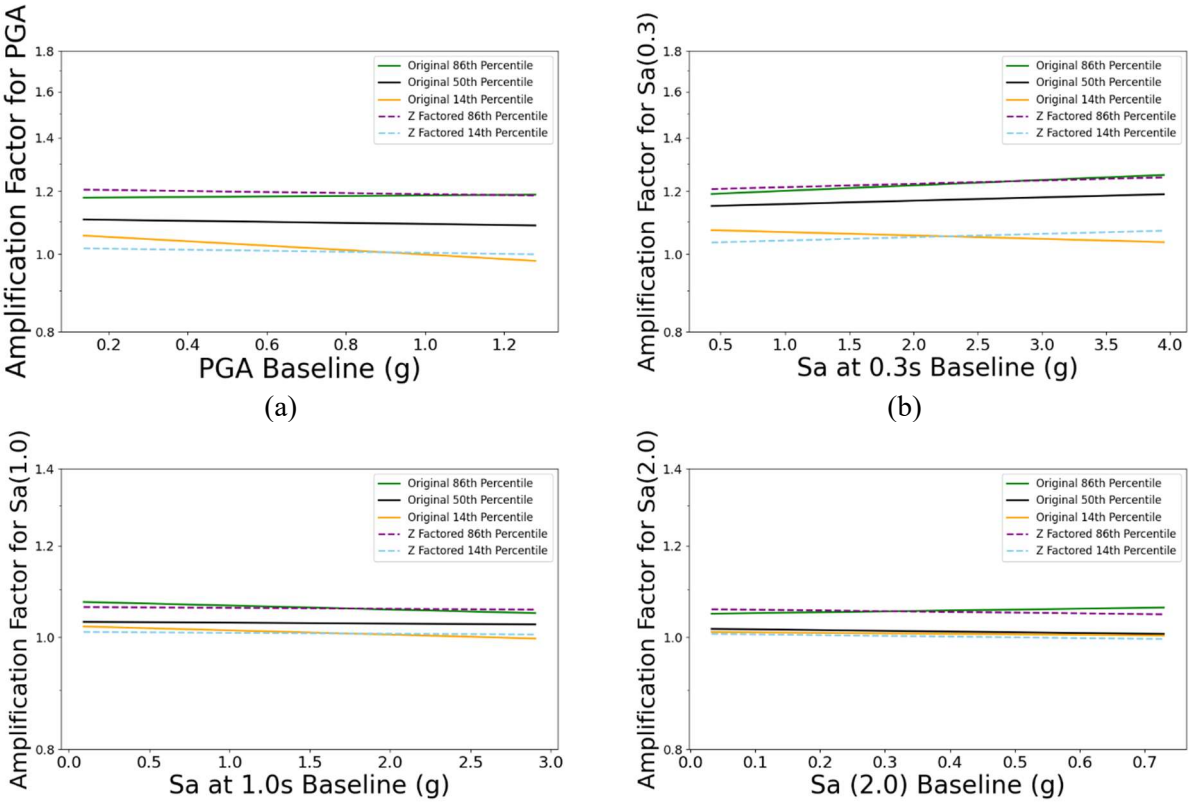

Figure 3.4 Comparison of Originally Linearly Regressed Lines with the Z Factored 86th and 14th Percentile Lines for Site Class C2 at Forks, WA for All Intensity Measures (a) PGA, (b) S_a(0.3 sec), (c) S_a(1.0 sec), and (d) S_a(2.0 sec)

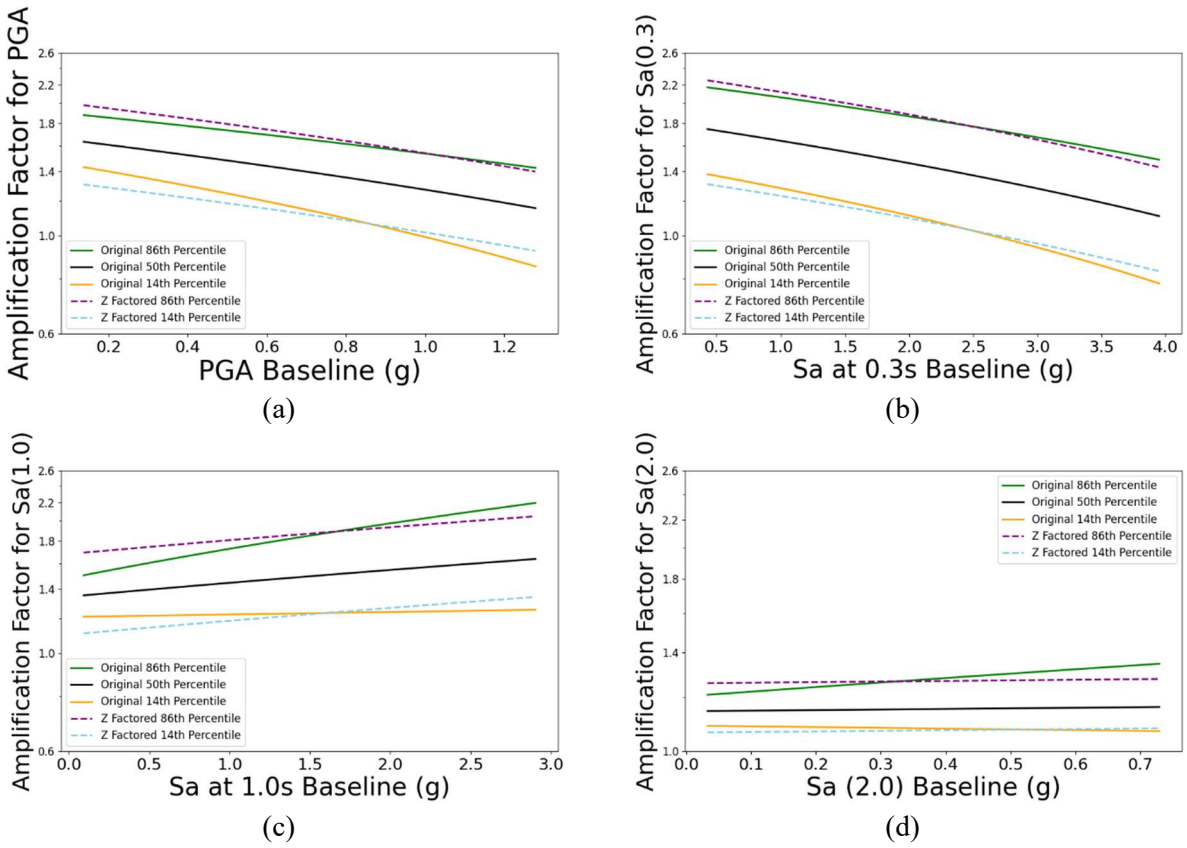

Figure 3.5 Comparison of Originally Linearly Regressed Lines with the Z Factored 86th and 14th Percentile Lines for Site Class D1 at Forks, WA for All Intensity Measures (a) PGA, (b) S_a(0.3 sec), (c) S_a(1.0 sec), and (d) S_a(2.0 sec)

3.4 RESULTING SOIL AMPLIFICATION MODELS FOR ALL 10 LOCATIONS

The following Figure 3.4 shows the fitted line for the 50th percentile soil amplification factors using the data for all 10 locations for all 7 site classes and for the 4 intensity measures. For the M9 baseline ground motions on Grid B, these combined fitted lines will be used to generate an amplification factor for a given baseline intensity at each soil site class. That is then multiplied by the baseline ground motion intensity to create an approximate amplified intensity. Figures 3.6 – 3.8 show the same lines but for the 14th and 86th percentiles. Specific values of the

equation for the fitted lines for the combination of all ten locations at each site class for the 50th percentile are in Table B.1 in Appendix B. Tables B.2 and B.3 also in Appendix B contain the values of the equation for the original fitted lines for the 14th and 86th percentiles. Regression (Z) values were created for the new combined fitted lines as well and are in Table 3.4 below.

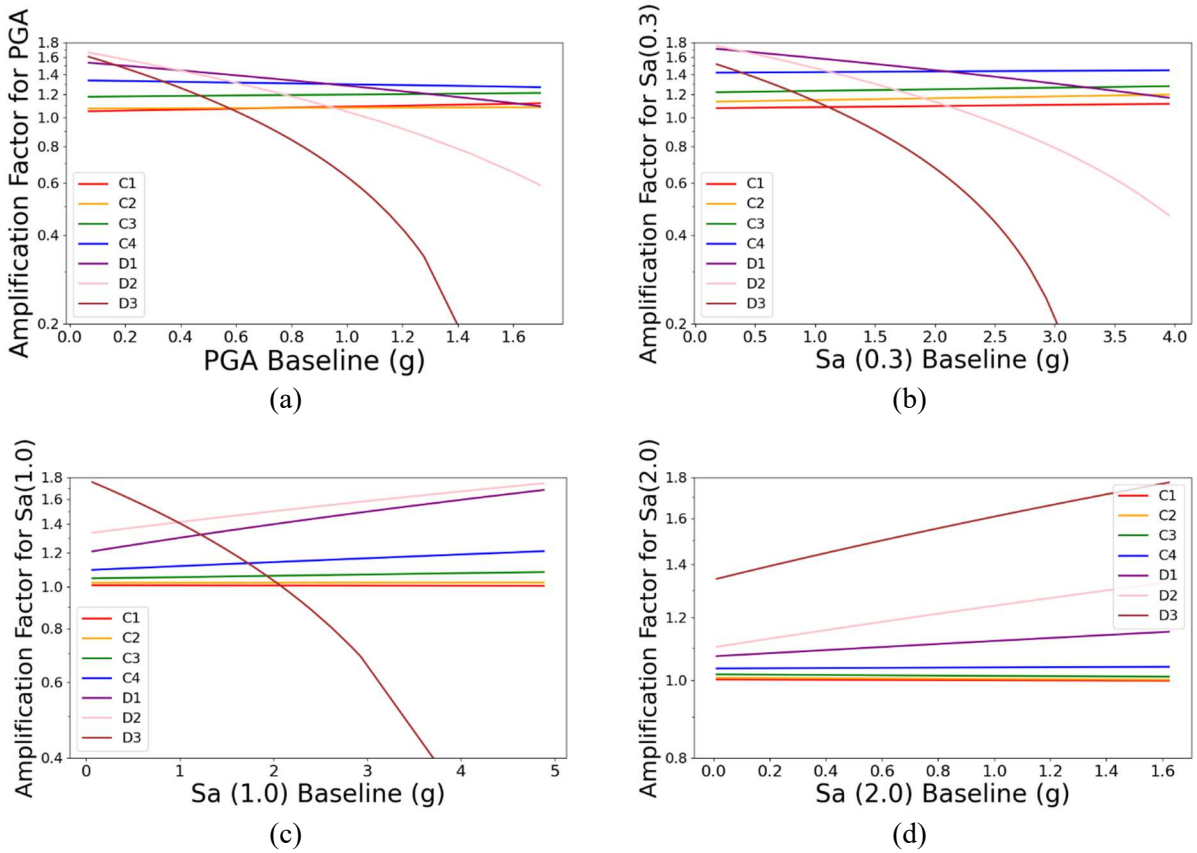

Figure 3.6 Fitted Lines for of the Soil Amplification Factor for Different Intensity Measures versus the Same Corresponding Intensity Measure Combining All 10 Locations at the 50th Percentile for Each Site Class

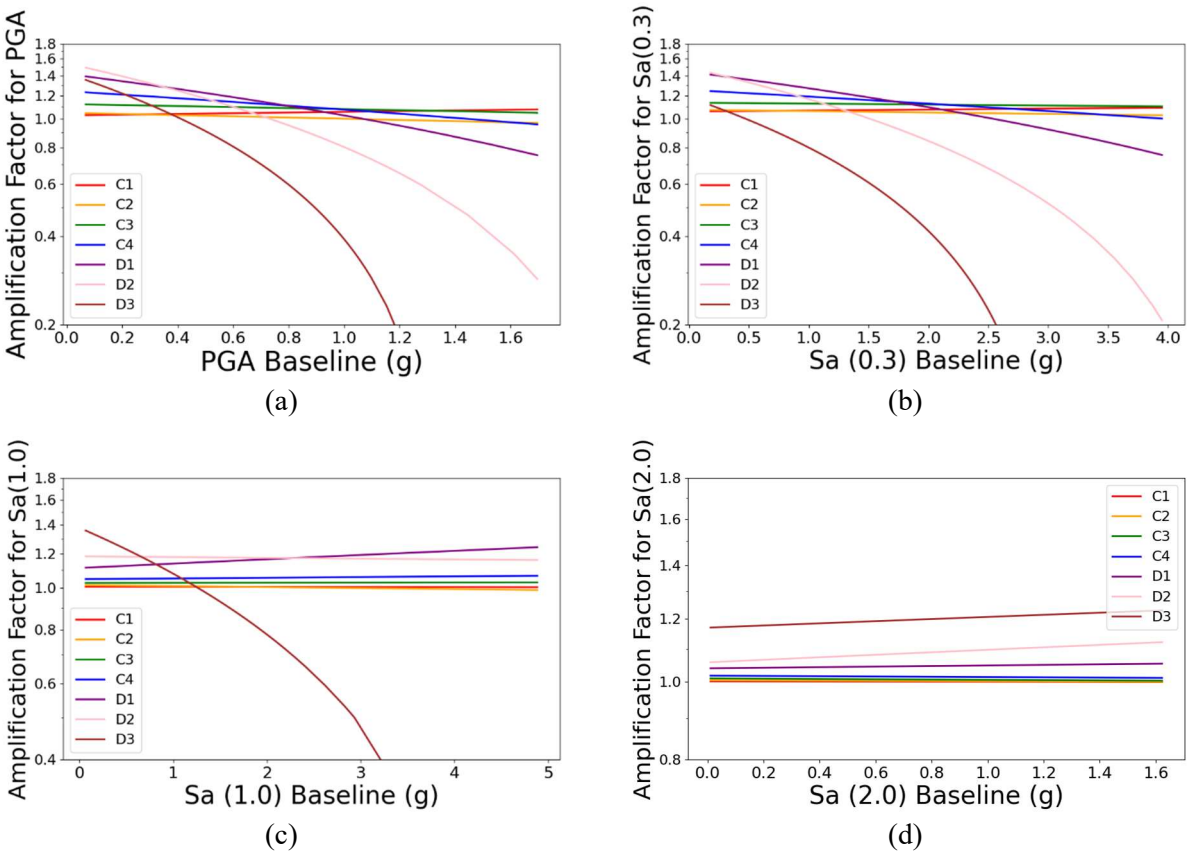

Figure 3.7 Fitted Lines for of the Soil Amplification Factor for Different Intensity Measures versus the Same Corresponding Intensity Measure Combining All 10 Locations at the 14th Percentile for Each Site Class

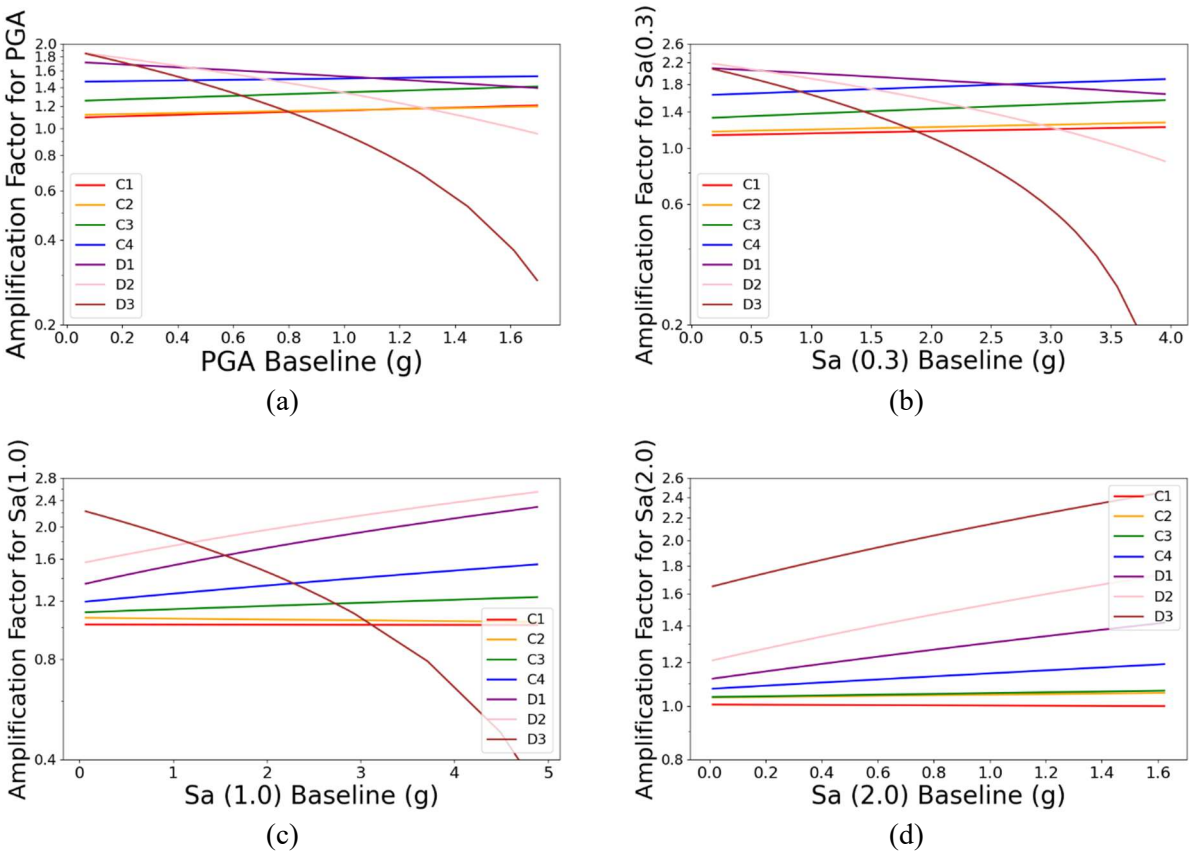

Figure 3.8 Fitted Lines for of the Soil Amplification Factor for Different Intensity Measures versus the Same Corresponding Intensity Measure Combining All 10 Locations at the 86th Percentile for Each Site Class

Table 3.4 Regressed Values of Z for the 14th and 86th Percentile Lines for Each Intensity Measure for Each Site Class

Site Class	**14th Percentile Regression Values (Z)**				**86th Percentile Regression Values (Z)**			
	PGA	$S_a(0.3)$	$S_a(1.0)$	$S_a(2.0)$	PGA	$S_a(0.3)$	$S_a(1.0)$	$S_a(2.0)$
C1	0.97	0.98	1.00	1.00	1.06	1.06	1.01	1.01
C2	0.93	0.90	0.97	1.00	1.07	1.05	1.02	1.06
C3	0.91	0.89	0.96	0.99	1.11	1.14	1.10	1.08
C4	0.84	0.79	0.92	0.98	1.14	1.22	1.20	1.20
D1	0.82	0.75	0.81	0.89	1.17	1.27	1.28	1.32
D2	0.82	0.76	0.77	0.79	1.21	1.33	1.34	1.42
D3	0.78	0.73	0.76	0.61	1.24	1.37	1.37	1.46

Chapter 4. FRAGILITY CURVES

In this chapter common bridge types on the Olympic Peninsula, as well as their corresponding fragility curves, will be identified. The fragility curves described in this chapter will include HAZUS relationships (FEMA 2024), as well as relationships developed by other researchers.

4.1 BRIDGE TYPES IN GRAY'S HARBOR AND PACIFIC COUNTIES

There are a total of 483 bridges in Gray's Harbor and Pacific counties according to the National Bridge Inventory (NBI), which documents properties of nearly all publicly owned bridges. For each of these bridges, the NBI assigns a three-digit code (bridge class), whose meaning are defined in the Recording and Coding Guide for the Structure Inventory and Appraisal of the Nation's Bridges (Federal Highway Administration 1995). The first number in that code indicates the material class (and continuity), and the last two numbers indicate the bridge type. Tables 4.1 and 4.2 gives the meaning of these codes. The last three columns of these tables list the number of single span bridges, multi-span bridges built before 1990 and multi-span bridges built in or after 1990 that have the corresponding code for the two counties.

Table 4.1 Number of Bridges in each NBI Material Class

Material Class Code	Description	Number of Single Span Bridges	Number of Multi-span Bridges Before 1990	Number of Multi-span Bridges After 1990
1	Concrete	20	21	2
2	Concrete Continuous	7	92	1
3	Steel	59	3	1
4	Steel Continuous	0	7	1
5	Prestressed Concrete	109	68	5
6	Prestressed Concrete Continuous	9	17	22
7	Timber	2	36	0
8	Masonry	0	0	0
9	Aluminum, Wrought Iron, or Cast Iron	0	0	1
0	Other	0	0	0
	Sum	206	244	33

Table 4.1 shows that:

a) The vast majority (77%, 373/483) of the bridges were constructed of reinforced or prestressed concrete. Steel bridges make up only 15% (71/483) of the inventory, with the remaining inventory consisting mainly of timber bridges (7.9%, 38/483).

b) 43% (206/483) of the bridges have a single span, including 39% (145/373) of the reinforced or prestressed bridges and 83% (59/71) of the steel bridges. Approximately half of the single span bridges, 53% (109/206), are simply supported prestressed concrete, 9.7% (20/206) are simply supported concrete and 29% (59/206) are simply supported steel.

c) 88% (244/277) of the multi-span bridges were constructed before 1990. Steel bridges were rarely built after 1990 (2/33), and the inventory lists no timber bridges built after 1990.

Table 4.2 Number of Bridges in each NBI Bridge Type

Bridge Type Code	Description	Number of Single Span Bridges	Number of Multi-span Bridges Before 1990	Number of Multi-span Bridges After 1990
01	Slab	51	113	3
02	Stringer/Multi-beam or Girder	66	65	20
03	Girder and Floor Beam System	2	1	0
04	Tee Beam	16	30	0
05	Box Beam or Girders – Multiple	4	10	0
06	Box Beam or Girders – Single or Spread	1	3	0
07	Frame	3	7	0
08	Orthotropic	0	0	0
09	Truss – Deck	1	0	0
10	Truss – Thru	8	2	1
11	Arch – Deck	8	0	0
12	Arch – Thru	2	0	0
13	Suspension	0	0	0
14	Stayed Girder	0	0	0
15	Movable – Lift	1	0	0
16	Movable – Bascule	3	0	0
17	Movable – Swing	0	1	0
18	Tunnel	0	0	0
19	Culvert	38	7	4
20	Mixed Types (applicable only to approach spans)	0	0	0
21	Segmental Box Girder	0	0	0
22	Channel Beam	2	5	5
00	Other	0	0	0
	Sum	206	244	33

Table 4.2 shows that most of the single span bridges are slabs or girders, with 25% (51/206) being slabs and 32% (66/206) being girders. Note that nine of the bridges are trusses and ten are arches.

For the multi-span bridges built before 1990, 46% (113/244) are slabs and 27% (65/244) are girders. The multi-span bridges built before 1990 are much more varied in material type

(Table 4.1), with concrete continuous and simply supported prestressed concrete each making up 38% (92/244) and 28% (68/244), respectively. Simply supported concrete, prestressed concrete continuous and timber make up 8.6% (21/244), 7% (17/244), and 15% (36/244), respectively. Whereas, the multi-span bridges built after 1990 only make up 6.8% (33/483) of total bridges. Of these bridges the vast majority are girder bridges and prestressed concrete continuous bridges.

Figure 4.1 shows the percentage of the most common multi-span bridge types in Gray's Harbor and Pacific counties as well as other group types of bridges that exist. Even though a timber girder bridge with NBI class of 702, may be the third most common specific bridge class in Gray's Harbor and Pacific counties, the combined concrete bridge classes heavily outweigh it. From Table 5.1 it is clear that concrete is the most common bridge material.

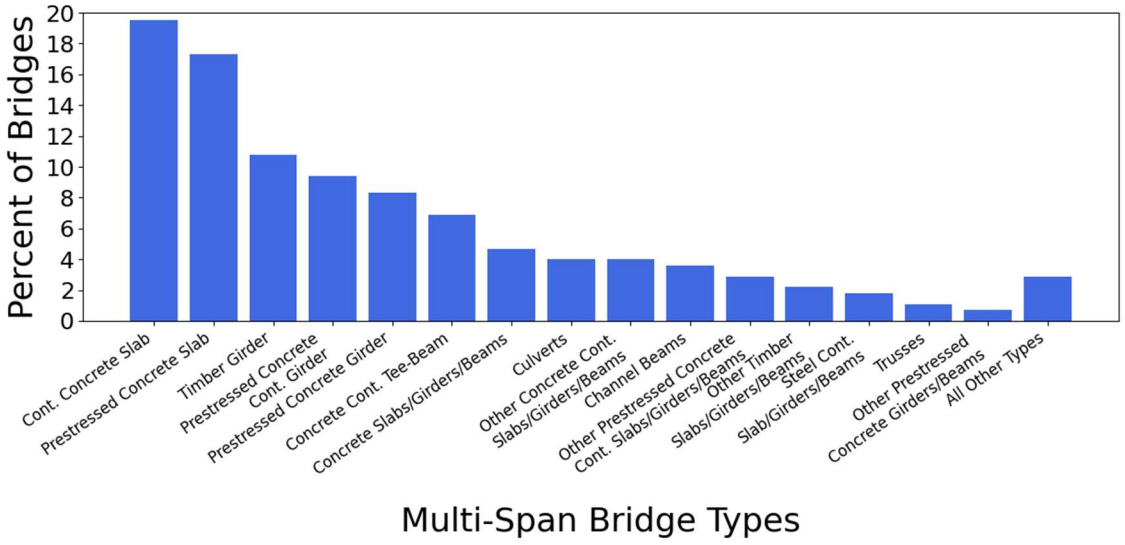

Figure 4.1 Multi-Span Bridge Types found in Gray's Harbor and Pacific Counties

4.2 SELECTION OF FOUR BRIDGE TYPES FOR FURTHER ANALYSIS

To make it possible to compare the vulnerability of bridges, four groups of bridges were chosen to be looked at in further detail. This study will focus on multi-span bridges, not only because they are more numerous, but because they are typically more vulnerable in an earthquake than single span bridges.

The second most common multi-span bridge group is prestressed simply supported concrete bridges, they make up 26% (48+23+2) of all multi-span bridges. The two most common bridge types of this group specifically correspond to the 501 and 502 bridge classes, which are denoted Prestressed Concrete Slab and Prestressed Concrete Girder in Figure 4.1. The material type 5 means the bridges are simply supported. From Table 4.1 it can be seen that the majority of bridges of this type were built before 1990, so this chapter will only focus on "older" simply supported (SS) concrete bridges.

The most common group of bridges are continuous concrete bridges, which includes prestressed and non-prestressed bridges, making up in total 46% (54+26+19+11+8/277) of multi-span bridges in the two counties. The two most dominant bridge classes being 201 and 602, named Cont. Concrete Slab and Prestressed Concrete Cont. Girder, respectively in Figure 4.1. While almost all of the bridges with material type 2 are built before 1990, for material type 6 there are a fair amount built before and after 1990. Therefore, an "older" continuous (Cont.) concrete bridge and a "newer" continuous (Cont.) concrete bridge will be considered. Since prestressed concrete continuous girder bridges (602) make up the vast majority of multi-span bridges built after 1990, this bridge type specifically will be considered. This also indicates that bridges being built from this time forward are likely to be of this bridge class.

The last bridge type that will be looked at is a movable bridge. While these bridges are not common, making up less than 5% of all bridge types in Gray's Harbor and Pacific counties, they have been found to be particularly vulnerable to earthquakes (Ranf et al. 2005), and they often provide vital links along major routes within a transportation network. Note that most movable bridges are single span. As previously stated, multi-span bridges are the main focus of this thesis, however the fragility curves detailed later in this chapter and analyzed in Chapter 5, do not differentiate between single span or multi-span bridges.

Table 4.3 lists the different types of fragility curves that will be used for each bridge type, their designation and their reference. They will be explained in more detail later in this chapter.

Table 4.3 Reference and Designation of Various Fragility Curves for their Corresponding Bridge Type and Category

Category	Bridge Type	Reference	Fragility Curve Designation in Original Work	Fragility Curve Designation Here
Older SS Concrete	Slabs and Girders	FEMA 2024	HWB17	HAZUS – HWB17
	Slab	Nielson and DesRoches 2007	MSSS Slab	MSSS Slab
	Girder	Nielson and DesRoches 2007	MSSS Concrete	MSSS Concrete
Older SS / Older Cont. Concrete	All Types	Ranf et al. 2005	1941 – 1975	Nisqually – 1941-1975
Older Cont. Concrete	Slabs and Girders	FEMA 2024	HWB10 / HWB22	HAZUS – HWB10/22
	Girder	Nielson and DesRoches 2007	MSC Concrete	MSC Concrete
	Girder	Liu et al. 2022	N/A	Concrete – NoShearKeys
Newer Cont. Concrete	Slabs and Girders	FEMA 2024	HWB11 / HWB23	HAZUS – HWB11/23
	All Types	Ranf et al. 2005	post – 1975	Nisqually – Post 1975
	Girder	Padgett and DesRoches 2009	MSC Concrete	MSC Concrete – Shear Keys
	Girder	Liu et al. 2022	N/A	Concrete – Shear Keys
	Girder	Xao and Xie 2024	CSE	CSE
Movable	All Types	FEMA 2024	HWB28	HAZUS – HWB28
	All Types	Ranf et al. 2005	movable	Nisqually – Movable

4.3 OLDER SIMPLY SUPPORTED CONCRETE BRIDGES

In Gray's Harbor and Pacific counties, the two most common bridge types, single span and multi-span combined, correspond to bridge classes 501 and 502. For multi-span bridges alone, they are the second most common bridge types. Bridge class 501 corresponds to a

simply supported prestressed concrete slab. Bridge class 502 corresponds to a simply supported prestressed concrete stringer/multi-beam or girder.

4.3.1 HAZUS Fragility Curves

According to the HAZUS method (FEMA 2024), both bridge types are assigned the same base fragility curves, HWB17 for bridges built before 1990, and HWB19 for bridges built on or after 1990. Bridges built before 1990 are assumed to not be seismically designed, and bridges built after 1990 are. Only HWB17 will be considered since there are few prestressed simply supported bridges built after 1990.

In actuality, two bridges classified as 501 and 502 might not have the same fragility curves depending on their individual parameters. HAZUS (FEMA 2024) includes factors that modify the HWB median values based on skew, number of spans, and the ground motion spectral acceleration at the particular location. To compare the fragility curves, just the unaltered medians and fragility curves will be considered. Table 4.4 and Figure 4.4 at the end of this section give the median values and plots of the fragility curves, respectively.

4.3.2 Nisqually Fragility Curves

The Nisqually fragility curves (Ranf et al. 2005) were developed from damage observations following the 2001 Nisqually earthquake in western Washington. That study provided specific fragility curves for movable bridges and truss bridges, which were particularly vulnerable during the earthquake. For all other bridges, the fragility curves are separated by year built, pre-1941, 1941 – 1975, and post 1975. For bridge class 501/502, the fragility curves for 1941 – 1975 will be used and will represent non-seismic bridges. The level of damage during the Nisqually earthquake was relatively low, so the authors only provided relationships for the Slight

damage state. For this study, the medians for the Moderate, Extensive, Complete damage states will be estimated by basing the values off of the proportions for the HAZUS medians. For example, the median for Moderate on the HWB17 curve is 1.4 times the median for Slight, therefore the median for Moderate for the Nisqually 1941-1975 curve will be 1.4 times the median for Slight which is 1.4, making the median for Moderate 1.96. All medians and fragility curves for bridge class 501/502 will be provided at the end of this section.

4.3.3 Similar Bridges in Central and Southern United States

Extensive research has been done in developing fragility curves for common bridge types in the Central and Southern region of the United States (Nielson 2005, Nielson and DesRoches 2007, Padgett and DesRoches 2009). The Multi-span Simply Supported Concrete Slab (MSSS Slab), is the central/southern bridge type that most closely resembles bridge class 501. Figure 4.2 shows the basic layout for a MSSS Slab bridge that was used to develop the fragility relationships.

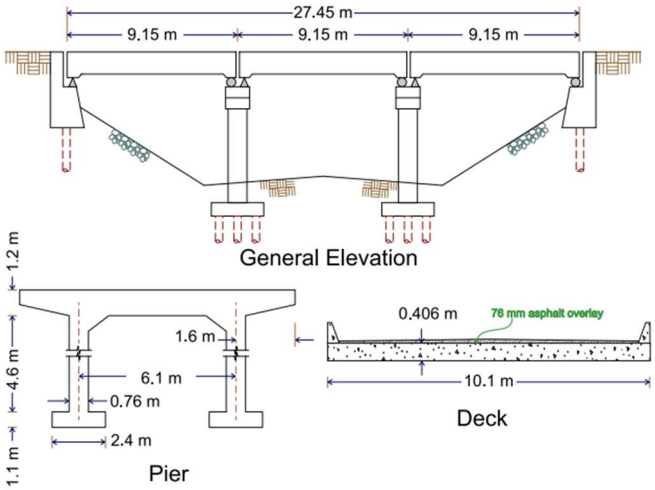

Figure 4.2 MSSS Slab Bridge Configuration (Nielson 2005)

The Multi-span Simple Supported Concrete Girder (MSSS Concrete), is the central/southern bridge type that most closely resembles bridge class 502. Figure 4.3 shows the basic design for a MSSS Concrete girder bridge that was used as a prototype to develop the fragility curves.

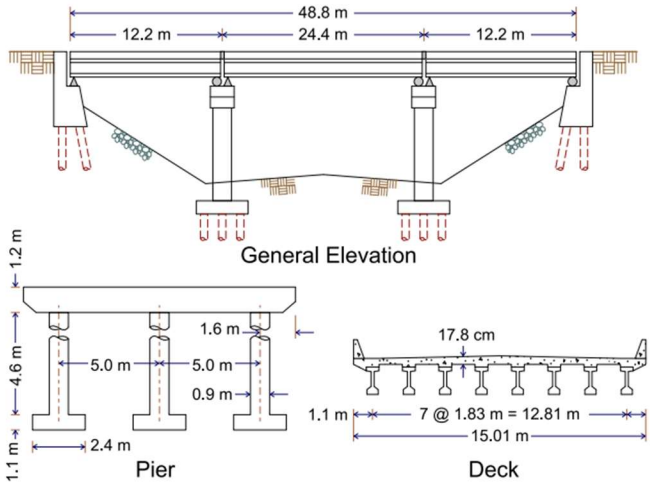

Figure 4.3 MSSS Concrete Bridge Configuration (Nielson 2005)

While there are many variations, this study will focus on the basic fragility curve for as-built bridges conventionally designed (Nielson and DesRoches 2007). Table 4.3 below list the median values for the fragility curves for each damage state, as well as the intensity measure used for those curves and the dispersion, β.

Table 4.4 Fragility Function Median and Dispersion Values for Bridge Class 501/502

Reference	**Fragility Function Designation**	**Intensity Measure**	**Damage State Median**				**β**
			Slight	Moderate	Extensive	Complete	
FEMA 2024	HAZUS – HWB17	S_a (1.0)	0.25	0.35	0.45	0.70	0.60
Ranf et al. 2005	Nisqually – 1941-1975	S_a (0.3)	1.40	1.96	2.52	3.92	0.60
Nielson and DesRoches 2007	MSSS Slab	PGA	0.18	0.52	0.94	1.92	0.75
Nielson and DesRoches 2007	MSSS Concrete	PGA	0.20	0.57	0.83	1.17	0.65

The fragility curves are hard to compare on their own, since most of them use different intensity measures. However, MSSS Slab and MSSS Concrete are both graphed on the same plot in Figure 4.4 since they do use the same intensity measure, being developed by the same authors in the same paper. Even though one is for a slab and one is for a girder, the fragility curves are similar, with the Slight and Moderate curves being almost identical. The biggest difference between the two is in the Complete damage state (Table 4.4 and Figure 4.4).

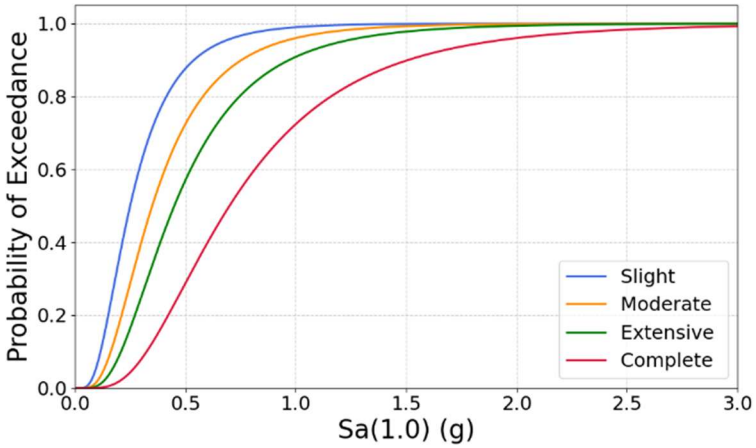

(a) HAZUS - HWB17 (FEMA)

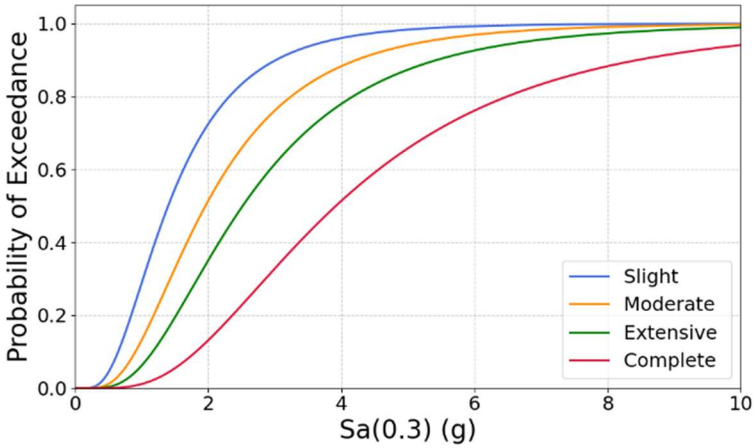

(b) Nisqually 1941-1975 (Ranf)

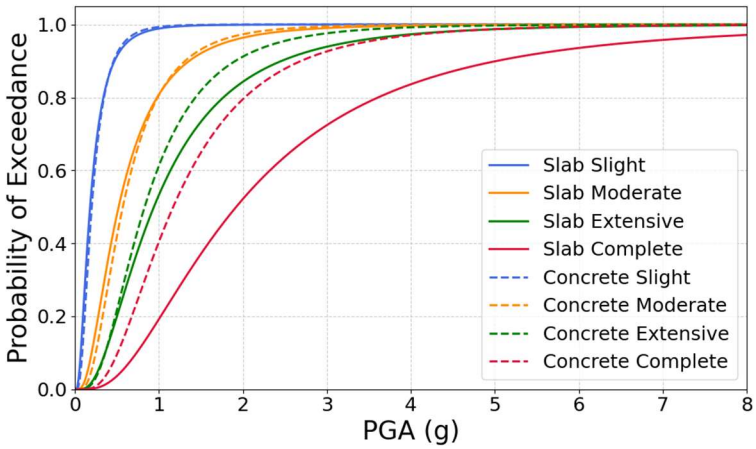

(c) MSSS Slab and MSSS Concrete (Nielson and DesRoches)

Figure 4.4 Fragility Functions for an Older Simply Supported Concrete Bridge

4.4 OLDER CONTINUOUS CONCRETE BRIDGES

Continuous concrete bridges are the next most common bridge class overall, and the most common bridge class for multi-span bridges. Continuous concrete bridges encompass material types 2 and 6. Fragility curves in this section will be for an "older" bridge, meaning it is not specifically seismically designed, and will be assumed to not include shear keys. The bridge in question will be the same model that was used in a WSDOT report on bridges in western Washington, minus the shear keys (Liu et al. 2022). Figure 4.5 shows the general bridge configuration. Given its continuous prestressed girders, it will also be classified as bridge class 602, which is also the classification of the 4th most common multi-span bridge type in Gray's Harbor and Pacific counties according to Figure 4.1.

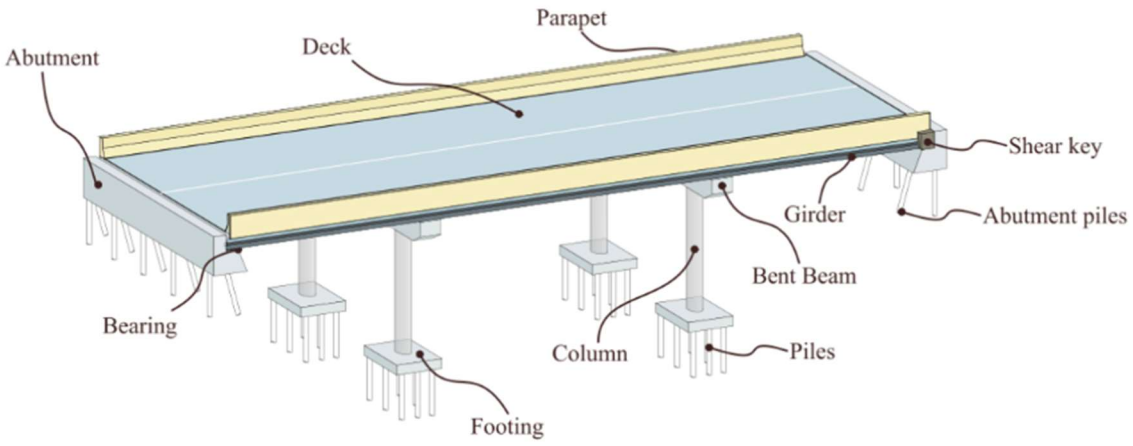

Figure 4.5 General Configuration of Continuous Concrete Bridge (Mangalathu 2017)

4.4.1 Fragility Curves Derived from Liu Analyses

The research described in the WSDOT report (Liu et al. 2022) is relevant to this study because it used a three-dimensional multi-degree of freedom bridge model with the same set of M9 ground motions. It was developed to represent a typical highway bridge in Washington (Liu 2022). While fragility curves were not developed in that study, another researcher, Andres Sanchez, used the data on the damage types that the model incurred, to create fragility curves. The median for Moderate damage came from concrete spalling, and the median for Extensive damage came from bar buckling. The medians for Slight and Complete were assumed base off of the ratios of the HAZUS curve.

4.4.2 HAZUS Fragility Curves

For a bridge classified as 602 built before 1990, the fragility curve classification is HWB22 (FEMA 2024). The most common bridge type in Figure 4.1 is technically classified as 201 or a Continuous Concrete Slab. In HAZUS (FEMA 2024) this type of bridge built before 1990 has a HWB10 fragility function. Coincidentally, HWB10 and HWB22 have the exact same base fragility functions, and so for this case they can be lumped together. Again, the individual parameters of a bridge might result in varying modification factors, but just the base medians will be listed in Table 4.5 at the end of this section.

4.4.3 Nisqually Fragility Curves

Because the Nisqually fragility curves (Ranf et al. 2005) only differentiate bridges based on the year built for all other bridges besides trusses or movable bridges, the same fragility function that was used in the previous section applies here as well. The similarity between the previous section and this section being that both consider bridges that are “older” or not

seismically designed. As with before, only the Slight median is given and the rest of the damage states are calculated based off of the proportions of the HAZUS fragility function, except the proportions from the HWB10/22 will be used instead of HWB17.

4.4.4 Similar Bridges in Central and Southern United States

The central/southern bridge type (Nielson and DesRoches 2009) that most closely resembles a prestressed concrete continuous girder bridge is Multi-span Continuous Concrete Girder (MSC Concrete). Figure 4.6 shows the general configuration. The girders are in fact prestressed, however there are no shear keys and the fragility curves used are for the conventional as-built design.

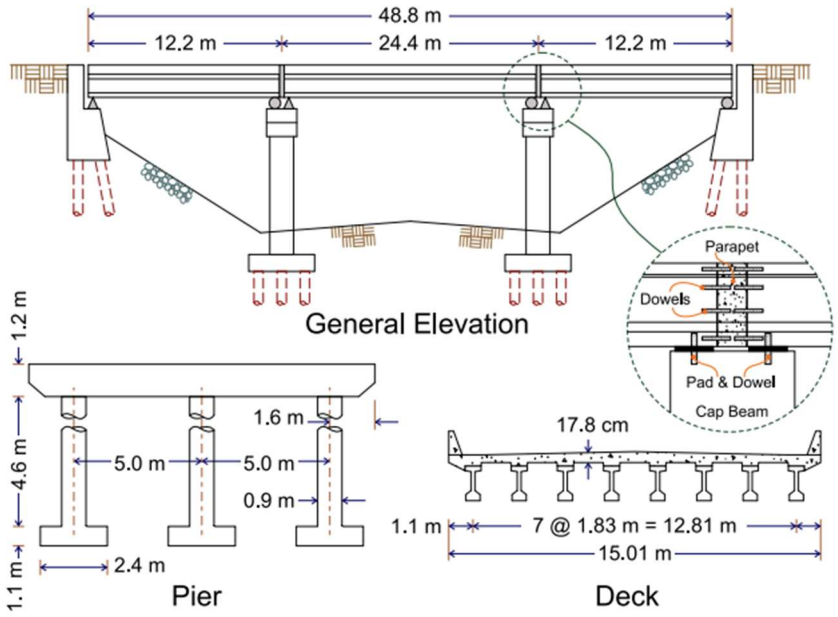

Figure 4.6 MSC Concrete Girder Bridge Configuration (Nielson 2005)

Table 4.5 Fragility Function Median Values for an Older Continuous Concrete Bridge

Reference	Fragility Function Designation	Intensity Measure	Damage State Median				β
			Slight	Moderate	Extensive	Complete	
FEMA 2024	HAZUS – HWB10/22	S_a (1.0)	0.60	0.90	1.10	1.50	0.60
Ranf et al. 2005	Nisqually – 1941-1975	S_a (0.3)	1.40	2.10	2.57	3.50	0.60
Nielson and DesRoches 2007	MSC Concrete	PGA	0.15	0.52	0.75	1.03	0.70
Liu et al. 2022	Concrete –No Shear Keys	S_a (1.0)	0.74	1.11	2.23	3.04	0.50

The HAZUS fragility curve and the Concrete-No Shear Keys from the WSDOT report data are the only comparable fragility curves since they share the same intensity measure. The curves for Slight and Moderate are not too far off from each other, but there is a substantial difference between the Extensive and Complete damage states.

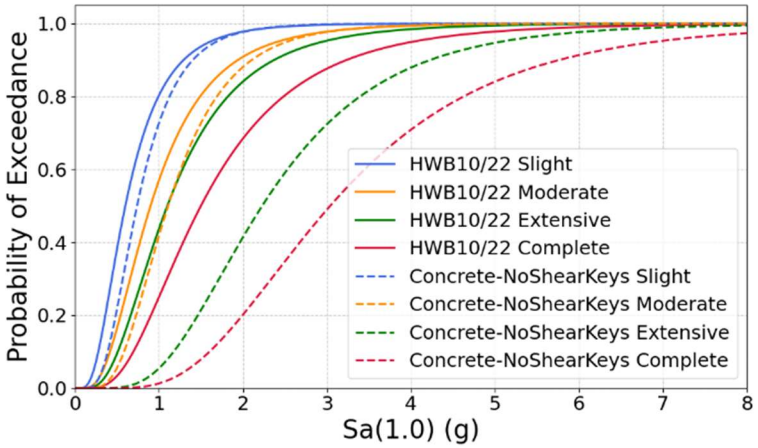

(a) HWB10/22 (FEMA) and Concrete-NoShearKeys (Liu)

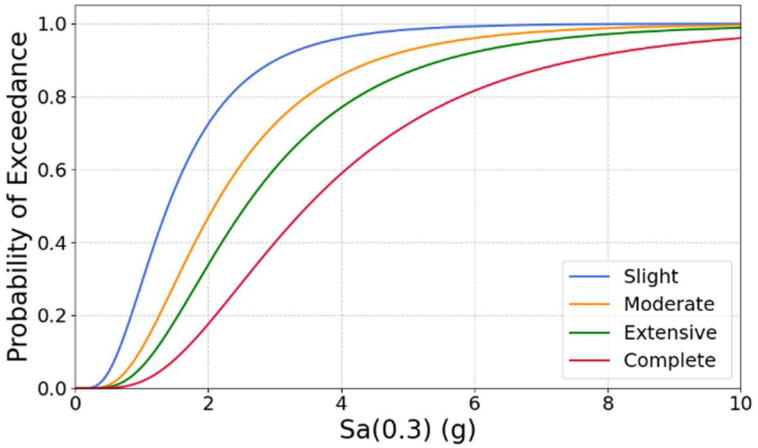

(b) Nisqually 1941-1975 (Ranf)

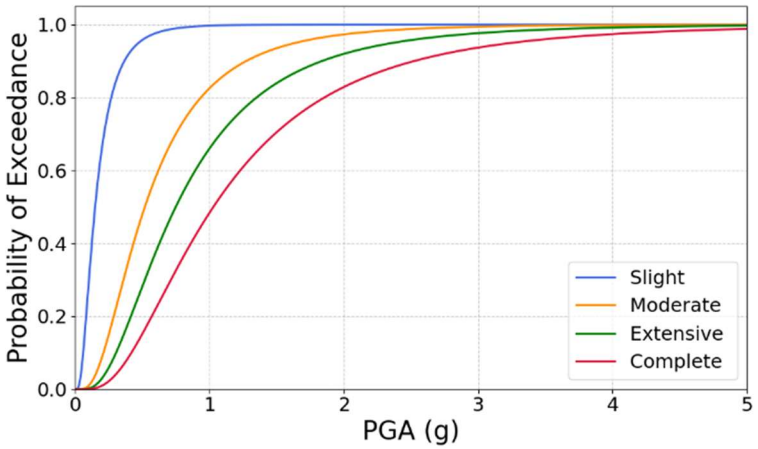

(c) MSC Concrete (Nielson and DesRoches)

Figure 4.7 Fragility Functions for an Older Continuous Concrete Bridge

4.5 NEWER CONTINUOUS CONCRETE BRIDGES

The bridge type considered for this section will be the same as the previous section except it will be considered to be of newer design or seismically designed. As such, this bridge will also assume to have shear keys and more transverse reinforcement steel in the columns. The general configuration will be the same as in Figure 4.5.

4.5.1 Fragility Curves Derived from Liu Analyses

Like before, specific damage types, spalling and bar buckling, were used to develop the medians for the fragility curve, but this time shear keys were included in the model.

4.5.2 HAZUS Fragility Curves

The HAZUS classification method doesn't account for whether or not a bridge has shear keys specifically but they differentiate seismic design by the year built. For bridge class 602 built after 1990, the fragility function classification is HWB23. Likewise for bridge class 201 built after 1990 the fragility function classification is HWB11 and just like in the previous section the median values are exactly the same for HWB11 and HWB23.

4.5.3 Nisqually Fragility Curves

Since this section is considering a newer or seismically designed bridge the Nisqually fragility function that will be used is the Post 1975 function. The proportions for the Moderate, Extensive and Complete damage state medians will be based off of the HAZUS HWB11/23 curves.

4.5.4 Similar Bridges in Central and Southern United States

The same central/southern bridge classification as in the previous section still applies, however that was for an as-built conventionally designed bridge and did not assume any shear keys. Fortunately, previous researchers have built off of those base bridge types in the Central and Southern United States to vary certain parameters and provide new fragility curves. One such was for a retrofit that included shear keys and that is the fragility function below in Table 4.6.

4.5.5 Cascadia Subduction Zone Fragility Curves

Another researcher took a basic reinforced concrete bridge modeled after typical highway bridges in Canada and produced fragility curves given 3 different types of earthquakes; Crustal Earthquake, Subcrustal Earthquake, and a Cascadia Subduction Zone Earthquake (Xao and Xie 2024). As stated in a previous chapter, the Cascadia Subduction Zone Earthquake is the earthquake that threatens the Olympic Peninsula region. The reinforced concrete girder bridge can be classified as having a seismic design because the bridge type it was modeled after assumes shear keys in the design (Xao and Xie 2024). Figure 4.8 below gives the general configuration of the model bridge.

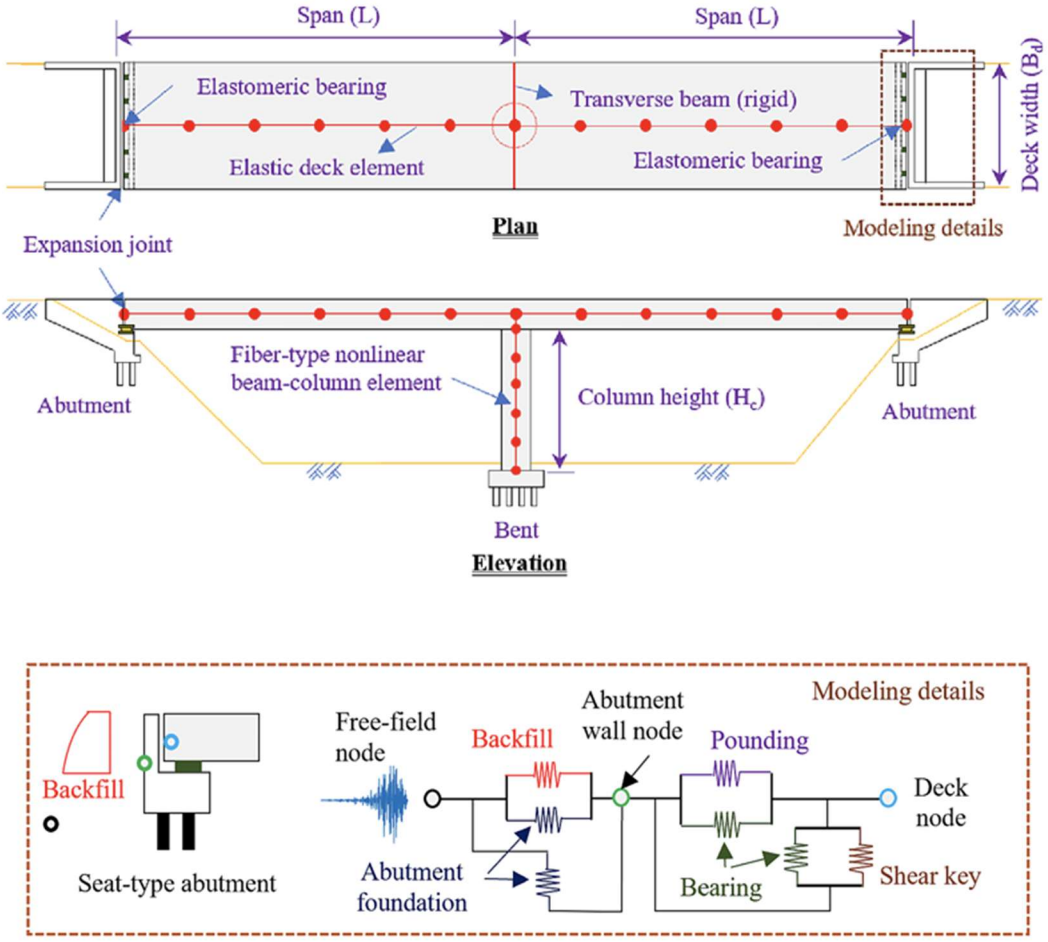

Figure 4.8 General Configuration of Canadian Reinforced Concrete Highway Bridge (Xao and Xie 2024)

The table below gives the values for the medians of each damage state for the different fragility methods. Certain fragility curves have a specific dispersion value for each damage state instead of one. Those specific values for β can be seen in Table 4.7. Since the Concrete – Shear Keys curves were only derived for the Moderate and Extensive damage states, and the other damage states were assumed, the dispersion used for Slight and Complete is the average value of the dispersions for Moderate and Extensive for that particular curve.

Table 4.6 Fragility Function Median Values for a Newer Continuous Concrete Bridge

Reference	Fragility Function Designation	Intensity Measure	Damage State Median				β
			Slight	Moderate	Extensive	Complete	
FEMA 2024	HAZUS – HWB11/23	S_a (1.0)	0.90	0.90	1.10	1.50	0.60
Ranf et al. 2005	Nisqually – Post 1975	S_a (0.3)	1.60	1.60	1.96	2.67	0.60
Padgett & DesRoches 2009	MSC Concrete – Shear Keys	PGA	0.16	0.57	0.84	1.62	Table 5.7
Xao and Xie 2024	CSE	S_a (1.0)	0.18	0.50	1.09	1.75	Table 5.7
Liu et al. 2022	Concrete – Shear Keys	S_a (1.0)	2.15	2.15	3.39	4.63	Table 5.7

Table 4.7 Dispersion Values for Individual Damage States

Fragility Function Method	β			
	Slight	Moderate	Extensive	Complete
MSC Concrete – Shear Keys	0.84	0.69	0.67	0.69
CSE	0.74	0.58	0.58	0.56
Concrete – Shear Keys	0.61	0.78	0.43	0.61

In the case of several of the fragility curves, the Slight and Moderate damage states have the same median. So, in Figure 4.9, the curve for Slight cannot be seen because it is under the Moderate curve for those cases. Comparing the HAZUS curve to the CSE curves, the Slight and Moderate curves are vastly different, however the Extensive curves are extremely close, and the Complete curve is not as far off either. The HAZUS curve and the Concrete – Shear Keys curve gives no resemblance whatsoever.

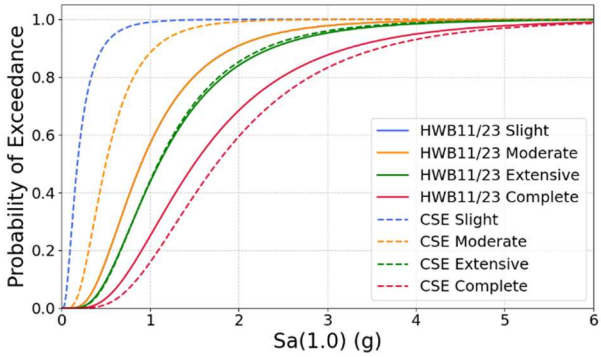

(a) HWB11/23 (FEMA) and CSE (Xao and Xie)

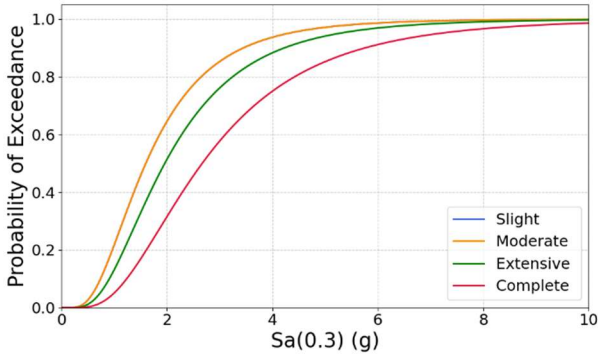

(b) Nisqually Post 1975 (Ranf)

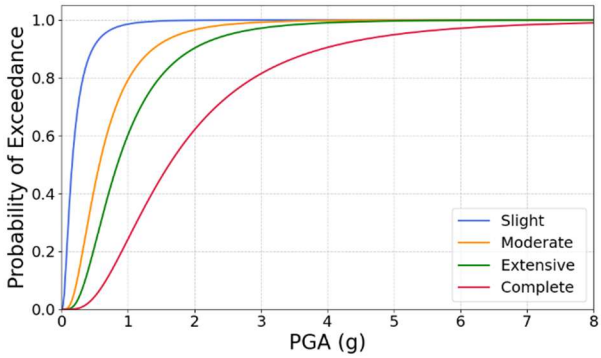

(c) MSC Concrete with Shear Keys (Padgett and DesRoches)

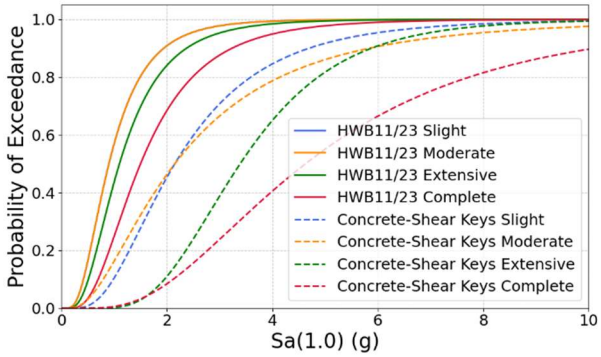

(d) HWB11/23 (FEMA) and Concrete-Shear Keys (Liu)

Figure 4.9 Fragility Functions for a Newer Continuous Concrete Bridge

4.6 MOVABLE BRIDGES

In Gray's Harbor and Pacific counties, there exists a few bridges that are classified as "movable", the most common being bridge class 316 making it a steel movable – bascule bridge. A movable bascule bridge is another term for a drawbridge where one or more spans can pivot and lift up by way of a counterweight, letting taller boats pass through. After the 2001 Nisqually earthquake which took place in western Washington, it was found that these types of bridges are particularly vulnerable and incur unique types of damage (Ranf et al. 2005). Unfortunately, HAZUS does not have a specific HWB classification for a movable bridge, so in a HAZUS analysis it would be assigned as HWB28 which can be used for arch bridges, suspension bridges, tunnels, culverts, channel beam bridges, and various other combinations of bridge types. HWB28 also uses no modification factors to modify the fragility curves to a given bridge, which also means there is no modification factor for the number of spans.

From the observations that were made after the Nisqually earthquake, new fragility relationships were proposed for movable bridges to more accurately predict the damages they might sustain. Table 4.8 gives the median values of the fragility curves at the different damage states. Similar to the previous sections in this chapter, only the median value for Slight is given for the Nisqually fragility curve, and the following damage state medians are proportional to the HAZUS medians. In both cases a dispersion value of 0.6 is used.

Table 4.8 Fragility Function Median Values for a Movable Bridge

Reference	Fragility Function Method	Intensity Measure	Damage State Median				β
			Slight	Moderate	Extensive	Complete	
FEMA 2024	HAZUS – HWB28	S_a (1.0)	0.80	1.00	1.20	1.70	0.60
Ranf et al. 2005	Nisqually - Movable	S_a (0.3)	0.60	0.75	0.90	1.28	0.60

Another difference in the methods is the intensity measure used. HAZUS uses the long period acceleration Sa (1.0) and the Nisqually method uses the short period acceleration Sa (0.3), so they cannot be plotted on the same graph unfortunately. Figure 4.10 shows the fragility curves of the four damage states for the HAZUS fragility function and the Nisqually fragility function for movable bridges respectively.

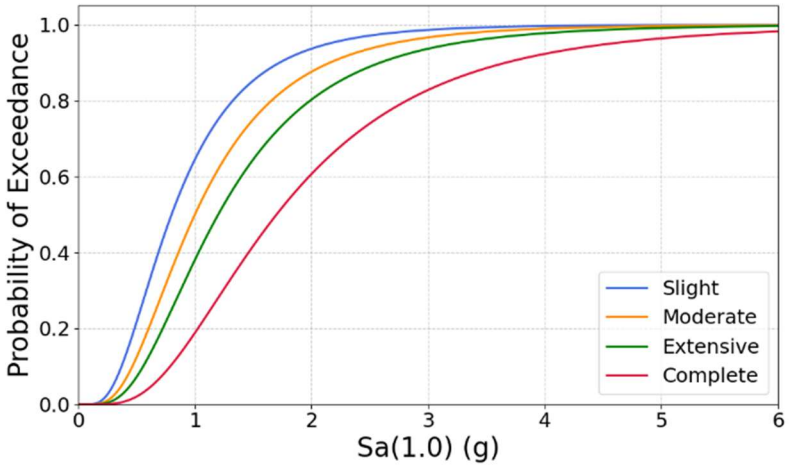

(a) HAZUS – HWB28 (FEMA)

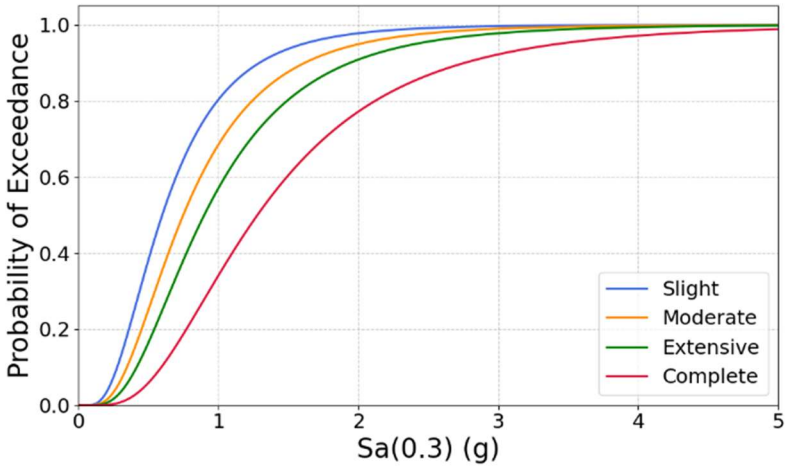

(b) Nisqually Movable (Ranf)

Figure 4.10 Fragility Functions for a Movable Bridge

Chapter 5. PARAMETRIC STUDIES OF INDIVIDUAL BRIDGES

In this chapter, parametric studies of individual bridges are described in which one bridge type is studied at a time. Each one is placed at the Reference point described in Chapter 2 and other parameters needed for assessing bridge performance are varied. The varied parameters are the ground motion realizations (Chapter 2), the soil site class amplification (Chapter 3), and the fragility curves used for the four bridge categories described in Chapter 4. For all bridge types, the following characteristics will be assumed unless otherwise noted: 3 spans, 0 skew, 10m deck width, and 30m maximum span length.

5.1 MODIFICATION FACTORS

For most of this chapter, the bridge fragility curves from HAZUS (FEMA 2024) will be used for damage assessment. The HAZUS technical manual outlines modification factors (K_{shape}, K_{3D}, and K_{skew}) that are primarily based on spectral shape, the number of spans, bridge skew, and bridge type. The K_{shape} modification factor only applies if I-shape is equal 1, otherwise if I-shape is 0, K_{shape} is 1. I-shape is either 0 or 1, indicating if long periods or short periods govern the bridge type, respectively. K_{3D} accounts for the effect of the 3-dimensional arch action in the deck given more than one span and depends on the number of spans of the bridge. Note that the equation to calculate K_{3D} also varies with bridge type. The modification factor K_{skew} accounts for the effect of skew on bridge response and likely damage. This factor depends on the bridge skew angle. For a bridge with no skew, the modification factor is 1. These modification factors are then used to modify the median values of the fragility curve that were given in the previous chapter.

Table 5.1 gives the modification factors for each of the HAZUS curves that will be used in this study. Note that K_{shape} is only applied to the Slight damage state, while both K_{3D} and K_{skew} are applied to damage states Moderate through Complete. A complete discussion of the modification factors can be found in the HAZUS Technical Manual, provided by FEMA.

Table 5.1 Modification Factors for the Medians of the HAZUS Fragility Curves

Category	Class	I-shape	K-shape	K-3D	K-skew
Older SS	HWB17	0	1.000	1.125	1.000
Older Cont.	HWB22	1	0.726	1.110	1.000
Newer Cont.	HWB23	1	0.726	1.165	1.000
Movable	HWB28	N/A	1.000	1.000	1.000

As described in Chapter 4, fragility curves from Ranf et al. (2005), derived from bridge data in the Nisqually Earthquake and denoted the Nisqually fragility curves herein, are only available for the Slight damage states. Fragility curve parameters for the rest of the damage state medians were approximated using the ratio of medians for those other damage states as given in the HAZUS fragility curves. To be consistent, the same modification factors used for HAZUS will be applied to the Nisqually curves that were assumed. Table 5.2 shows the modified median value for each of the Nisqually fragility curves after multiplying the original median by the modification factors specified above. The original median for Slight is also shown and will be kept the same.

Table 5.2 Modified Medians for the Nisqually Fragility Curves after Applying the HAZUS Modification Factors

Category	Fragility Function	Original Median	Modified Median		
		Slight	Moderate	Extensive	Complete
Older SS	Nisqually 1941-1975	1.400	2.205	2.835	4.410
Older Cont.	Nisqually 1941-1975	1.400	2.331	2.853	3.885
Newer Cont.	Nisqually – Post 1975	1.600	1.864	2.283	3.111
Movable	Nisqually – Movable	0.600	0.750	0.900	1.280

Similarly, the same approach is sued to augment the Moderate and Extensive damage states developed from the data found in Liu et al. (2022). In this case the Complete and Slight damage states are derived using the ratio of the medians for those damage states relative to the Moderate and Extensive damage states from the HAZUS fragility curves. Table 5.3 shows the updated medians for the four state fragility curves where the HAZUS modification factors have also been applied.

Table 5.3 Modified Damage State Fragility Curve Medians after Scaling Moderate and Extensive and Applying the HAZUS Modification Factors for the Corresponding Liu Fragility Curves

Category	Fragility Function	Modified Median	Original Median		Modified Median
		Slight	Moderate	Extensive	Complete
Older Cont.	Concrete – No Shear Keys	0.537	1.110	2.230	3.374
Newer Cont.	Concrete – Shear Keys	1.560	2.150	3.390	5.394

5.2 STUDY 1: OLDER SIMPLY SUPPORTED CONCRETE BRIDGE TYPE WITH VARYING REALIZATIONS

For this portion of the parametric study, the site class will be held constant and assumed to have the sub-site class C2 with ground motion amplification set at the 50th percentile for all

intensity measures. The amplification factors for all 30 realizations at the four intensity measures are given in Table C.1 in Appendix C.

Further, the bridge type is held constant and is set as "older simply supported concrete bridge" which comprises bridge classes 501 and 502 in HAZUS. The HAZUS fragility curves will be the default fragilities and as specified in the previous chapter, specifically those for HWB17 for this case will be used. Again, modification factors that are multiplied to the base medians specified in Chapter 4, were shown in Table 5.1.

5.2.1 Thirty Realizations with Median Site Amplification

Here, the ground motions from Chapter 2 have been multiplied by the amplification factors for site class C2 at the 50^{th} percentile. Table C.2 in Appendix C shows the amplified intensity measures for all 30 ground motion realizations at the Reference Point. Each realization was applied to the HWB17 modified fragility curve, giving a unique set of probabilities for each damage state at each realization. Figure 5.1 shows the probability of each damage state and how it varies across the realizations. The None and Complete damage states show the most variability across realization, while the probabilities for the middle damage states are more similar across all 30 realizations. The variability is larger for the None and Complete Damage States likely because the medians of the curves for each damage state are all relatively close together. This means there isn't as big of a difference between the $S_a(1.0)$ value that gives None as the most probable damage state and the $S_a(1.0)$ value that gives Complete as the most probable damage state. This in turn leads to a small range by which the $S_a(1.0)$ value would yield Slight, Moderate, or Extensive as the most probable damage state. See Table C.3 in Appendix C for a complete list of the specific values of damage state probabilities for the 30 realizations.

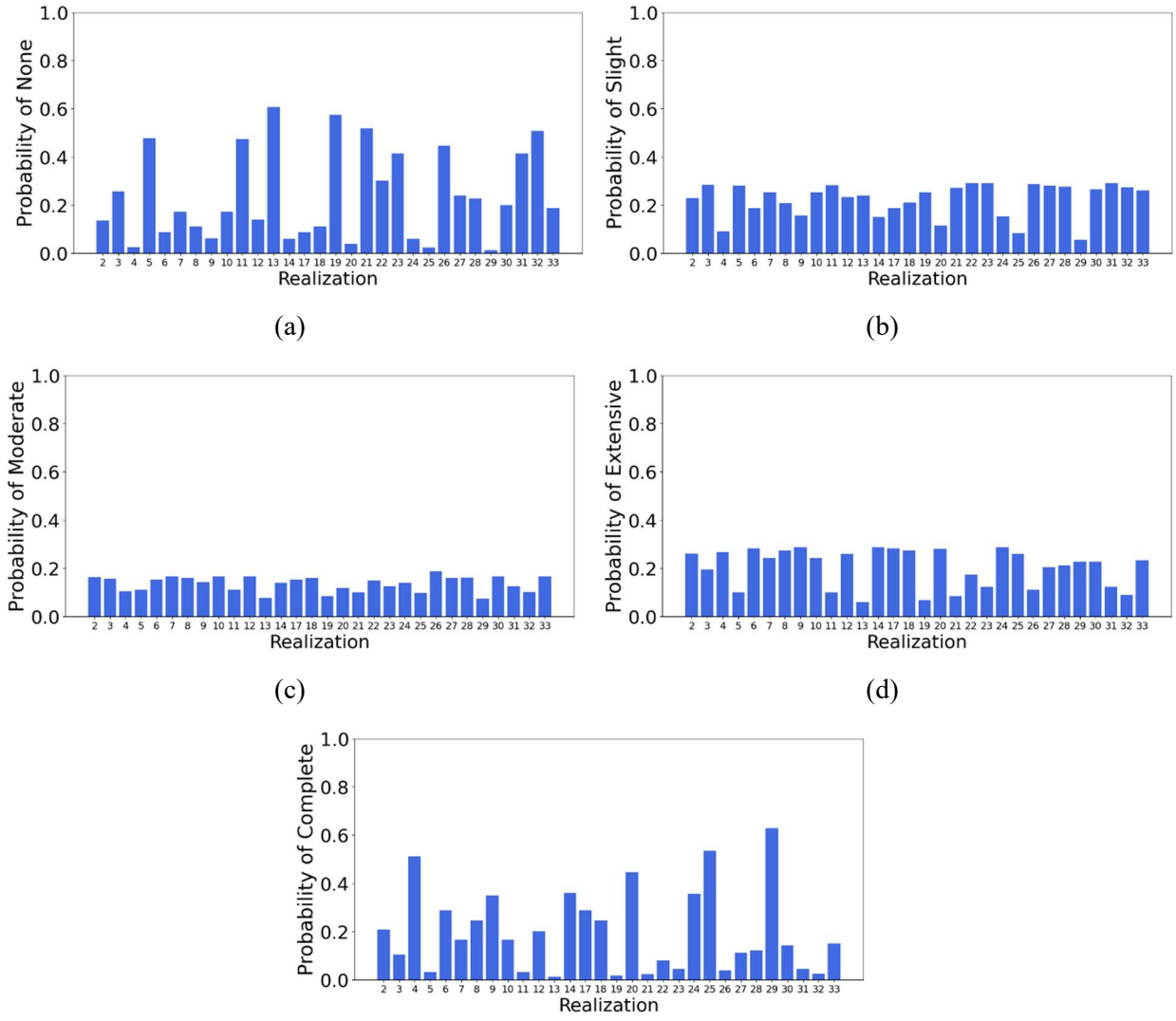

Figure 5.1 Probability of Each Damage State, (a) None, (b) Slight, (c) Moderate, (d) Extensive, and (e) Complete Across All 30 Realizations with 50th Percentile Site Class C2 Amplification for HWB17 at the Reference Point

For each realization, a most likely damage state can be identified as the damage state that has the highest probability for that realization. Table 5.4 gives the percentage, out of the 30 realizations, that each damage state was the most likely damage state. Assuming that all realizations are equally probable, the table also shows the combined probability of each damage

state at the Reference Point with HWB17 given an M9 Cascadia Subduction Earthquake with 50th percentile Site Class C2 amplification.

Table 5.4 Likelihood of Each Damage State Given All 30 Realizations Equally Probable

None	Slight	Moderate	Extensive	Complete
33.3%	23.3%	0.0%	13.3%	30.0%

However, the margin at which a damage state is the most likely can vary greatly. For example, for one instance there may be several damage states that are almost as equally probable (e.g., Realization 10 in Figure 5.1). Conversely, there may be a scenario where one of the damage states has a much higher probability than the rest of the damage states (e.g., Realizations 29 in Figure 5.1). Generally, there are not cases where one damage state is 100% while the rest are 0%. Rather than just reporting the most likely damage state, which can be miss-interpreted when several damage states have similar likelihood, the average across the damage states was calculated at each realization. To do this, the damage states None, Slight, Moderate, Extensive, and Complete are represented numerically by 0, 1, 2, 3, and 4, respectively. The average of the probability of each damage state, denoted the average damage state herein, is then calculated by multiplying the probability of each damage state for a given realization by its numerical value and adding them all together for the realization. Figure 5.2 shows the average damage state for each realization. Table 5.5 provides statistical measures on all the average damage state across the 30 realizations. As shown, the average damage state varies greatly with realization, reflecting the large variation in ground motion intensity across the realizations. The maximum average damage is 3.41, which is greater than severe damage and near complete damage while the minimum is 0.63, near the None Damage State. The median average damage state is 1.94 indicating near moderate damage would be expected for an older reinforced concrete bridge at

the Reference Point location assuming all realizations of the Cascadia Subduction Zone Earthquake are equally likely.

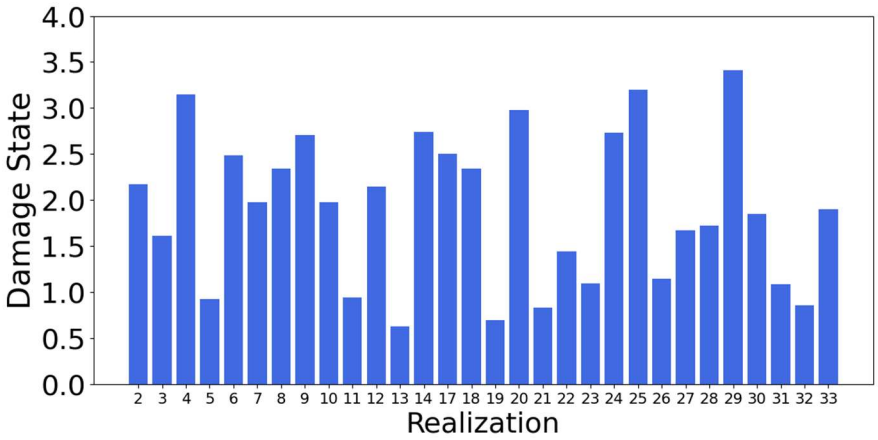

Figure 5.2 Average of the Probability of Each Damage State (Denoted Average Damage State) at Each Realization for HWB17 at the Reference Point

Table 5.5 Statistics on Average Damage State Across All 30 Realizations

Statistical Measure	Value
Maximum	3.41
Minimum	0.63
Range	2.78
Median	1.94
Mean	1.91
Standard Deviation	0.80
Variance	0.65

5.2.2 Effect of Ground Motion Intensity

Table 5.6 summarizes ground motion intensity with four different intensity measures for the 30 realizations at the Reference Point with 50th percentile Site Class C2 soil amplification. Specifically, the 14th, median, and 86th percentile values across the 30 realizations for PGA, S_a(0.3 sec), S_a(1.0 sec), and S_a(2.0 sec) intensity measures are shown. This table can be

compared with Table 3.1, the similar table for the baseline ground motions in Chapter 2, to see how ground motion intensity and variability have changed with consideration of median Site Class C2 soil amplification. This section explores how this impacts the predicted bridge damage at the Reference Point.

Table 5.6 Intensity Measure Variation at the Reference Point with C2 – 50% Amplification Factors

Percentile	**PGA** (g)	**S_a (0.3)** (g)	**S_a (1.0)** (g)	**S_a (2.0)** (g)
14th	0.340	0.958	0.259	0.087
50th	0.526	1.542	0.433	0.194
86th	0.770	2.086	0.637	0.325

To examine the effect of ground motion intensity on the damage estimate, specific realizations were chosen that most closely approximate the 14th, 50th, and 86th percentile intensity measure values from Table 5.6. Those realizations are shown in Table 5.7. Because the HAZUS fragility curves use $S_a(1.0)$ as its intensity measure, the values from those realizations that correspond to the 14th, 50th and 86th percentile (csz005, csz007, csz014) will be used when applying the HAZUS fragility curve. Later in this chapter, other fragility curves will be used that use different intensity measures, the corresponding realization at the 50th percentile will be used in those cases.

Table 5.7 Ground Motion Realizations Corresponding to a Certain Intensity Measure Percentile at the Reference Point

Percentile	**Realizations**			
	PGA	$S_a(0.3)$	$S_a(1.0)$	$S_a(2.0)$
14th	Csz005	Csz008	Csz005	Csz032
50th	Csz007	Csz004	Csz007	Csz020
86th	Csz009	Csz017	Csz014	Csz007

Table 5.8 lists the probability at each damage state given the 14th, 50th, and 86th percentile realizations. The most likely damage states are None, Slight, and Complete for the 14th, 50th, and 86th percentile, respectively. Even though Slight is the most likely damage state at the 50th percentile, Extensive is also almost equally probable, unlike at the 14th and 86th percentiles, there is not a clear front-runner.

Table 5.8 Likelihood of Each Damage State at Specified Percentile Intensity Measure for $S_a(1.0)$ for HWB17

Percentile	None	Slight	Moderate	Extensive	Complete
14	47.6%	28.1%	11.1%	10.0%	3.2%
50	17.2%	25.3%	16.6%	24.2%	16.7%
86	5.9%	15.2%	14.0%	28.7%	36.2%

By visualizing the probabilities on a bar chart, as seen in Figure 5.2, expected trends can be clearly seen such as the probabilities at the 50th percentile is consistently around 20%. At the 14th percentile, the probabilities go from highest to lowest across the damage states from None to Complete. Whereas the opposite occurs at the 86th percentile, the probabilities go from low to high across the damage states None to Complete. This data provides confidence in the analyses computed at the regional scale in the next chapter.

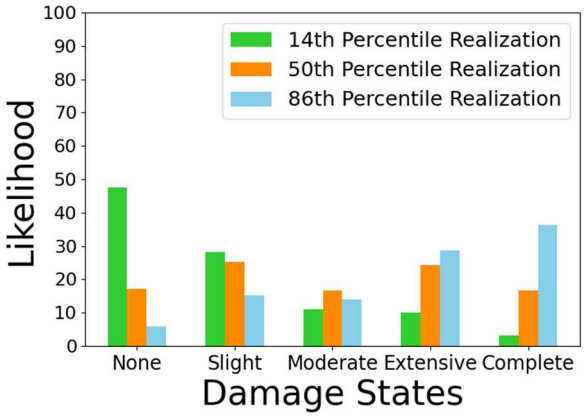

Figure 5.2 Likelihood of Each Damage State at Specified $S_a(1.0)$ Percentile for $S_a(1.0)$ for HWB17 at the Reference Point

5.3 STUDY 2: OLDER SIMPLY SUPPORTED CONCRETE BRIDGE TYPE WITH VARYING SITE CLASS AMPLIFICATION

For this case study the impact of soil amplification will be on bridge damage prediction will be studied by varying the site class-based amplifications derived in Chapter 3, while the bridge type/fragility curve and ground motion used will be kept the same. Again, the bridge will be an older simply supported concrete bridge classified as HWB17 with the associated fragility curves from HAZUS and the same modification factors applied to the medians of the curves for each damage state as described in Section 5.2 above. The ground motion intensity measure values will be from Realization Csz007, since that is the realization nearest to the median value of $S_a(1.0)$ across all realizations at the Reference Point which is the intensity measure the HAZUS fragility curves use (Table 5.7). The site classes that will be considered are the sub-site classes C2 and D1 described in Chapter 3. Within each of those site classes the 14^{th}, 50^{th}, and 86^{th} percentile amplification factors will be examined.

Table 5.9 shows the probability of each damage state for HWB17 at the Reference Point for Realization Csz007 considering variable soil amplification represented using Site Classes C2 and D1. Figure 5.4 shows those same values represented in a bar graph along with the probability of each damage state for the same ground motion without soil amplification. From the figure it can be seen that there is little difference in the probability of each damage state for varying soil amplification factor within the Site Class C2, as well as little difference between those damage state probabilities when compared with the results for the baseline ground motion. This is congruent with the fact that the baseline ground motions were generated with a minimum shear wave velocity of 600 m/s which lies close to the upper bound of Site Class C. The Site Class D1 results in Table 5.9 and Figure 5.4 show greater variability with soil amplification factor. Amplifying the ground motions by the 14th percentile Site Class D1 amplification factor yields damage state probabilities most akin to those for Site Class C2 and the baseline ground motion. However, when considering the 50th and 86th percentile amplification factors for Site Class D1 the probability of more severe damage state increases.

Table 5.9 Likelihood of Each Damage State with Variable Soil Amplification Factors Applied to the Median $S_a(1.0)$ Realization for HWB17 at the Reference Point

Site Class	Amplification Percentile	Damage State				
		None	Slight	Moderate	Extensive	Complete
C2	14	18.4%	25.9%	16.6%	23.6%	15.6%
	50	17.2%	25.3%	16.6%	24.2%	16.7%
	86	16.2%	24.8%	16.6%	24.7%	17.7%
D1	14	17.6%	25.5%	16.6%	24.0%	16.3%
	50	10.1%	20.1%	15.8%	27.8%	26.2%
	86	4.6%	13.1%	12.9%	28.5%	40.9%

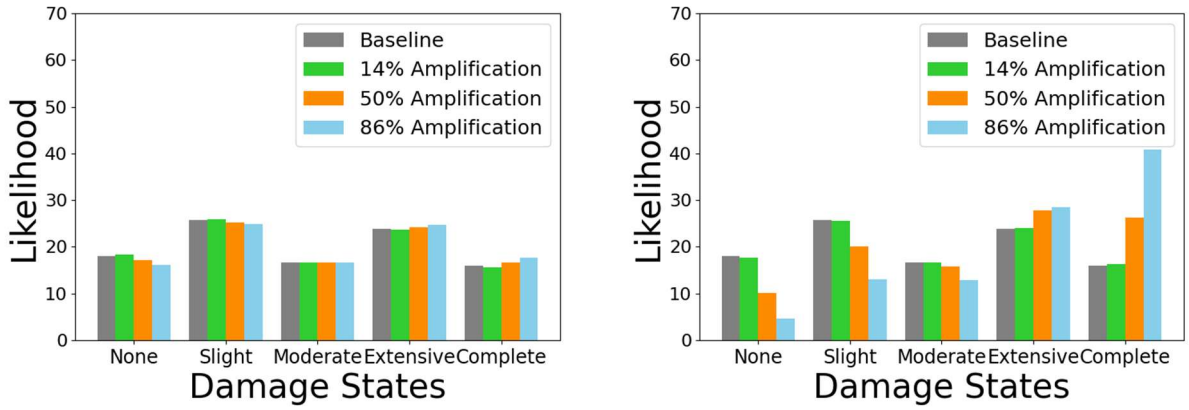

Figure 5.4 Likelihood of Each Damage State for Site Class (a) C2 and (b) D1 Considering Variable Amplification Compared Against the Baseline Ground Motions using the Median $S_a(1.0)$ at the Reference Point with HWB17

5.4 STUDY 3: VARYING FRAGILITY CURVES FOR OLDER SIMPLY SUPPORTED CONCRETE BRIDGES

For this case study, the soil amplification will be taken as the 50th percentile amplification for Site Class C2. As with the previous sections, the bridge will be an older simply supported reinforced concrete bridge. The different fragility curves from the sources described in Chapter 4 that can apply to this type of bridge are listed in Table 4.4 and will be tested one by one to examine the differences in predicted damage. Because not every fragility curve uses the same intensity measure as input, the same exact spectral acceleration value will not be applied to every fragility curve. Instead for each fragility curve, the realization with the median intensity measure at the Reference Point that is needed for input for the fragility curve will be used, where the specific realizations were presented in Table 5.6. For example, for the Nisqually curves Realization Csz004 is used because that is the realization with the median value of spectral acceleration for $S_a(0.3)$ at the Reference Point, which is the input intensity measure for those fragility curves.

Table 5.10 below gives the probability of each damage state using the different fragility functions, and Figure 5.5 represents that same information in a bar chart. From the figure it can be observed that the MSSS Slab and MSSS Concrete fragility curves yield the most similar results. This makes sense as they were both developed by the same research group and the differences between the bridge types is not substantial for seismic loading. It is not expected that a simply supported reinforced concrete slab bridge would behave differently from a simply supported reinforced concrete girder bridge. Both have Slight as the most likely damage state. HWB17 also has Slight as the most likely damage state, but otherwise produces results that are somewhat different from MSSS Slab or MSSS Concrete. The fragility curve that is most different from the others is the Nisqually 1941-1965 fragility curve which has None as its most likely damage state. This makes sense as the Nisqually 1941-1975 fragility curve is not specific to a particular bridge class, and is for the most part only different based on the year built.

Table 5.10 Likelihood of Each Damage State for Older Simply Supported Concrete Bridges for the Realizations with Median Intensity Measures with Site Class C2 50th Percentile Amplification Factors using Different Fragilities

Fragility Function	**Intensity Measure**	**None**	**Slight**	**Moderate**	**Extensive**	**Complete**
HWB17	$S_a(1.0)$	17.2%	25.3%	16.6%	24.2%	16.7%
Nisqually 1941-1975	$S_a(0.3)$	42.7%	29.0%	12.3%	11.9%	4.2%
MSSS Slab	PGA	7.0%	40.6%	29.1%	18.7%	4.6%
MSSS Concrete	PGA	6.2%	46.7%	21.4%	13.8%	11.9%

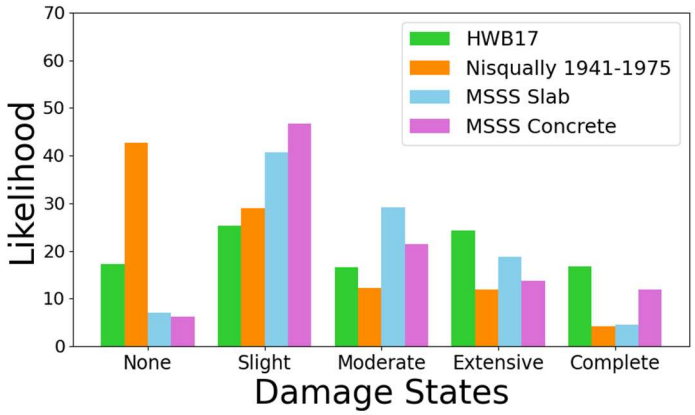

Figure 5.5 Likelihood of Each Damage State for Older Simply Supported Concrete Bridges for the Realizations with Median Intensity Measures with Site Class C2 50th Percentiles Amplification Factors using Different Fragilities

The average damage state for each set of fragility curves is shown in Figure 6.6. It is seen that the average damage state for HWB17, MSSS Slab and MSSS Concrete are very similar, with the Nisqually 1941-1975 again being the outlier. Note that the closer the average damage state is to the most likely damage state, the higher the probability of that damage state is in Figure 5.5. Whereas, a larger discrepancy between the average damage state and the most likely damage state indicates that there are other damage states with significant probability of occurring.

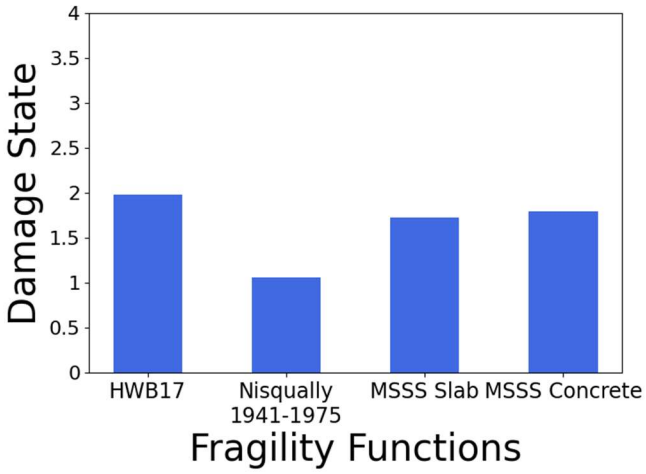

Figure 5.6 Average Damage State for Each Fragility Function for the Older Simply Supported Concrete Bridge Category with the Median Intensity Measure Realizations and Site Class C2 50th Percentile Amplification

5.5 STUDY 4: VARYING FRAGILITY CURVES FOR OLDER CONTINUOUS CONCRETE BRIDGES

The same procedure used in the previous section will be repeated except the fragility curves will come from Table 4.5 for older continuous concrete bridges. Table 5.11 shows the probability of each damage state given a certain fragility curve (HWB22 from HAZUS, Nisqually 1941-1975 from Ranf et al. (2005), MSC Concrete from Nielson and DesRoches (2007), and Concrete-No Shear Keys from Andres Sanchez using Liu et al 2022 data) and Figure 5.7 visually represents this information. Interestingly, HWB22 from HAZUS and the Nisqually 1941-1975 fragility curves produce the most similar results for this set of fragility curves. However, it is likely coincidental as the Nisqually 1941-1975 is not specific to bridge type but instead generally captures the lack of seismic design considerations in such older bridges. The fragilities HWB22, Nisqually 1941-1975, and Concrete – No Shear Keys all produce None as the most likely damage state, and MSC Concrete produces Slight as its most likely fragility curve.

Overall compared to the previous bridge category of older simply supported concrete bridges and its fragility curves, older continuous concrete bridges perform better with less expected damage given a magnitude 9 earthquake. This is consistent for all sources of fragility curve data.

The average of the probability of each damage state for each fragility function is provided in Figure 5.8. The average damage state for HWB22 is much lower than that of HWB17, indicating that a continuous bridge is better equipped for earthquake loading than a simply supported bridge. There was little no change in the average damage state for the Nisqually 1941-1975 curve because essentially the same curve was used. Only slight differences in the ratios between the medians of the damage states exist due to one being based off of the HWB17 median ratios and the other HWB22 median ratios. Surprisingly, the average damage state for MSC Concrete appears to be slightly higher than the MSSS Slab and MSSS Concrete average damage state. This contradicts the conclusion based off of the HAZUS curves that continuous bridges perform better in earthquakes.

Table 5.11 Likelihood of Each Damage State for Older Continuous Concrete Bridges for the Realizations with Median Intensity Measures with Site Class C2 50th Percentile Amplification Factors using Different Fragilities

Fragility Function	**Intensity Measure**	**None**	**Slight**	**Moderate**	**Extensive**	**Complete**
HWB22	$S_a(1.0)$	49.2%	42.2%	4.2%	3.1%	1.3%
Nisqually 1941-1975	$S_a(0.3)$	42.7%	32.0%	9.5%	9.4%	6.5%
MSC Concrete	PGA	3.3%	44.1%	20.2%	14.2%	18.1%
Concrete – No Shear Keys	$S_a(1.0)$	65.3%	31.4%	3.2%	0.1%	0.0%

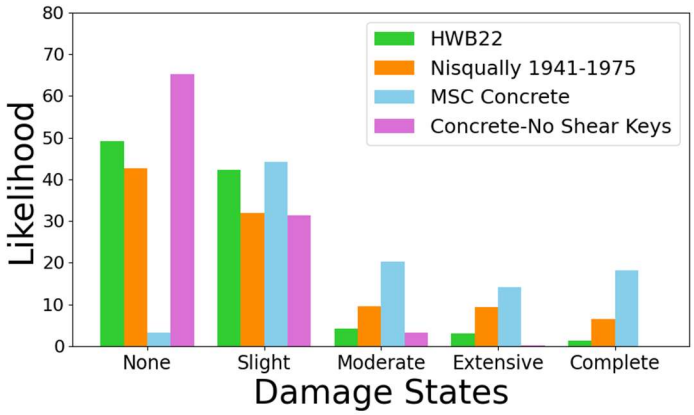

Figure 5.7 Likelihood of Each Damage State for Older Continuous Concrete Bridges for the Realizations with Median Intensity Measures with Site Class C2 50th Percentiles Amplification Factors using Different Fragilities

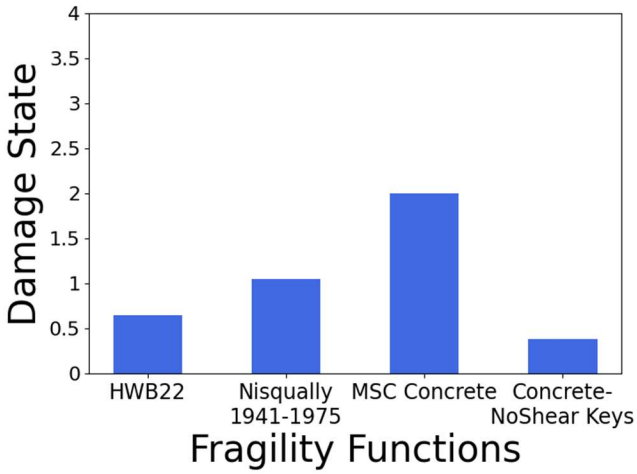

Figure 5.8 Average Damage State for Each Fragility Function for the Older Continuous Concrete Bridge Category with the Median Intensity Measure Realizations and Site Class C2 50th Percentile Amplification

5.6 STUDY 5: VARYING FRAGILITY CURVES FOR NEWER CONTINUOUS CONCRETE BRIDGES

Again, the process is continued, but for newer continuous concrete bridges. The table of probabilities and corresponding bar chart are shown below. It is worth noting that for the fragility

curve Concrete – Shear Keys, different dispersions are specified for each damage states. Depending on the applied spectral acceleration value, this might not always yield a positive probability since sometimes the probability of being in a damage state is the difference between the probability of that damage occurring and the probability of the less severe damage state occurring. Different dispersions can result in the fragility curves for two damage states crossing and make that difference negative. This was the case for the probability of damage state Slight for Concrete – Shear Keys, but since a negative probability cannot actually exist, it will be represented as 0.0%.

Overall, there is substantial variability between the fragility curves and their damage state probabilities, but general trends can be observed. Similar to the previous section, most of the fragility curves yield a most likely damage state of None, with the remaining curves producing a most likely damage state of Slight. In fact, the prediction of no damage is larger than that for older continuous concrete bridges. This is indicative that newer continuous concrete bridges are even better designed and equipped for seismic hazards than older continuous concrete bridges.

Table 5.12 Likelihood of Each Damage State for Newer Continuous Concrete Bridges for the Realizations with Median Intensity Measures with Site Class C2 50th Percentile Amplification Factors using Different Fragilities

Fragility Function	**Intensity Measure**	**None**	**Slight**	**Moderate**	**Extensive**	**Complete**
HWB23	$S_a(1.0)$	74.4%	18.2%	3.7%	2.7%	1.1%
Nisqually Post 1975	$S_a(0.3)$	51.5%	10.0%	12.1%	13.8%	12.6%
MSC Concrete – Shear Keys	PGA	7.3%	45.4%	21.5%	20.1%	5.7%
Concrete – Shear Keys	$S_a(1.0)$	98.1%	0.0%	2.1%	0.0%	0.0%
CSE	$S_a(1.0)$	11.3%	47.3%	35.5%	5.2%	0.7%

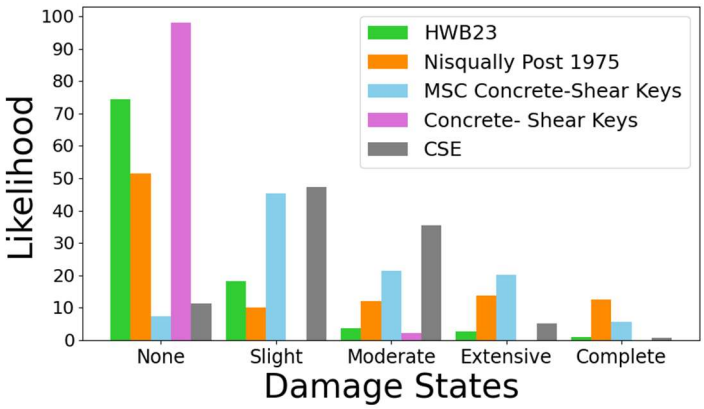

Figure 5.9 Likelihood of Each Damage State for Newer Continuous Concrete Bridges for the Realizations with Median Intensity Measures with Site Class C2 50th Percentiles Amplification Factors using Different Fragilities

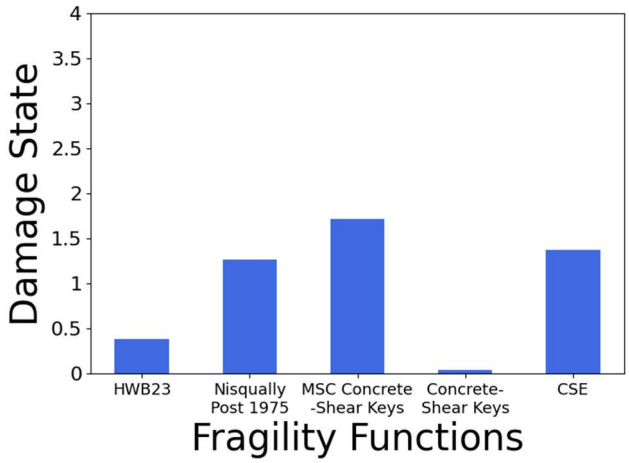

Figure 5.10 Average Damage State for Each Fragility Function for the Newer Continuous Concrete Bridge Category with the Median Intensity Measure Realizations and Site Class C2 50th Percentile Amplification

5.7 STUDY 6: VARYING FRAGILITY CURVES FOR MOVABLE BRIDGES

This section will explore damage predictions for movable bridges as there are several critical movable bridges in the communities in coastal Washington State. Because HAZUS has no specific fragility curve for a movable bridge it is lumped into a HWB classification that can

encompass vastly different bridges. Fragility curves were developed for movable bridges by Ranf et al. (2005) and are denoted here as Nisqually – Movable and were discussed in Chapter 4. Recall that the Nisqually – Movable fragility curves were developed by Ranf et al. only for the Slight Damage State and that the median values for the other damage states were approximated using the HWB28 fragility curves, where the ratio of the median for other damage states to Slight were calculated and used to scale the medians of the other damage states for Nisqually – Movable.

Table 5.13 and Figure 5.11 compare the predicted damage using the two fragility curves and as shown the results contrast one another. Even though the medians for the Nisqually – Movable fragility curves for damage states Moderate, Extensive and Complete are based off the proportions of the HAZUS curves, the initial median for Slight was developed specifically for a movable bridge. For a magnitude 9 earthquake, HWB28 predicts an 84% chance of no damage to a movable bridge. With the Nisqually – Movable fragility curve that possibility goes down to 5.5% of no damage and a 63.1% chance of complete and total damage of the bridge. This is more in line with what was observed during the 2001 Nisqually Earthquake, and for movable bridges HAZUS fragility curves should not be considered a reliable method of predicting damage in a movable bridge.

Table 5.13 Likelihood of Each Damage State for Movable Bridges for the Realizations with Median Intensity Measures with Site Class C2 50th Percentile Amplification Factors using Different Fragilities

Fragility Function	**Intensity Measure**	**None**	**Slight**	**Moderate**	**Extensive**	**Complete**
HWB28	$S_a(1.0)$	84.0%	7.4%	3.9%	3.5%	1.2%
Nisqually - Movable	$S_a(0.3)$	5.5%	5.5%	6.8%	19.1%	63.1%

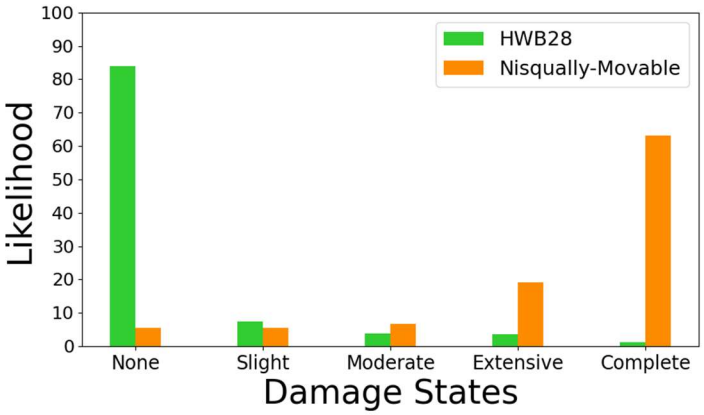

5.11 Likelihood of Each Damage State for Movable Bridges for the Realizations with Median Intensity Measures with Site Class C2 50th Percentiles Amplification Factors using Different Fragilities

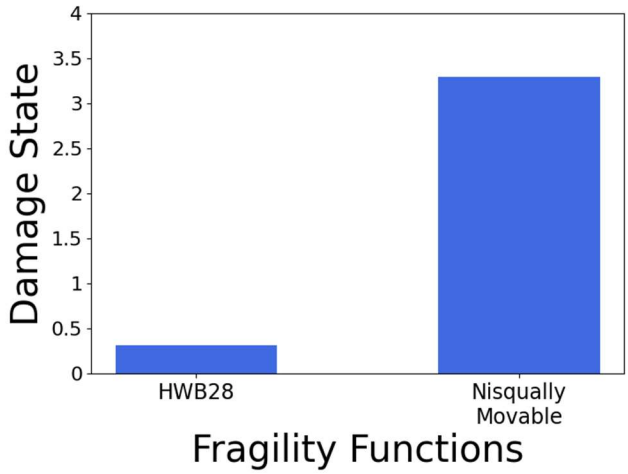

Figure 5.12 Average Damage State for Each Fragility Function for the Movable Bridge Category with the Median Intensity Measure Realizations and Site Class C2 50th Percentile Amplification

5.8 DISCUSSION ON VARYING BRIDGE TYPE

Figure 5.13 below shows the probability of various damage states for median intensity measure ground motions with Site Class C2 50th percentile amplification at the Reference Point for different bridge types with fragility data from each source discussed in Chapter 4 (e.g., HAZUS of Nisqually). For the HAZUS curves, the chances of no damage increase as the bridge

type changes from older simply supported bridges, older continuous bridges, to newer continuous bridges. This makes sense as each of the bridges are progressively designed for earthquake loading. First with the change from simply supported to a continuous bridge, then from an older design that possibly does not include shear keys to one that does.

The Nisqually derived functions follow similar trends to one another with the exception of the movable bridge. This is to be expected as a movable bridge is vastly different from a concrete simply supported or continuous bridge. The Nisqually Post 1975 fragility function is also expected to yield a higher probability of no damage because it assumes a more modern and resistant design. The Nisqually 1941-1975 fragility functions show a larger probability of damage relative to the Nisqually 1975 fragility functions at least at the Slight Damage State.

As for the curves that were derived from the bridges in the Central and Southern United States, they are all comparable, with some important trends observed. For example, the MSSS Concrete (Multi-span Simply Supported) bridge fragility has a slightly lower probability of being in the Complete Damage State than the MSC Concrete. This is surprising because the HAZUS curves indicate the lower probabilities of damage for the continuous bridge relative to the simply supported bridge as the continuous bridge eliminates several possible damage states (pounding at expansion joints and unseating for example). When shear keys are added the MSC Concrete bridge damage is reduced, especially for the Complete Damage State.

Not as much can be observed from the fragility functions derived from the Liu analyses of the WSDOT report (Lie et al. 2022), other than it makes sense that the Concrete-Shear Keys fragility curves would have a higher likelihood of no damage.

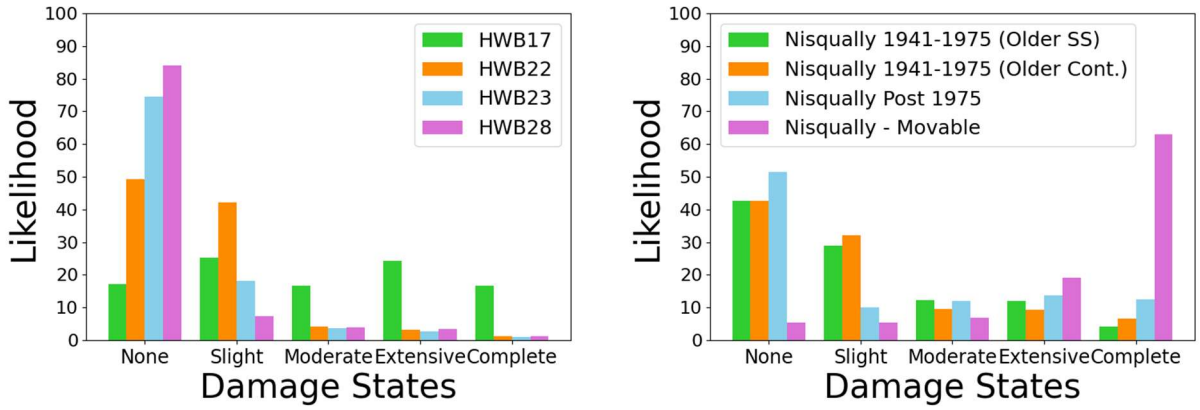

(a) HAZUS (FEMA 2024)

(b) Nisqually (Ranf et al. 2005)

(c) Central and Southern United States (Neilson and DesRoches 2007, Padgett and DesRoches 2009)

(d) Liu Analyses (Liu et al. 2022)

Figure 5.13 Comparison of the Probabilities of Each Damage State for Different Bridge Types Given Fragility Data Derived from Four Sources

Chapter 6. CASE STUDIES OF REGIONAL BRIDGE INVENTORY

In the previous chapter, the impacts of key modeling assumptions were evaluated for individual bridges. In this chapters, the impacts of the M9 CSZ ground motions were evaluated for all of the bridges listed in the NBI database for Gray's Harbor and Pacific counties in Washington State (Figure 6.1). To quantify the impacts of key assumptions, the evaluation was performed for 12 cases, consisting of all combinations of the following assumptions:

1. Two sets of ground motion realizations (all 30 motions or the five more intense motions)
2. Two types of site classes (C2 and D1)
3. Three sets of fragility curves (HAZUS, Nisqually and Combined)

This chapter provides an overview of the process by which the bridge inventory was analyzed, followed by the corresponding results for each of the cases.

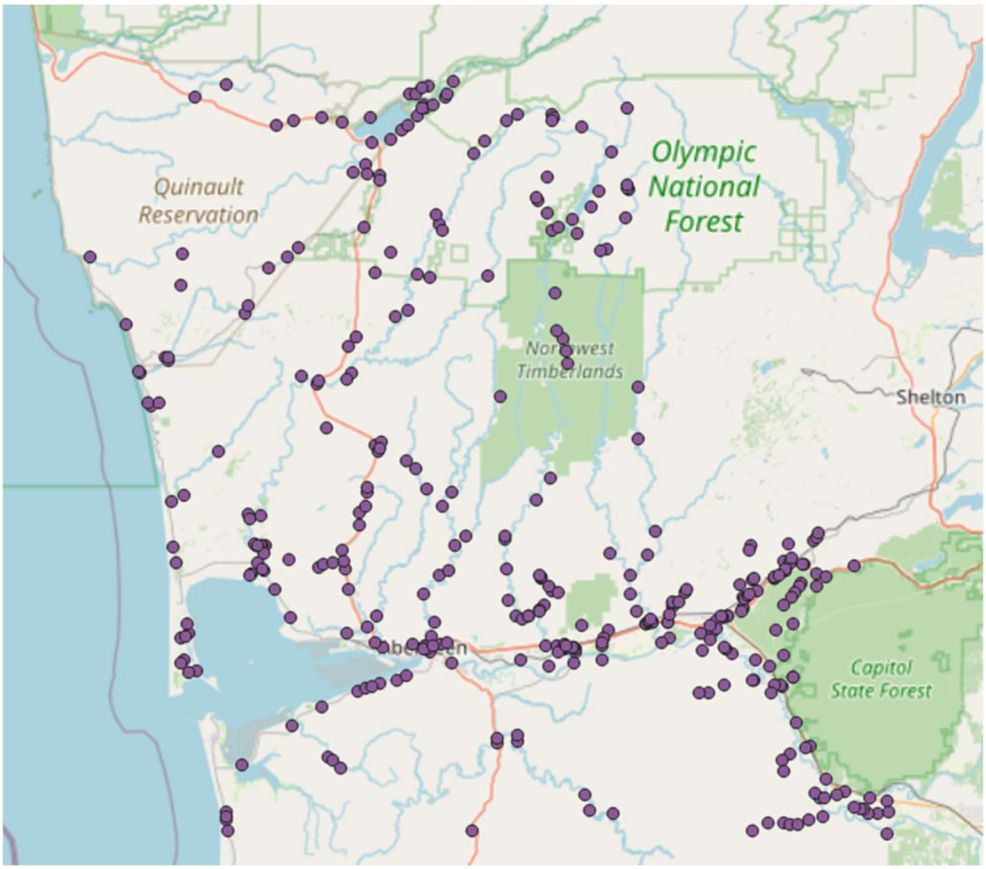

Figure 6.1 Locations of all Bridges in the NBI Database for Gray's Harbor and Pacific Counties

6.1 VARIATIONS IN GROUND MOTION INTENSITIES

To evaluate the impacts of variations in intensities among the 30 ground motion realizations, two options were considered: using all 30 realizations and using the top 5 realizations. The top five M9 most-intense realizations were selected based on the intensities of the ground motions at the Reference Point for the $S_a(1.0)$ intensity measure. This set of motions includes the realization corresponding to the 86^{th} percentile and above for that intensity measure. The five realizations specifically are: Csz014, Csz020, Csz004, Csz025, and Csz029. The two sets of ground motions can be summarized as:

- All Realizations

- Top 5 Realizations

6.2 APPLYING SITE AMPLIFICATION FACTORS TO GROUND MOTIONS

The two soil site classes chosen to illustrate the impacts of site conditions are Site Class C2 and Site Class D1. To account for the variability in site amplification, 30 sample amplification factors were generated by randomly sampling a lognormal distribution at each grid location and for each intensity measure. To create the sample distribution, the median was set to the value along the fitted line at the 50^{th} percentile for a given value of intensity identified in Chapter 3. The dispersion was calculated based off of the regressed Z factor lines for the 86^{th} and 14^{th} percentile values, also identified in Chapter 3.

Figure 6.2 shows examples of a distribution of 30 samples at the Reference Point for the amplification factor for PGA. For this figure, each distribution was generated for Realization Csz032; so, the variation among the six histograms is due to the random selection process. As shown in the figure, 30 samples provide only a crude approximation of a lognormal distribution; however, these histograms correspond to only one realization. When all 30 realizations are considered, and 30 samples are taken for each realization, a total of 900 values of the amplification factor are sampled for each intensity measure at a single grid point. In Figure 6.3, it can be seen that 900 samples provide a much better approximation for a lognormal distribution. Note that these histograms also reflect the variations in intensities among the motions, which increase the variability in amplification factor at that point.

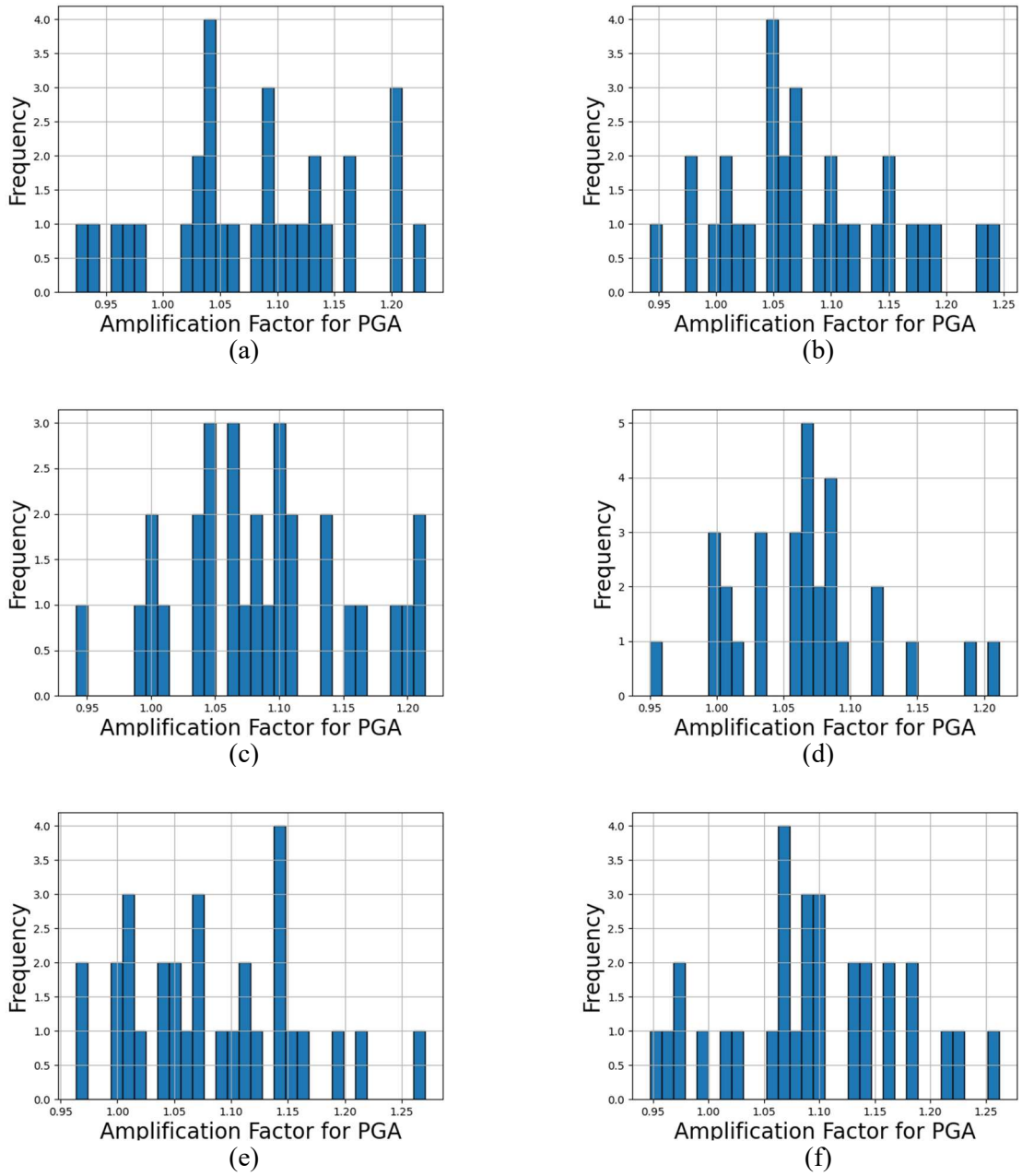

Figure 6.2 Examples of the Sampling Distribution of the Amplification for PGA for Site Class C2 for 30 Samples at the Reference Point. Histograms (a), (b), (c), (d), (e), and (f) Each Represent a Different Set of Sampling Points for Csz032

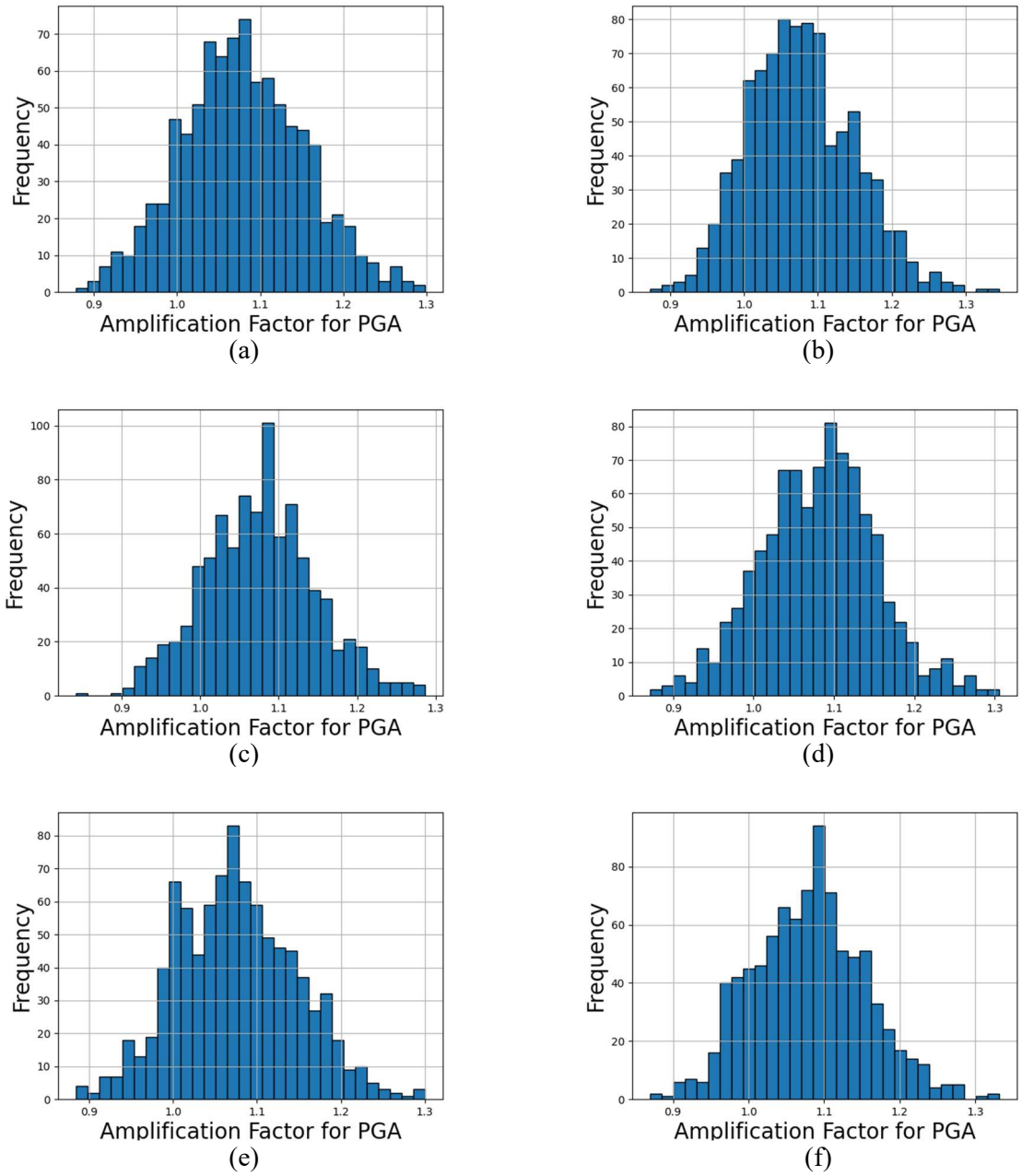

Figure 6.3 Examples of the Sampling Distribution of the Amplification for PGA for Site Class C2 for 900 Samples where 30 Samples were Taken for All 30 Realizations at the Reference Point. Histograms (a), (b), (c), (d), (e), and (f) Each Represent a Different Iteration

Note that, when only the top 5 realizations were considered in the analyses, there were only 150 samples at each grid point. Figure 6.4 shows the sampling distribution for 150 samples. While not as representative of the estimates based on 900 samples, there distributions were still

roughly similar. Likewise, there will be 150 values for each intensity measure at a single grid point.

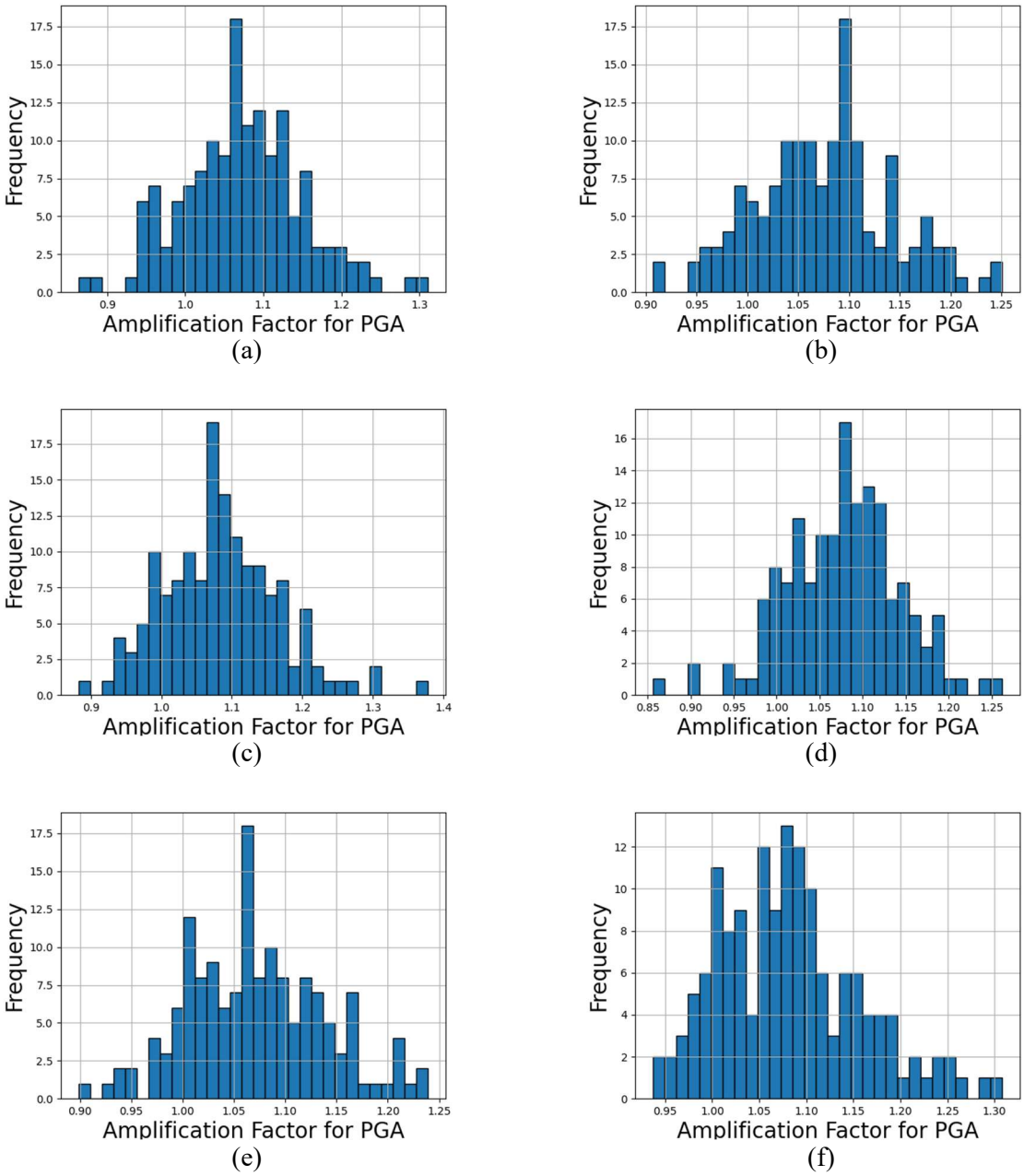

Figure 6.4 Examples of the Sampling Distribution of the Amplification for PGA for Site Class C2 for 150 Samples where 30 Samples were Taken for the Top Five Realizations at the Reference Point. Histograms (a), (b), (c), (d), (e), and (f) Each Represent a Different Iteration

6.3 GROUND MOTION INTENSITY AT A BRIDGE LOCATION

Once all the intensities of the surface ground motions (including site amplification) were generated at each grid point on Grid B, they were uploaded into R2D. As previously mentioned in Chapter 2, R2D uses the nearest neighbor event to connect the ground motions to a bridge since the grid points don't match up with locations of the bridges. R2D typically takes five samples from the four nearest gird points to the bridge. Again, the samples are proportionally to the distance the grid point is to the bridge to get a single value at a given intensity measure. So even though up to 900 samples may be provided, not all will be sampled during a single iteration of the nearest neighbor event. This is why when R2D runs its Damage and Loss Simulation, it will iterate through the nearest neighbor event for a large sample size, generating a unique ground motion value for each iteration. With a large enough sample size, it is likely that all 900 possible values for a given intensity measure will be sampled. The samples that R2D takes are random and are generated by a seed value. A different value of the seed was used for each of the 12 cases.

6.4 SAMPLE SIZE FOR DAMAGE SIMULATION

To determine the optimal sample size to use in the Damage Simulation, five test options were considered: 250, 500, 1000, and 2000 samples. These options were evaluated for a bridge located at longitude and latitude coordinates -123.39533, 47.00283, which is approximately 42.3 km east of the Reference Point. Bridge 101 was chosen because it was built 1964, NBI bridge class 502, and therefore classifies as HWB17 in HAZUS. For each of the five options a different random seed was used for the nearest neighbor event. After iterating through the nearest

neighbor event and the Damage Simulation for the total amount of the sample size, a single value for a damage state is calculated.

- 0 corresponds to None,
- 1 to Slight,
- 2 to Moderate,
- 3 to Extensive, and
- 4 to Complete.

The probability of reaching each damage state for a particular bridge was then calculated by adding up the number of times a damage state occurs and then dividing it by the total sample size. For example, if 0 (None) appears 100 times during the 500-sample test, the probability for the None damage state would be 20%. This process was repeated 5 times for each sample size.

The results across all five tests were compared and the median value of the five tests for each sample size is displayed in Table 6.1. There is little difference in the median values among the various sample sizes. The coefficients of variation for each set of five repetitions are plotted in Figure 6.5. From Figure 6.5, it appears that 1000 samples provided more stable results, with little to benefit from increasing the sample size to 2000. Besides having a tighter range of values, for Complete and Moderate damage states, 1000 samples provide the lowest coefficient of variation.

Table 6.1 Median Probability of Each Damage State for Each Sample Size

Damage State	250 Samples	500 Samples	1000 Samples	2000 Samples
None	0.536	0.542	0.524	0.531
Slight	0.260	0.266	0.269	0.267
Moderate	0.100	0.090	0.098	0.100
Extensive	0.080	0.080	0.087	0.085
Complete	0.024	0.022	0.025	0.026

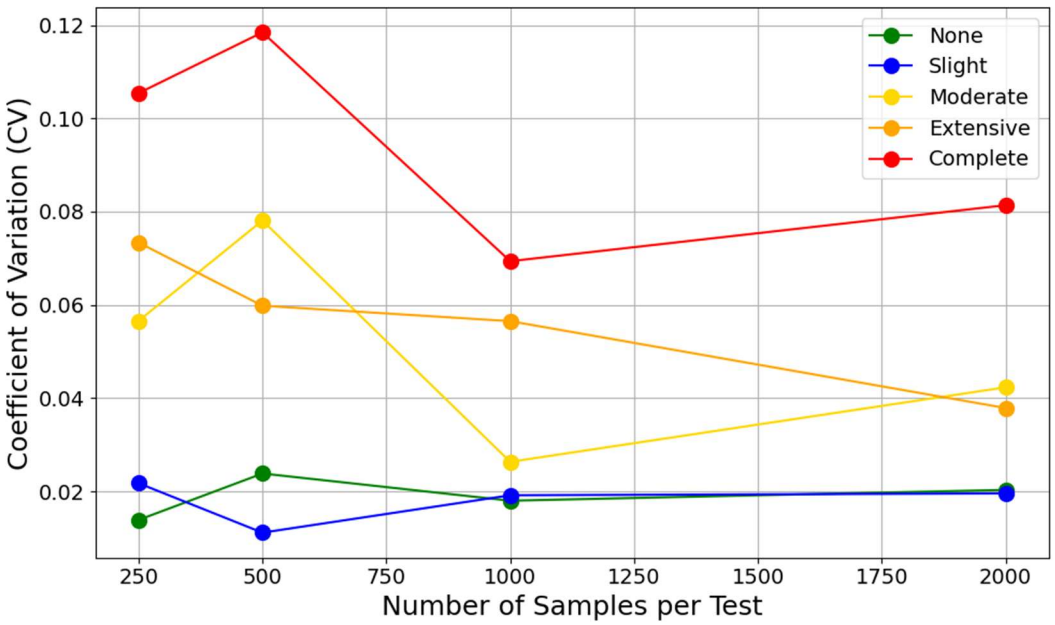

Figure 6.5 Coefficient of Variation VS Number of Samples for Each Damage State) with HWB17 Using the Median Spectral Acceleration at 1.0 sec for a Given Sample Size

6.5 SETS OF BRIDGE FRAGILITY RELATIONSHIPS

Three sets of fragility relationships were considered in the 12 case studies. The first set of fragility curves that were used are the HAZUS (FEMA 2024) fragility curves.

HAZUS specified a total of 28 base fragility curves for various types of bridges, and so the fragility curves used for this case will go beyond just the fragility curves specified in Chapter 4. These fragility curves are the default fragility curves that R2D uses. HAZUS can read the given parameters for each bridge in the inventory, and can apply the modification factors.

The second set of fragility curves were based on the Nisqually fragility curves (Ranf et al. 2005), because they can broadly be applied to all bridge types, and they are based on actual observations of bridge damage. As previously mentioned, these curves provide separate fragility relationships for movable and truss bridges, while all other bridge types are sorted by year built. The medians for damage states Moderate – Complete were based off of the proportions in HAZUS also previously discussed. Table D.1 in Appendix D provides the full list of medians and dispersions for the Nisqually fragility relationships.

The third set of fragility curves considered were a combination of the curves provided by Nielson and DesRoches (2007), Padgett and DesRoches (2009), and the Nisqually curves (Ranf et al. 2005). The Nisqually relationships were used only to describe the fragilities of bridges not specified by Nielson and DesRoches or Padgett and DesRoches. The cases involving the fragility curves developed in the Central and Southern part of the United States will expand beyond the bridge types specified in Chapter 5 and include all bridge types and their corresponding fragility curves outlined in Nielson and DesRoches, and Padgett and DesRoches. Nine bridge types in total are identified in Nielson and DesRoches and they are as follows:

- multi-span simply supported concrete slab (MSSS Slab),
- multi-span simply supported concrete girder (MSSS Concrete),
- multi-span continuous concrete girder (MSC Concrete),
- multi-span continuous concrete slab (MSC Slab),
- multi-span continuous steel beam (MSC Steel),
- multi-span simply supported concrete box girder (MSSS Box),
- multi-span simply supported steel beam (MSSS Steel),
- single span simply supported concrete girder (SSSS Steel) and

- single span simply supported steel beam (SSSS Steel).

Padgett and DesRoches expanded on four of these types of bridges and developed fragility curves for retrofitted bridges of these types including the addition of shear keys. The four types that have the addition of the shear keys are

- MSC Concrete,
- MSC Steel,
- MSSS Concrete, and
- MSSS Steel.

Bridges of these types built after 1990 will be considered to have the shear keys, and will be relabeled as MSC Concrete SK, MSC Steel SK, MSSS Concrete SK, and MSSS Steel SK. Table 6.2 shows the Central and Southern bridge types and their corresponding NBI bridge class used in this case study. NBI Bridge Type 02 – 06 are all considered girders of some type, because there was a specific bridge type for simply supported concrete box girder bridges, it is excluded from some of the generic concrete girder category. For a full list of the median of their fragility curves and their dispersion, see Tables D.2 and D.3 in Appendix D.

Table 6.2 Bridge Types in the Central and Southern United States and Their Corresponding NBI Bridge Class Categorized for this Case

Bridge Types	Single Span	Multi-Span Pre 1990	Multi-Span Post 1990
MSSS Slab		101, 501	101, 501
MSSS Concrete		102, 103, 104, 106, 502, 503, 504, 506	
MSC Concrete		202, 203, 204, 205, 206, 602, 603, 604, 605, 606	
MSC Slab		201, 601	201, 601
MSC Steel		402, 403, 404, 405, 406	
MSSS Box		105, 505	105, 505
MSSS Steel		302, 303, 304, 305, 306	
SSSS Steel	302, 303, 304, 305, 306		
SSSS Concrete	102, 103, 104, 106, 502, 503, 504, 506		
MSC Concrete SK			202, 203, 204, 205, 206, 602, 603, 604, 605, 606
MSC Steel SK			402, 403, 404, 405, 406
MSSS Concrete SK			102, 103, 104, 106, 502, 503, 504, 506
MSSS Steel SK			302, 303, 304, 305, 306

The three categories of fragility curves can be summarized as:

- HAZUS
- Nisqually
- Combined

6.6 MOST LIKELY DAMAGE STATE

For each of the twelve cases, the most likely damage state of each bridge was calculated. The most likely damage state means the damage state with the highest probability for a given bridge. Figure 6.6 shows the colors that correspond to each most-likely damage state.

Figure 6.6 Damage State Colors

Figures 6.7 to 6.9 show maps of the most likely damage state results for all 12 cases. Figure 6.7 shows the effects of ground motion selection (all vs 5) and site class (C2 vs D1) using the HAZUS fragility relationships. Figure 6.8 and 6.9 shows the same set of plots, but for the Nisqually and the Combined sets of fragility relationships.

- For all twelve cases there tended to be a higher level of damage in the southern part of the study region, mainly corresponding to Pacific County.
- The level of damage was consistently higher for Site Class D1 than Site Class C2.
- When just the top realizations were considered, the damage tended to increase compared to when all motions were used, but the effect was not uniform. As expected, the damage in the middle area of Gray's Harbor and Pacific counties increases. This is probably because the bridges within this region are located relatively near the Reference Point, where the top 5 motions were selected. However, the damage to the southern portion of the region did not increase consistently. These trends show some realizations are likely to produce the highest damage in a certain area, but those same realizations might not produce as much damage in other areas.

Across the different sets of fragility relationships, the Combined Fragility Curves show the most damage, then Nisqually, and then the HAZUS fragility curves with the least amount of damage overall based on the most likely damage state. However, each of the different fragility relationships used different intensity measures, $S_a(1.0)$ for HAZUS, $S_a(0.3)$ for Nisqually and for the fragilities that are derived from the Central and Southern part of the United States, PGA is used. This makes it hard to definitively compare the sets, due to this variable. This also can explain why the top 5 realization ground motions for either Site Class C2 or Site Class D1, don't make as big of an impact around the area where the Reference Point is. The top 5 realizations were based off of the spectral acceleration at 1.0 second. A realization that may be in the top percentile for one intensity measure may not be for another intensity measure.

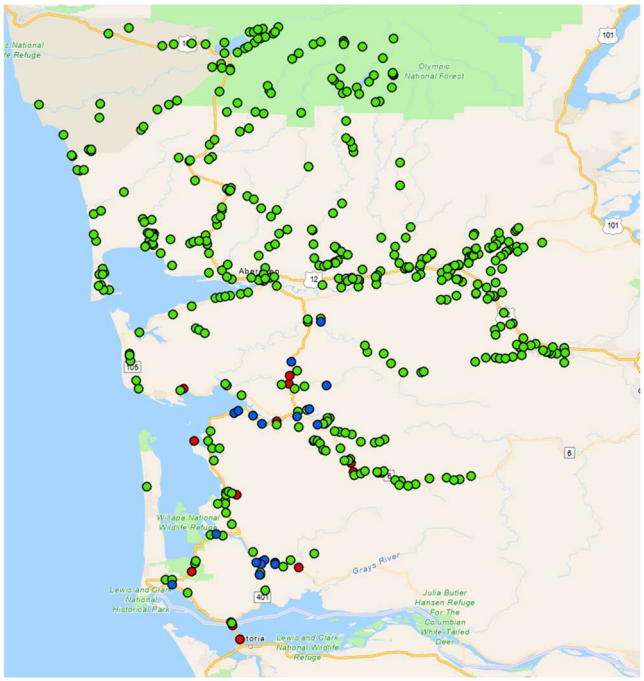

(a) All Realizations – Site Class C2

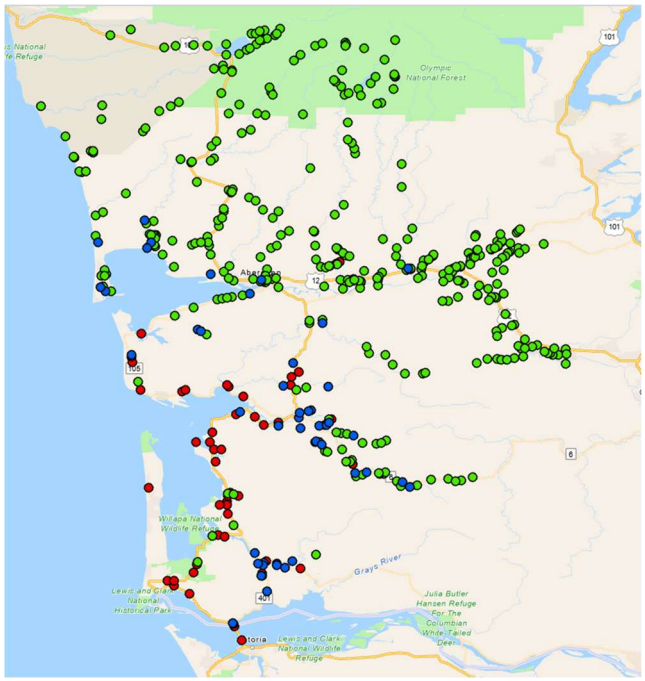

(b) All Realizations – Site Class D1

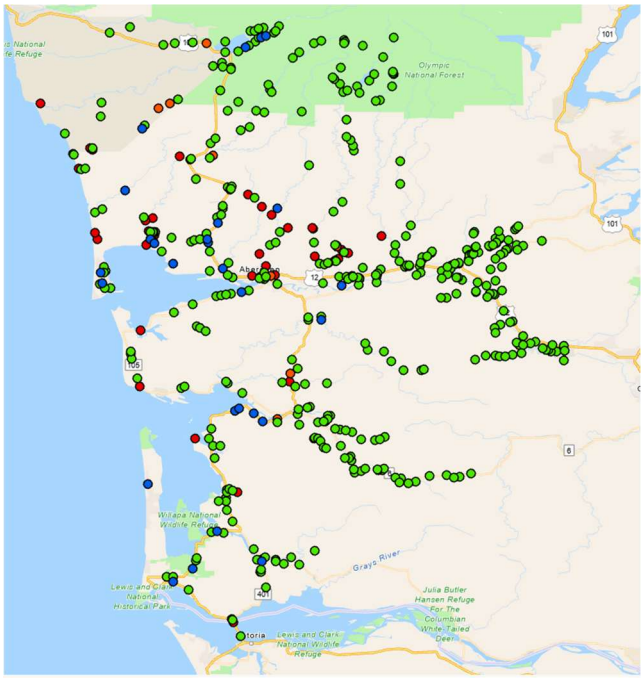

(c) Top 5 Realizations – Site Class C2

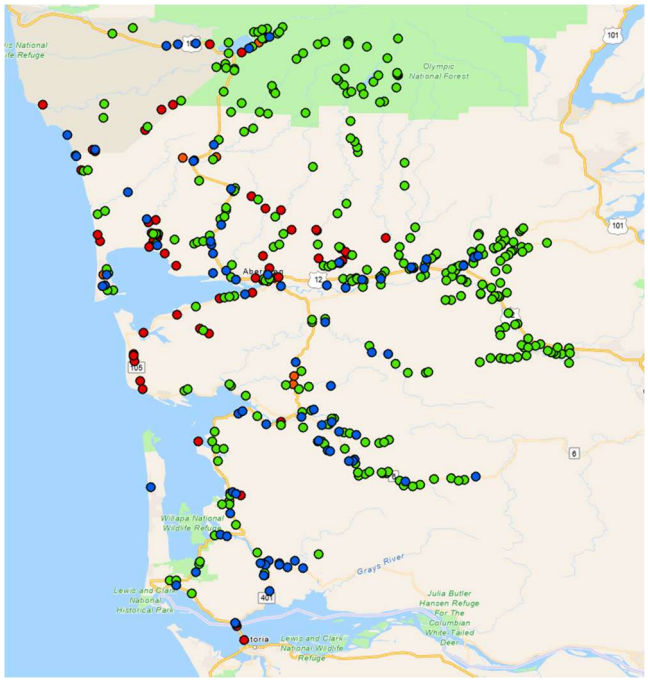

(d) Top 5 Realizations – Site Class D1

Figure 6.7 Most Likely Damage States for Bridges in Gray's Harbor and Pacific Counties using HAZUS Fragility Curves

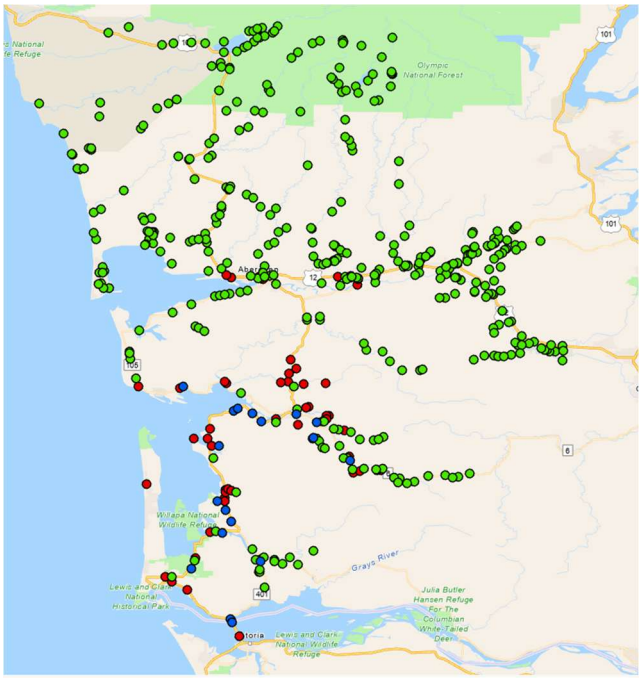

(a) All Realizations – Site Class C2

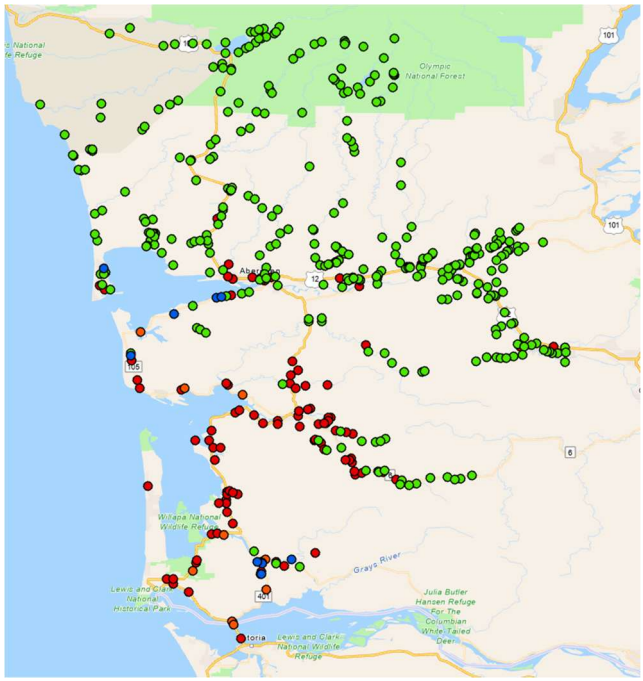

(b) All Realizations – Site Class D1

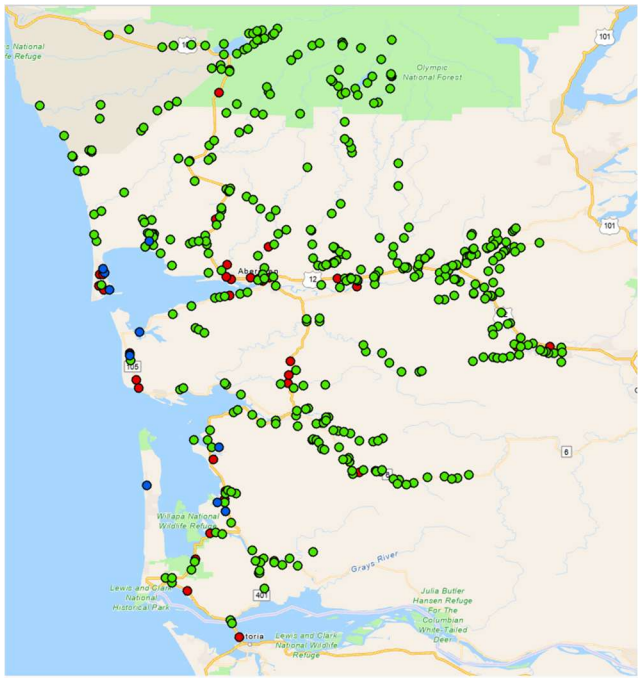

(c) Top 5 Realizations – Site Class C2

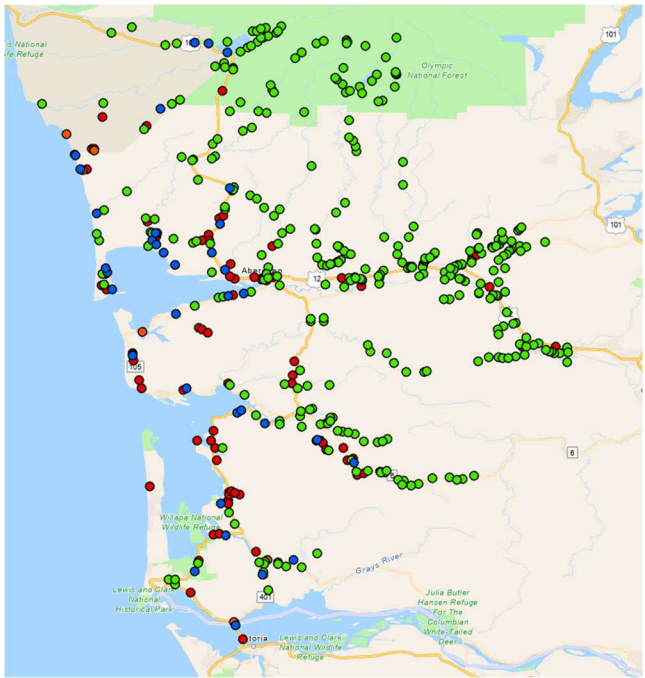

(d) Top 5 Realizations – Site Class D1

Figure 6.8 Most Likely Damage States for Bridges in Gray's Harbor and Pacific Counties using Nisqually Fragility Curves

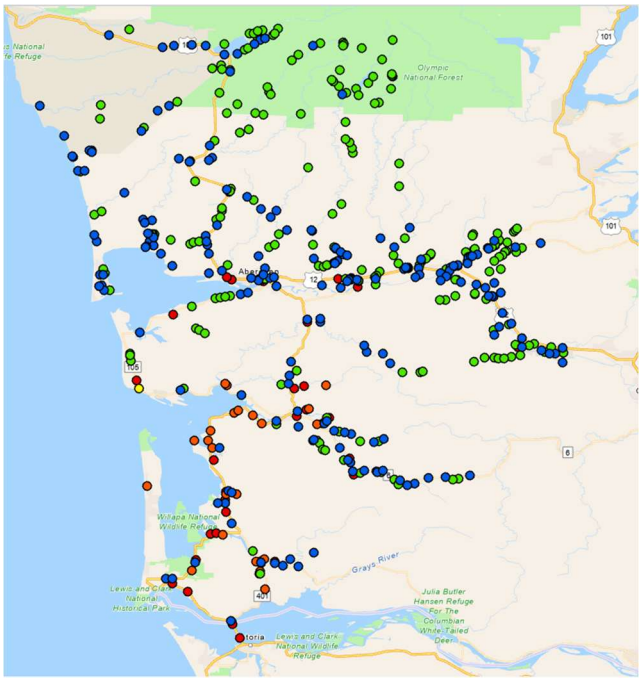

(a) All Realizations – Site Class C2

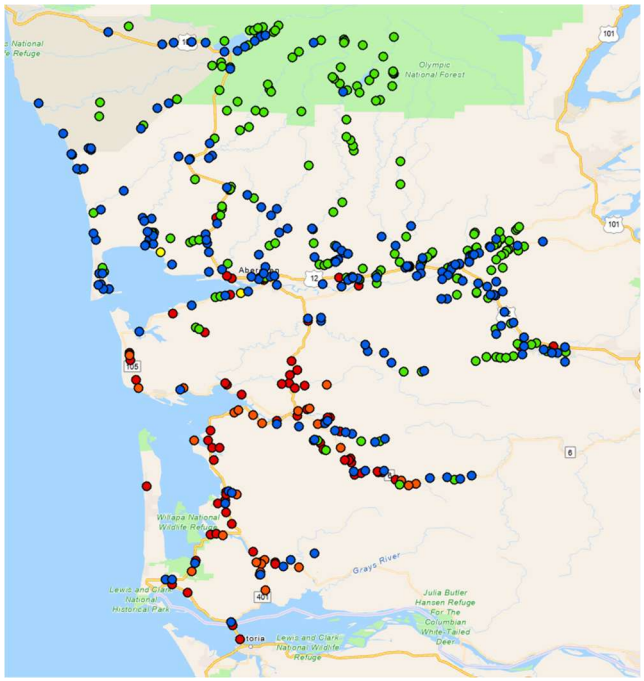

(b) All Realizations – Site Class D1

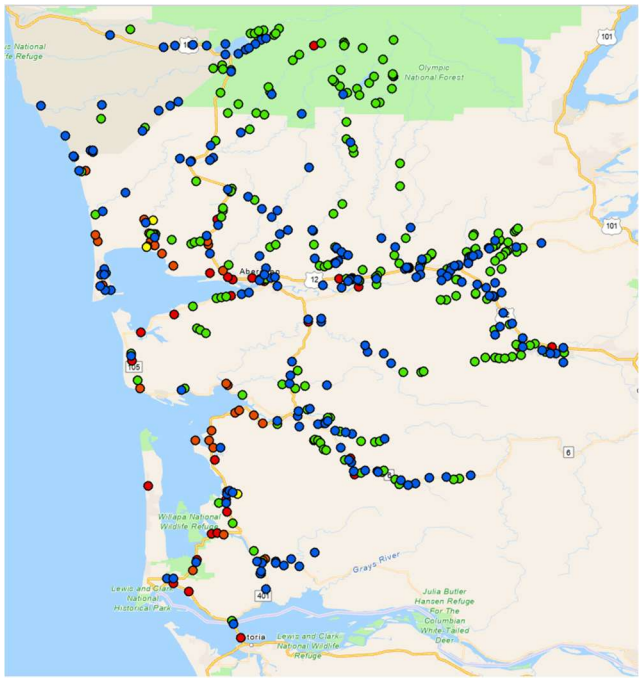

(c) Top 5 Realizations – Site Class C2

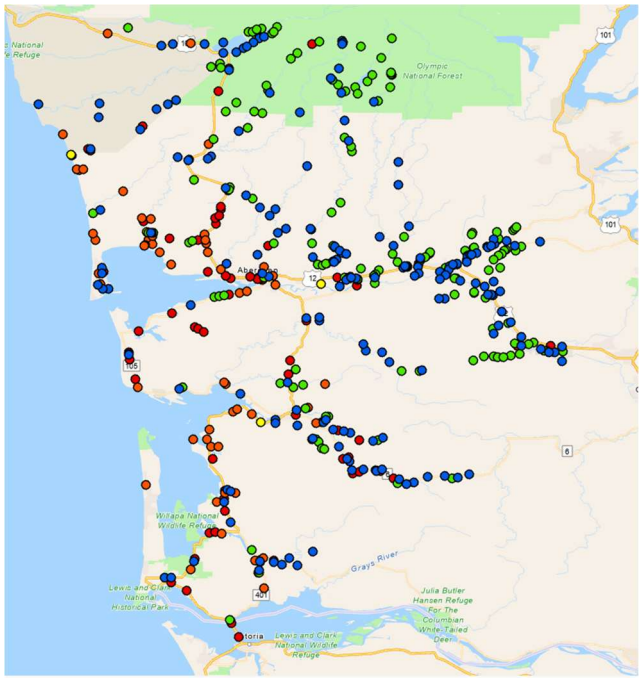

(d) Top 5 Realizations – Site Class D1

Figure 6.9 Most Likely Damage States for Bridges in Gray's Harbor and Pacific Counties using Combined Fragility Curves

6.7 AVERAGE DAMAGE STATE

Showing the most likely damage state is not always the most useful way to express the level of damage the bridges might experience. The probability of the damage state for some bridges may barely be in favor of None, so that is the damage state that is shown and represented, but it hides the fact that there is still significant probability of other damage states. For instance, in theory, a bridge could have a probability of 25% for None and a probability of 20% for Complete, so no damage is displayed even though a collapse probability of 30% would still be important.

To better represent the damage state of a bridge, the average damage state was calculated for each bridge as well. The average is calculated by multiplying the numerical representation of the damage states, 0-4, by their corresponding probability of occurrence and adding them together. This the average is unlikely to be an integer. Table 6.3 shows the range of values for the average that correspond to each damage state.

Table 6.3 Range of Average Values that Correspond to a Damage State

Damage State	**Range of Average Values**
None	0.0 – 0.5
Slight	0.5 – 1.5
Moderate	1.5 – 2.5
Extensive	2.5 – 3.5
Complete	3.5 – 4.0

Figures 6.10 through 6.12 show the average damage state for all bridges in Gray's Harbor and Pacific counties. The same color scheme that was used in the previous most-likely damage state figures are used in the figures of average. Comparing figures 6.10 – 6.12 to 6.7 – 6.9, it can

be seen that the average shows much more variation in damage state incorporating more of the damage states in the middle. Similar trends were observed in these distributions. For example, more damage occurred in the southern area for ground motions with all realizations, and more damage occurred around the Reference Point for ground motions with the top 5 realizations. Similarly, the Combined fragility curves showing the most damage, and the HAZUS fragility curves showing the least amount of damage.

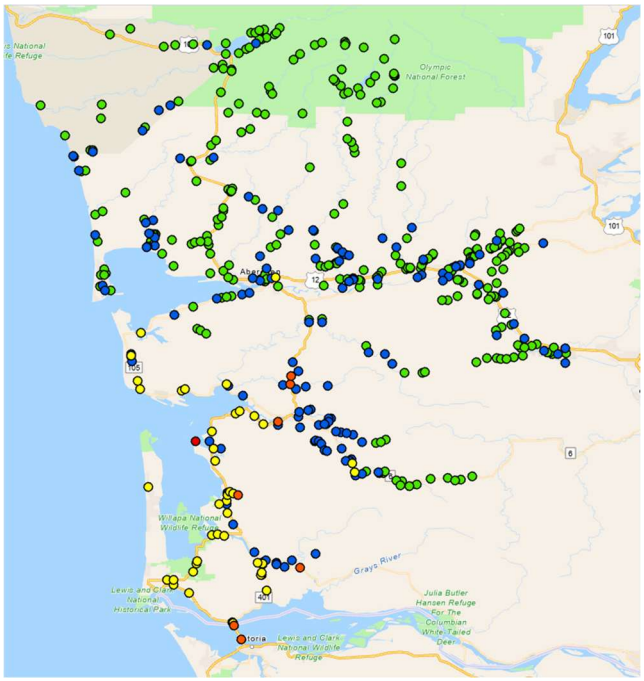

(a) All Realizations – Site Class C2

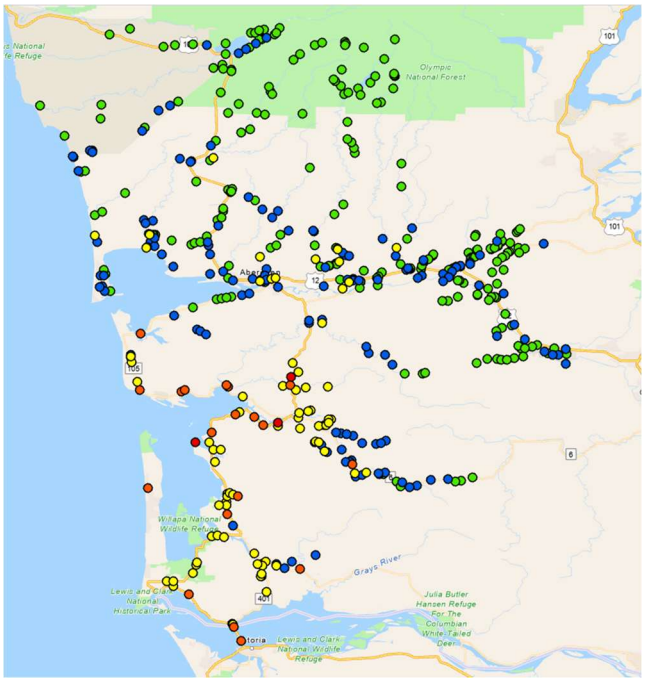

(b) All Realizations – Site Class D1

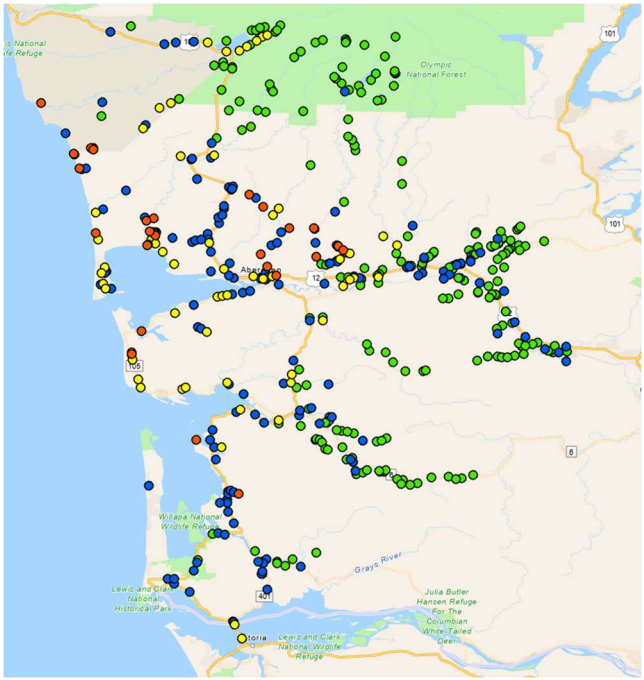

(c) Top 5 Realizations – Site Class C2

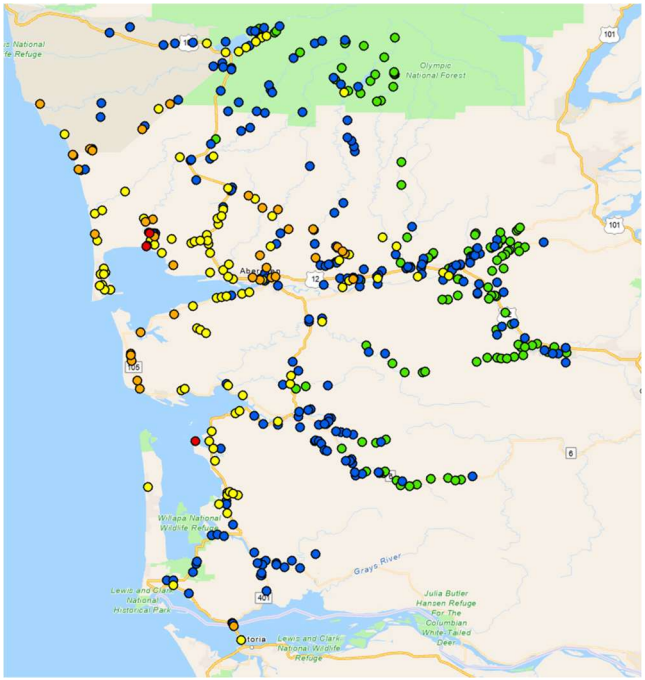

(d) Top Realizations – Site Class D1

Figure 6.10 Average Damage States for Bridges in Gray's Harbor and Pacific Counties using HAZUS Fragility Curves

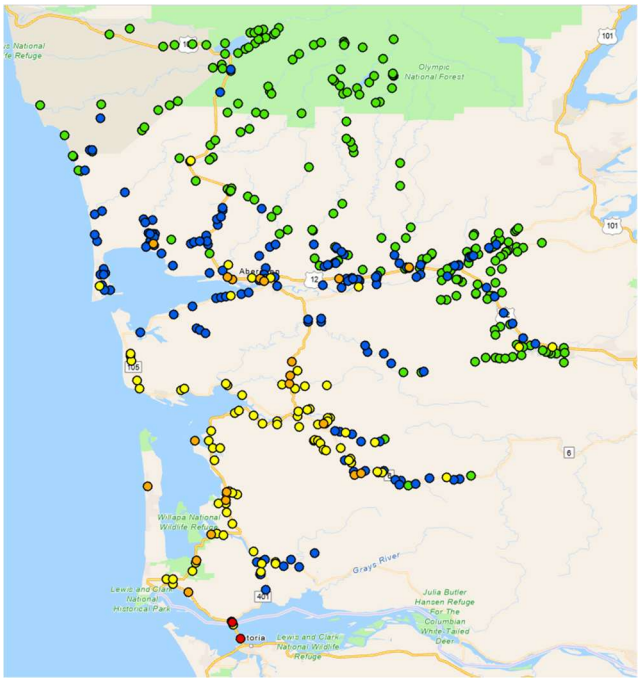

(a) All Realizations – Site Class C2

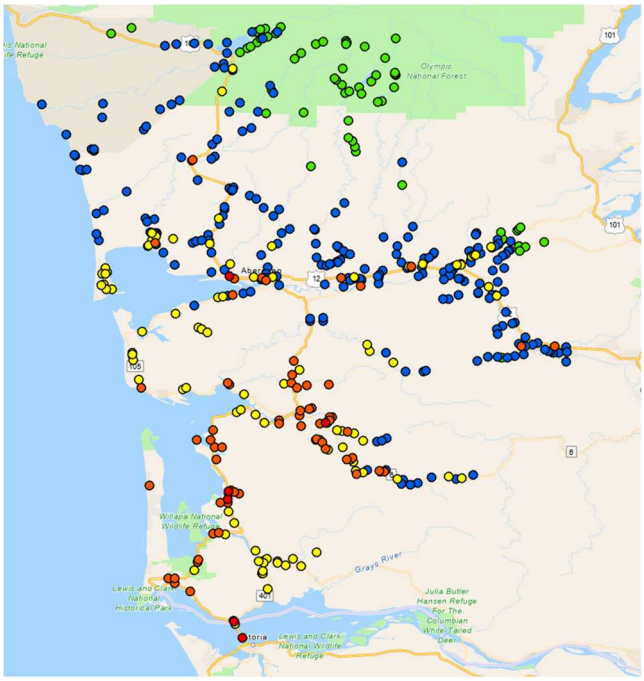

(b) All Realizations – Site Class D1

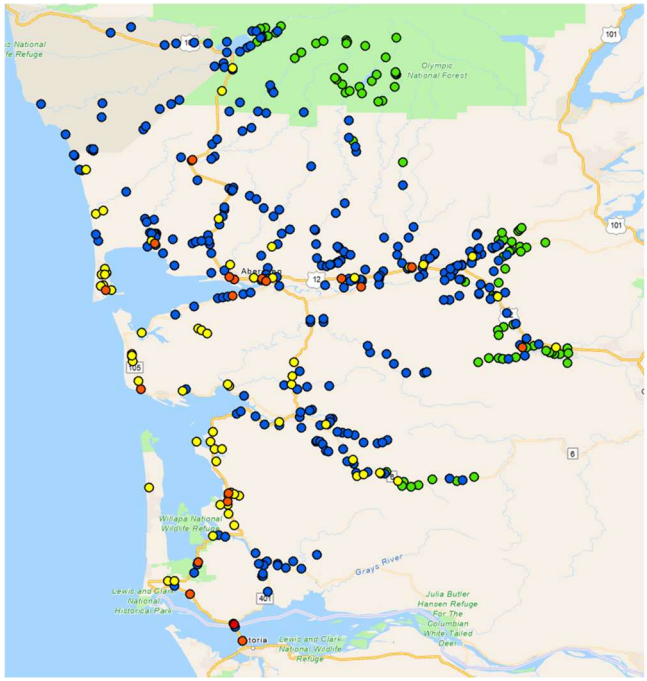

(c) Top 5 Realizations – Site Class C2

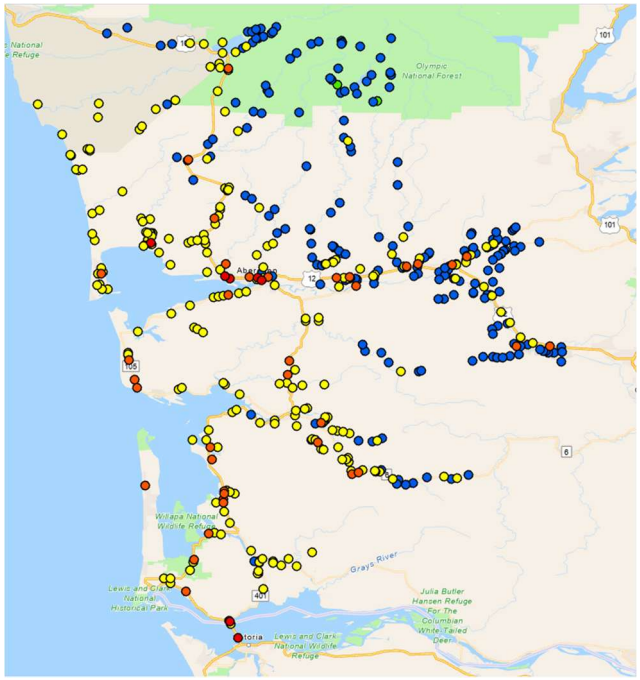

(d) Top Realizations – Site Class D1

Figure 6.11 Average Damage States for Bridges in Gray's Harbor and Pacific Counties using Nisqually Fragility Curves

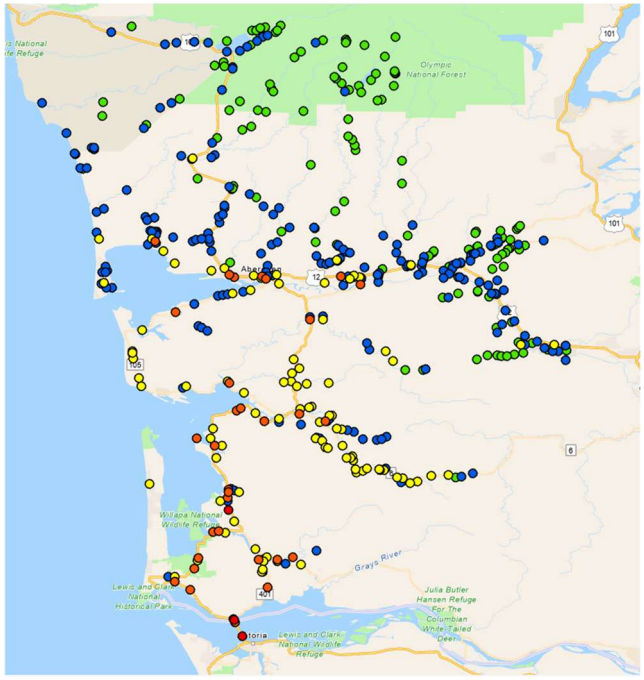

(a) All Realizations – Site Class C2

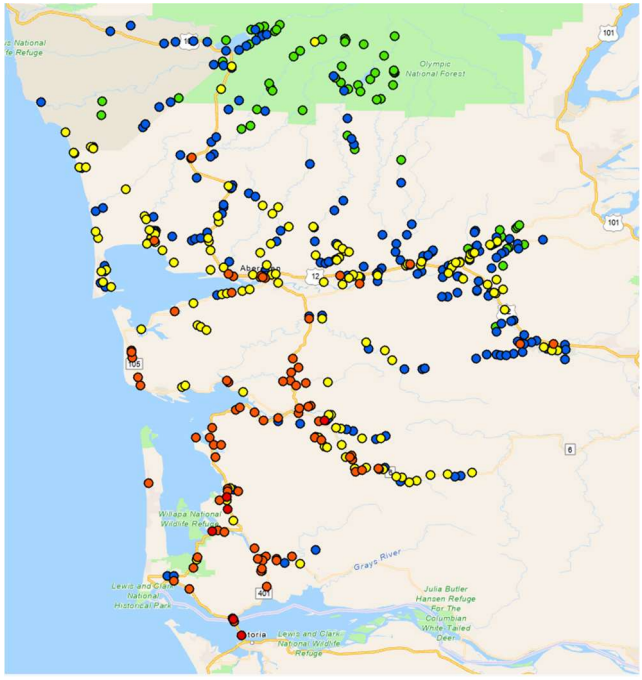

(b) All Realizations – Site Class D1

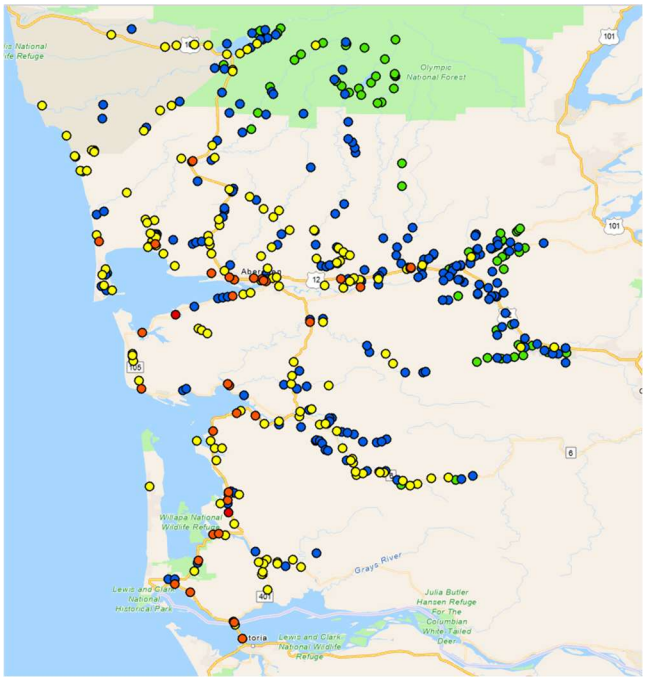

(c) Top 5 Realizations – Site Class C2

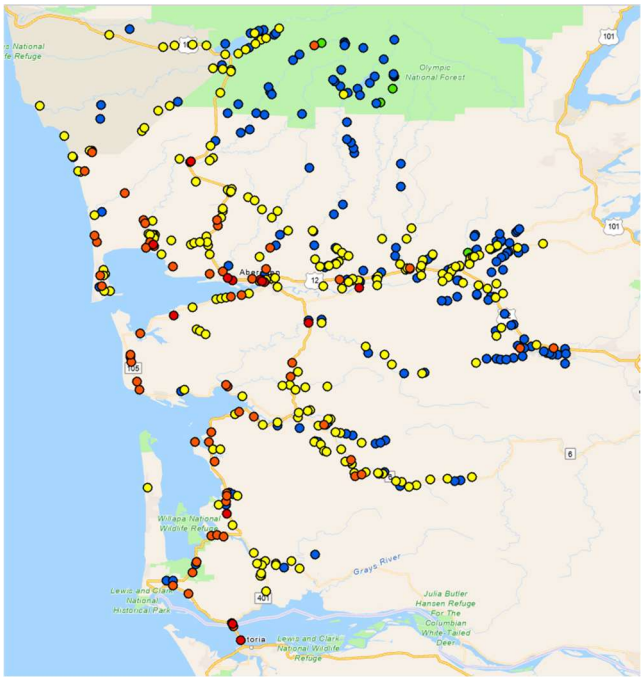

(d) Top Realizations – Site Class D1

Figure 6.12 Average Damage States for Bridges in Gray's Harbor and Pacific Counties using Combined Fragility Curves

The previous plots show the impacts of ground motion realization selection, site amplification and fragility curve selection on the distribution of expected bridge damage. Such plots are useful, but they do not show the relationships between bridge type and level of damage. To illustrate the impacts of bridge type, Figures 6.13 and 6.14 show the average damage state for a bridge separated into three categories, single span bridges, multi-span bridges built before 1990, and multi-span bridges built on or after 1990. Each category for each damage state is shown as a percentage of total bridges in each category. The amount in each category was previously identified in Chapter 4 as 206, 244, and 33 for single span, multi-span bridges built before 1990, and multi-span bridges built on or after 1990, respectively.

Figure 6.13 shows that for all realizations, the average damage state for most single span bridges fall within having a damage state of None. For the top 5 realization (Figure 6.14), most single span bridges fell within the range of Slight. For multi-span bridges there was not a stark of a contrast between the bridges built before 1990 and the bridges built on or after 1990. Because bridges built after 1990 are assumed to perform better seismically, the post 1990 bridges should have a higher amount of the average in the None or Slight Damage State. The pre 1990 bridges should have a higher percentage for the Extensive and Complete Damage State compared to post 1990 bridges, but this not always the case that is observed.

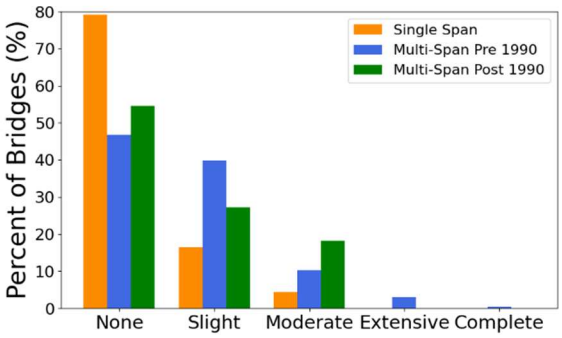

(a) HAZUS – Site Class C2

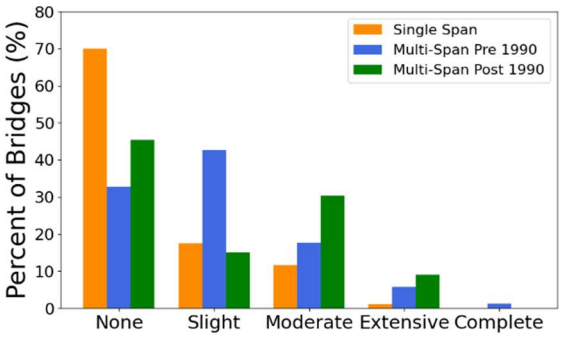

(b) HAZUS – Site Class D1

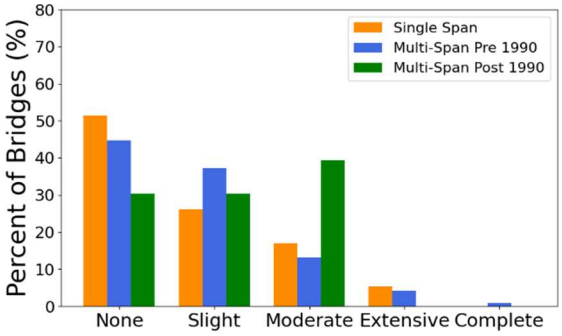

(c) Nisqually – Site Class C2

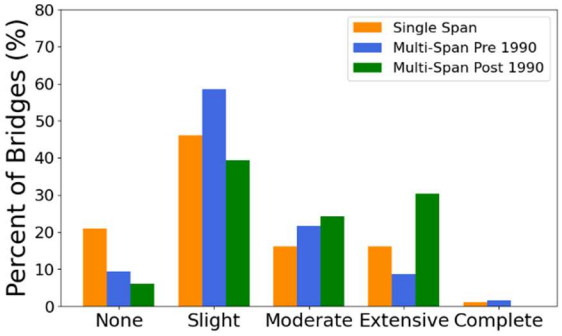

(d) Nisqually – Site Class D1

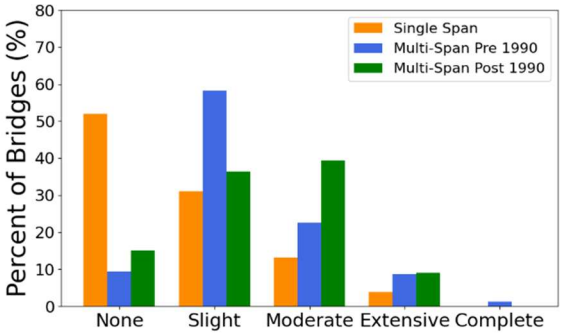

(e) Combined – Site Class C2

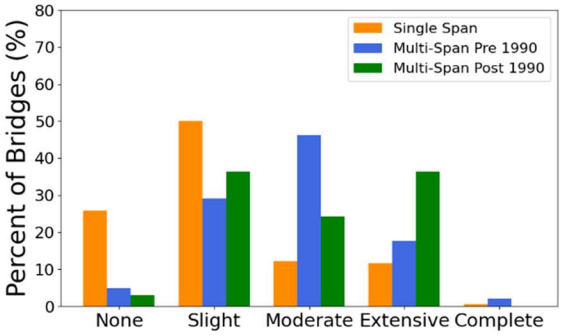

(f) Combined – Site Class D1

Figure 6.13 The Average of All Bridges in Gray's Harbor and Pacific Counties Separated by Category Given All Realizations. The Percent of Bridges is the Percent of Total Bridges in Each Category

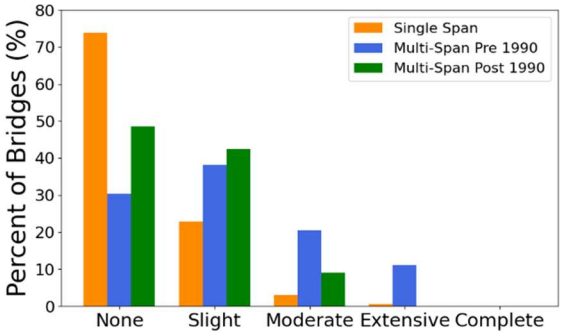

(a) HAZUS – Site Class C2

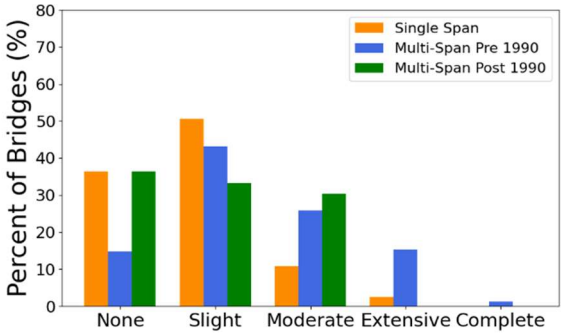

(b) HAZUS – Site Class D1

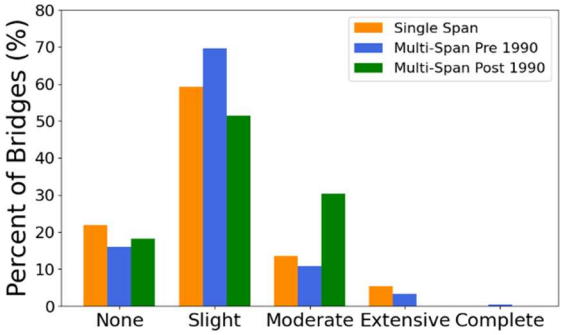

(c) Nisqually – Site Class C2

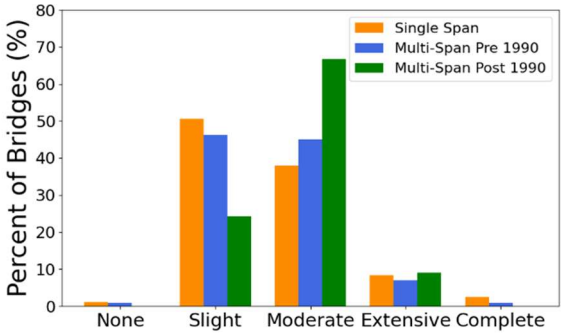

(d) Nisqually – Site Class D1

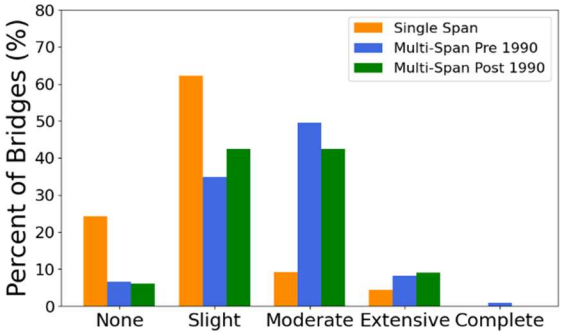

(e) Combined – Site Class C2

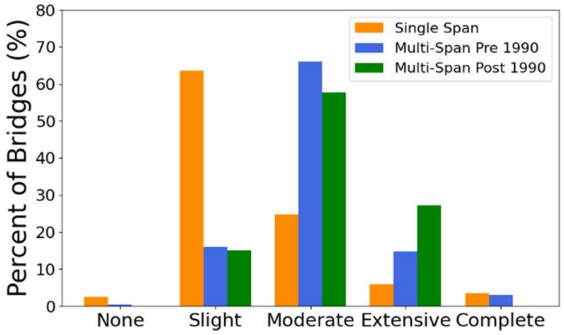

(f) Combined – Site Class D1

Figure 6.14 The Average of All Bridges in Gray's Harbor and Pacific Counties Separated by Category Given the Top 5 Realizations. The Percent of Bridges is the Percent of Total Bridges in Each Category

To summarize the results for each bridge type, the mean of the average damage state was taken for each of the 3 categories. Figure 6.15 displays the values for the mean for each of the 12 cases.

- Site Class D1 had more damage for all combinations of realization selection and bridge fragility curves.
- For eleven of the twelve sets of bars in Figure 6.15 (three bars per set). HAZUS predicted the least amount of damage.
- For multi-span bridges, the Combined fragility set predicted the most damage.
- For single span bridges the Nisqually fragility curves predicted the most damage, on average. This result is likely attributed to the fact that the Nisqually earthquake fragility curves do not have a separate category for single-span bridges.
- The single span group as a whole has a lower mean average than the multi-span bridges, as would be expected.
- The mean average for pre-1990 multi-span bridges as a whole is lower than the mean average for post 1990 multi-span bridges. These results are consistent with previous discussion in this chapter, but it was unexpected.

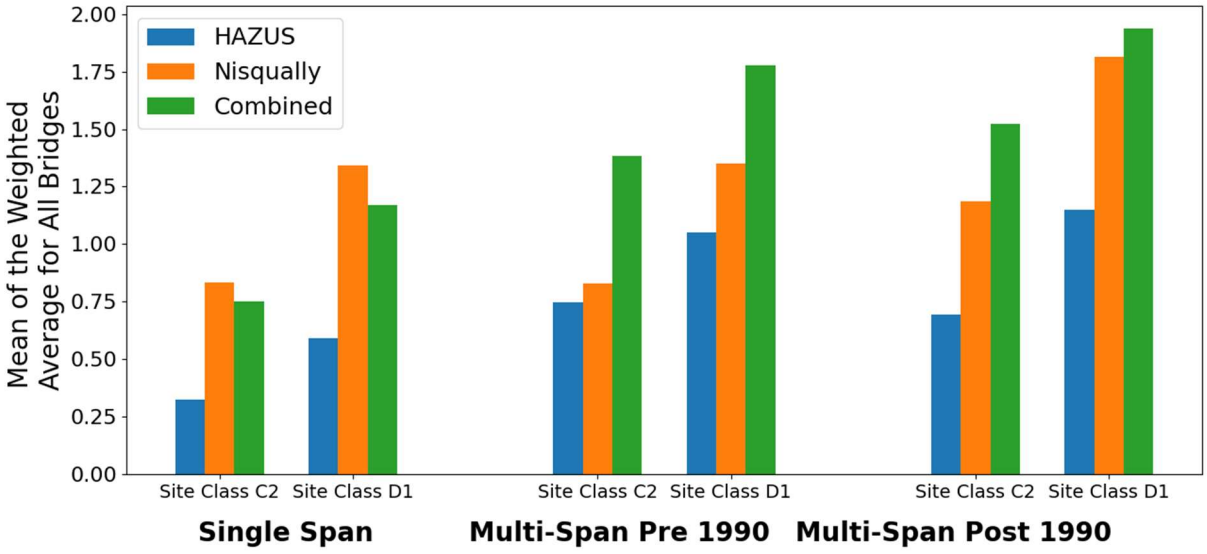

(a) All Realizations

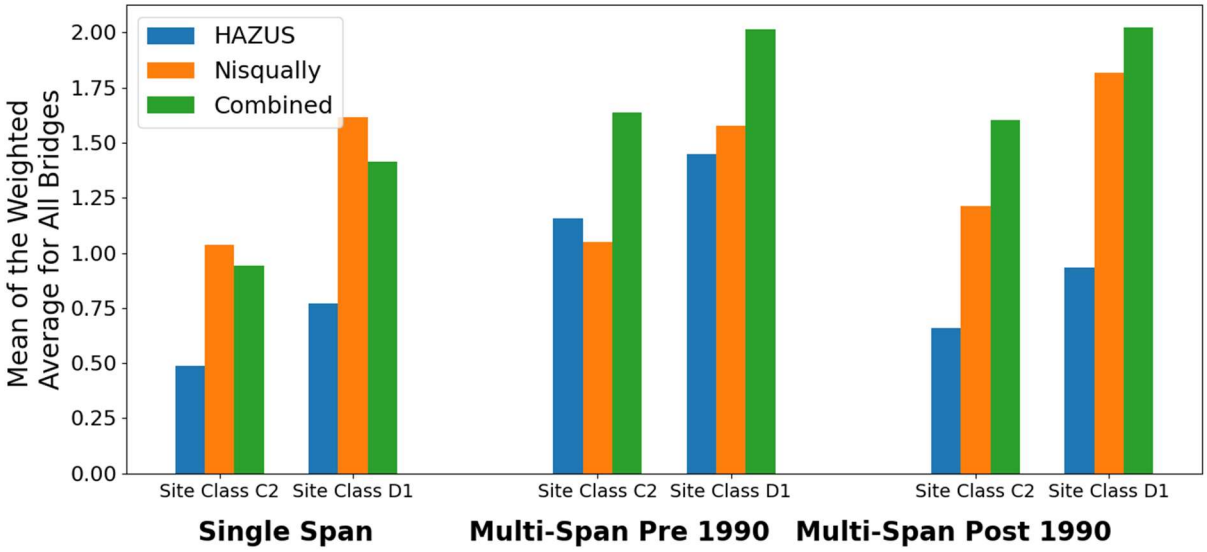

(b) Top 5 Realizations

Figure 6.15 Mean of the Average of All Bridges Combined in Each Category

6.8 LIKELIHOOD OF SOME DAMAGE

Another way of describing the damage of bridges is the likelihood of achieving a level of damage or more. For example, the likelihood of any or some damage occurring can be calculated by combining all of the probabilities above None for a single bridge.

Figures 6.16 and 6.17 are set up in a similar format to Figures 6.13 and 6.14. However, the horizontal axis represents ranges of percentages and the vertical axis represents the percentage of bridges whose probability of some damage occurring falls in those ranges. For the Combined fragility curves at all ground motion variations, around 80% of multi-span bridges have a likelihood of some damage in the 60-100% range meaning the vast majority of bridges with those fragility curves experience some damage. Interestingly, for single span bridges the likelihood of some damage doesn't vary as much across the different fragility sets. Another trend that can be observed it that the site class amplification D1 does slightly increase the probability of some damage overall.

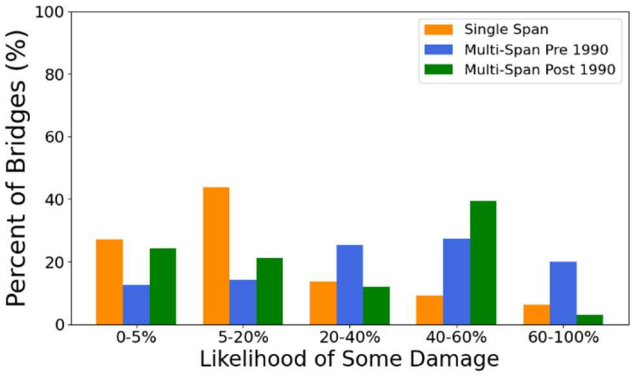

(a) HAZUS – Site Class C2

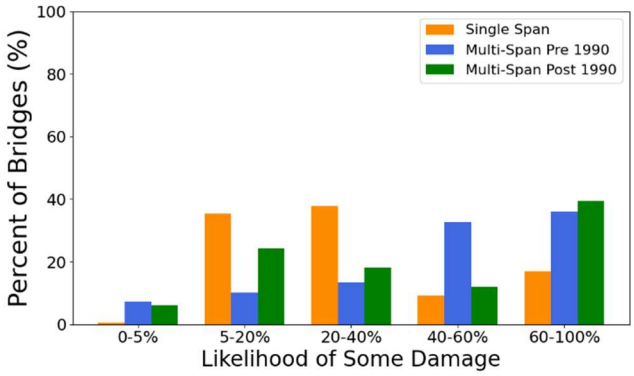

(b) HAZUS – Site Class D1

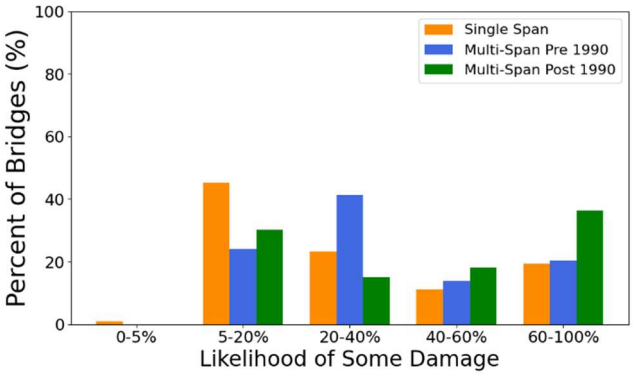

(c) Nisqually – Site Class C2

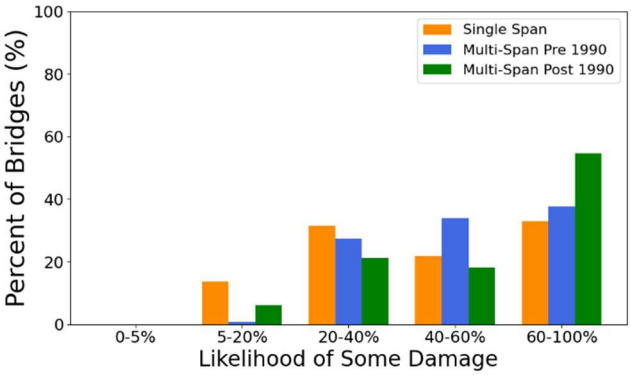

(d) Nisqually – Site Class D1

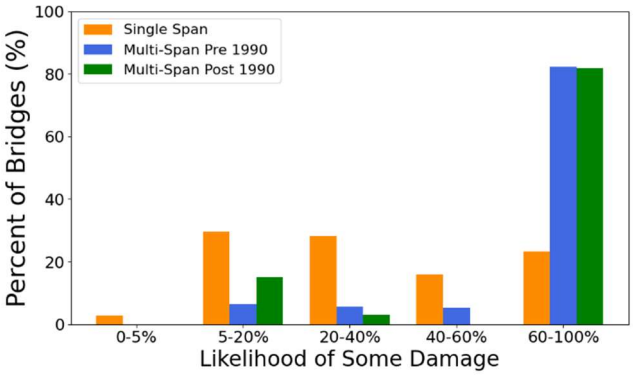

(e) Combined – Site Class C2

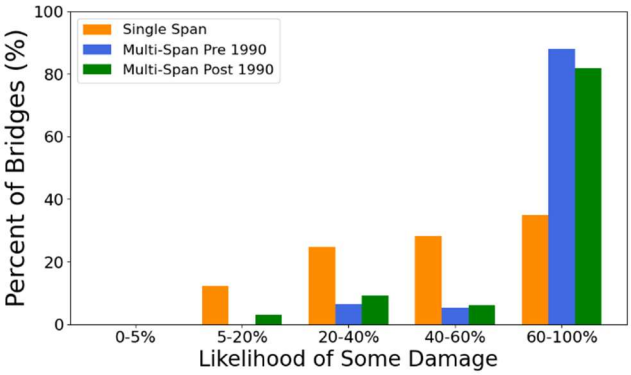

(f) Combined – Site Class D1

Figure 6.16 The Likelihood of Any Damage Occurring for All Bridges in Gray's Harbor and Pacific Counties Separated by Category Given All Realizations. The Percent of Bridges is the Percent of Total Bridges in Each Category

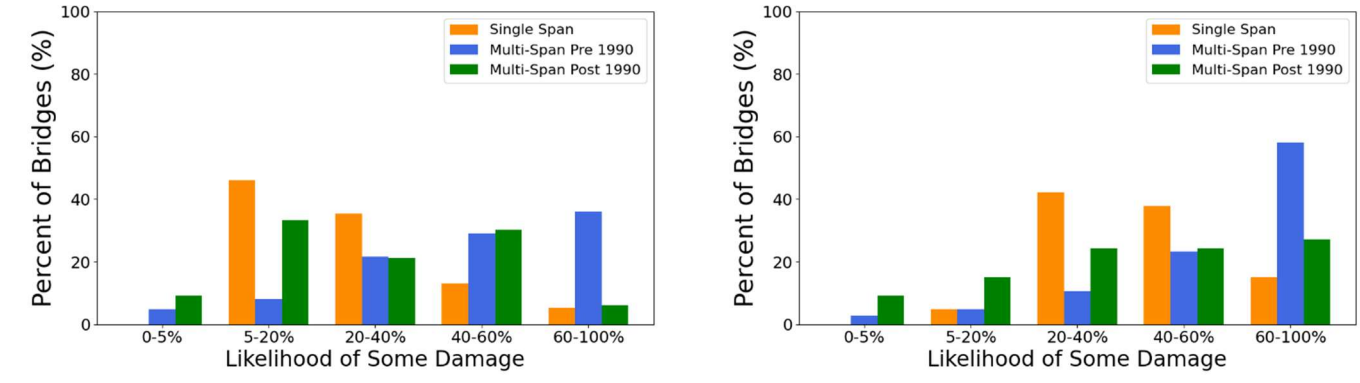

(a) HAZUS – Site Class C2

(b) HAZUS – Site Class D1

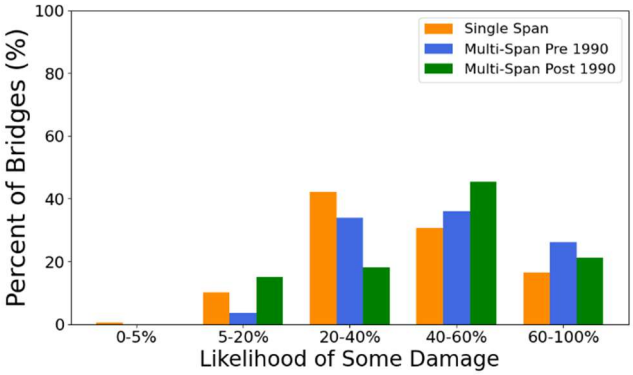

(c) Nisqually – Site Class C2

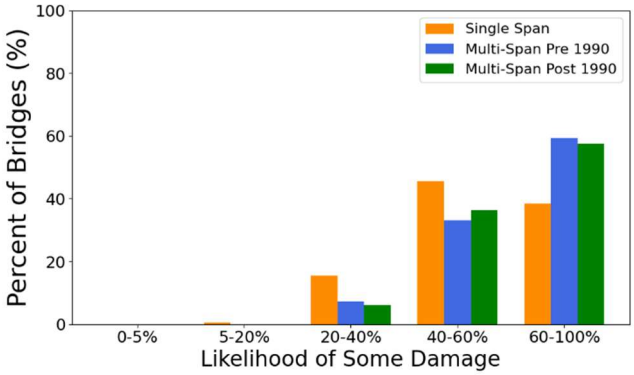

(d) Nisqually – Site Class D1

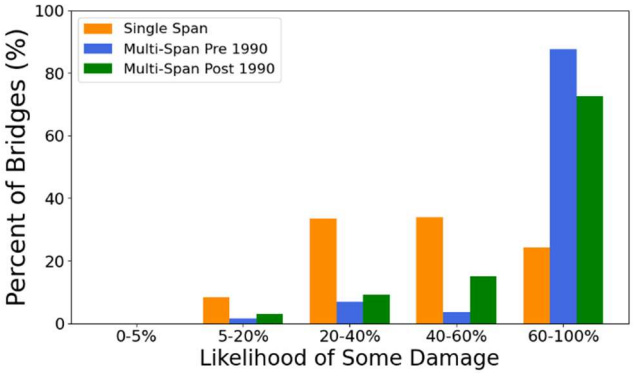

(e) Combined – Site Class C2

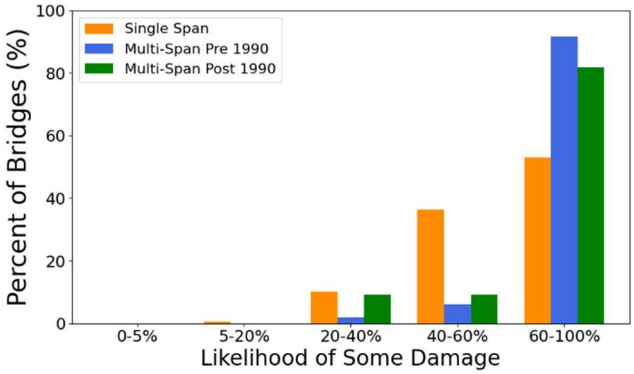

(f) Combined – Site Class D1

Figure 6.17 The Likelihood of Any Damage Occurring for All Bridges in Gray's Harbor and Pacific Counties Separated by Category Given the Top 5 Realizations. The Percent of Bridges is the Percent of Total Bridges in Each Category

Figure 6.18 shows the mean of the percentage of having some damage for all bridges in each of the three bridge categories. Single span bridges have the lowest percentage of having some damage overall meaning that the likelihood of no damage at all is high. For multi-span

bridges whether all realizations are used or the top 5 realizations are used there isn't as big of a difference, especially for the Combined fragility curves. For the HAZUS fragility curves multi-span bridges built before 1990, have a higher percentage of some damage, which would be the expected trend across all fragility relationships

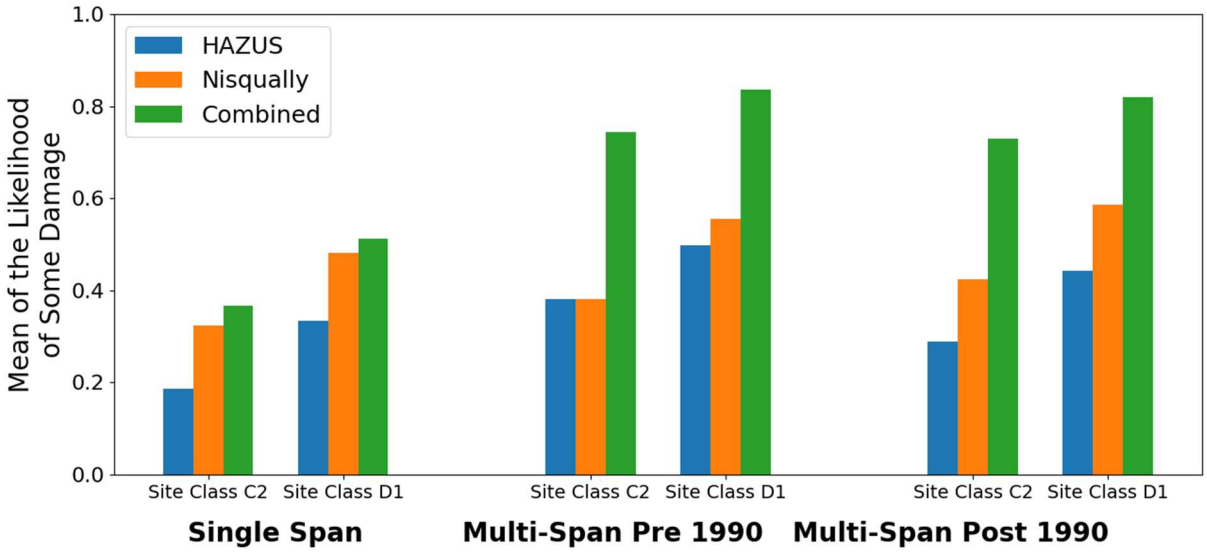

(a) All Realizations

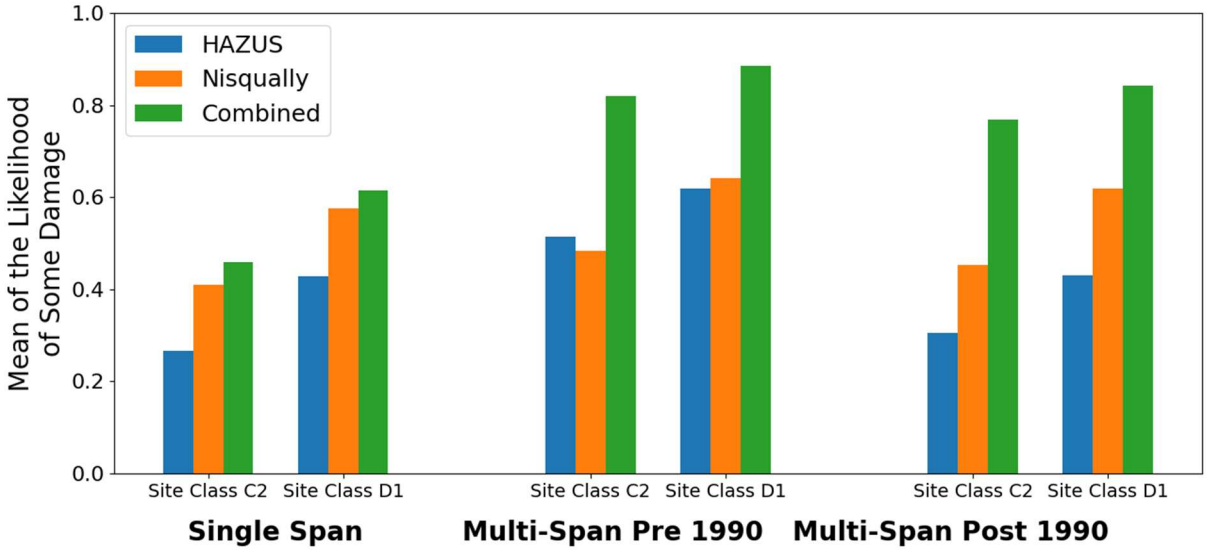

(b) Top 5 Realizations

Figure 6.18 Mean of the Likelihood of Some Damage for All Bridges Combined in Each Category

6.9 LIKELIHOOD OF EXTENSIVE DAMAGE OR COLLAPSE

Similar to the previous section, the likelihood of extensive damage to total collapse can be calculated by combining the probabilities above the Moderate damage state which include the Extensive Damage State and the Complete Damage state. Figures 6.19 and 6.20 are set up in a similar fashion to Figures 6.16 and 6.17. For HAZUS fragility curves there is the strongest correlation to single span bridges, showing that the majority of single span bridges have a low chance of Extensive to Complete damage when using HAZUS. This again corroborates that single span bridges generally experience less damage than multi-span bridges. For the Nisqually and Combined fragility relationship, there is less noticeable trends. This also corroborates what has been observed with the Nisqually fragility set as they don't have separate fragility curves for single span bridges.

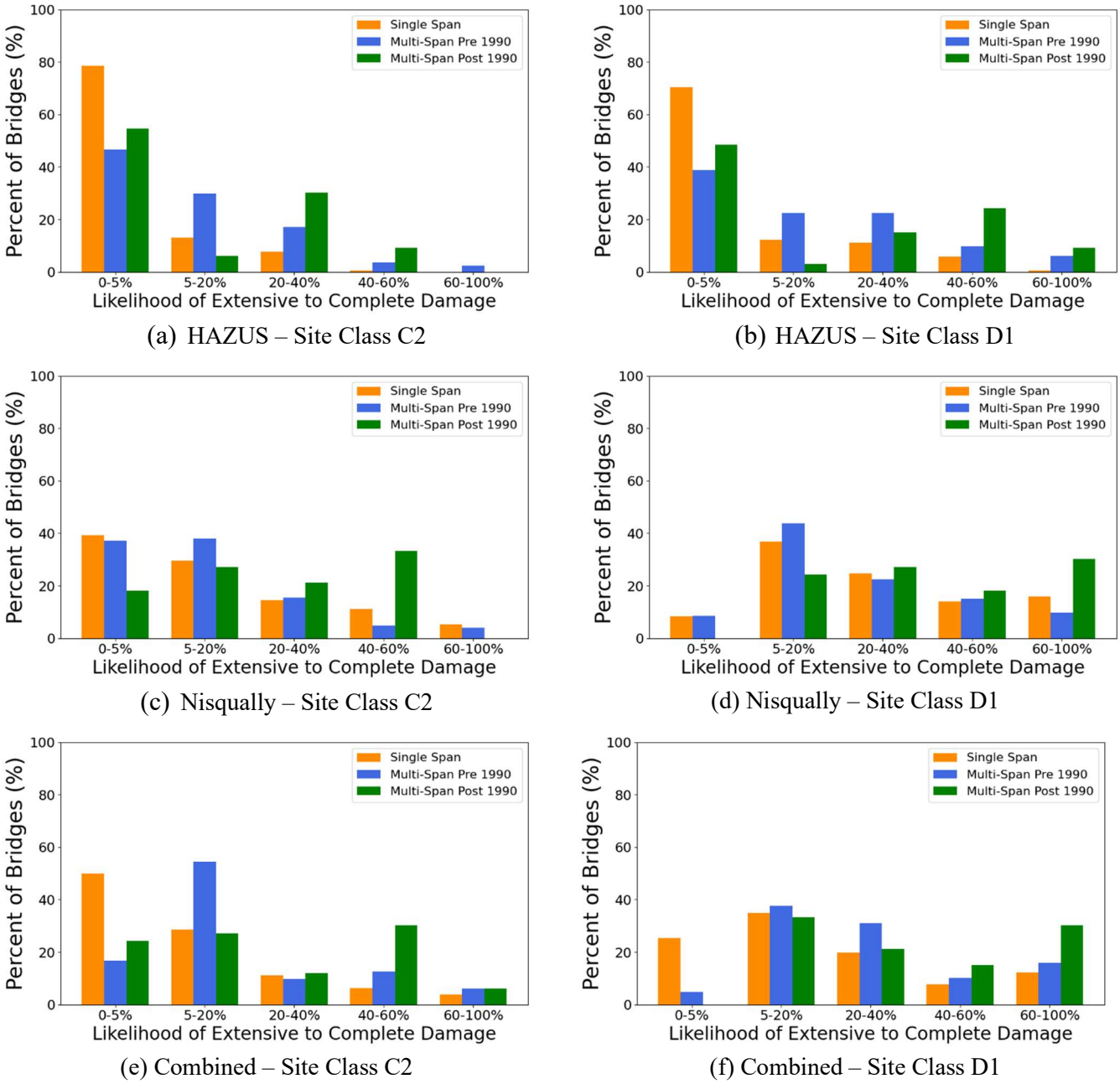

(a) HAZUS – Site Class C2

(b) HAZUS – Site Class D1

(c) Nisqually – Site Class C2

(d) Nisqually – Site Class D1

(e) Combined – Site Class C2

(f) Combined – Site Class D1

Figure 6.19 The Likelihood of Extensive Damage to Complete Failure Occurring for All Bridges in Gray's Harbor and Pacific Counties Separated by Category Given All Realizations. The Percent of Bridges is the Percent of Total Bridges in Each Category

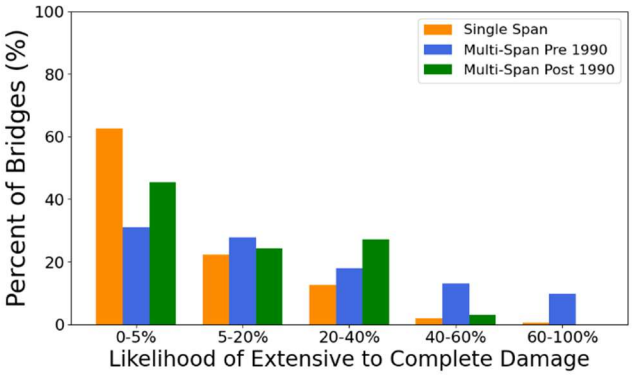

(a) HAZUS – Site Class C2

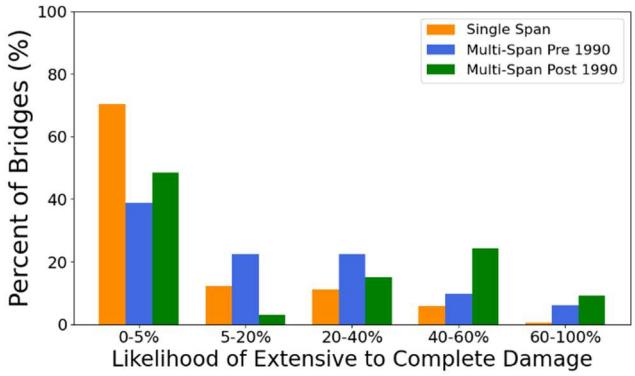

(b) HAZUS – Site Class D1

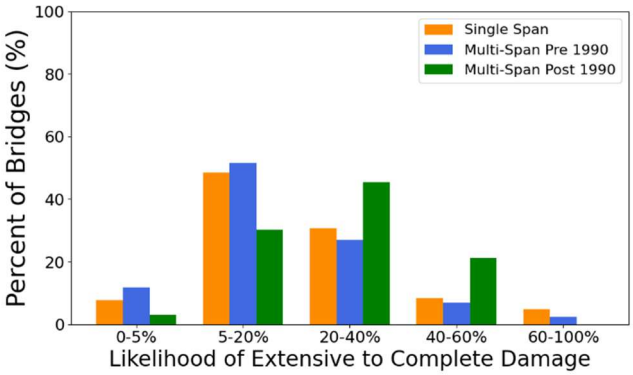

(c) Nisqually – Site Class C2

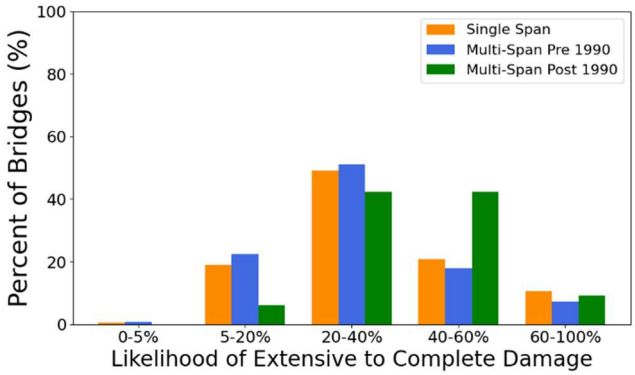

(d) Nisqually – Site Class D1

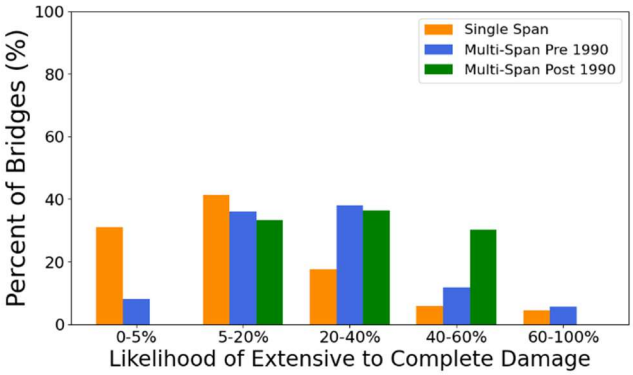

(e) Combined – Site Class C2

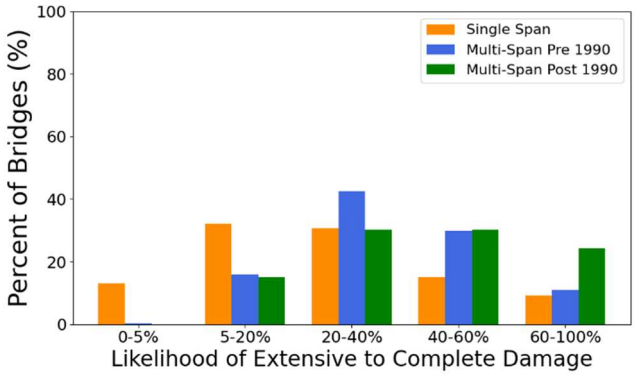

(f) Combined – Site Class D1

Figure 6.20 The Likelihood of Extensive Damage to Complete Failure Occurring for All Bridges in Gray's Harbor and Pacific Counties Separated by Category Given the Top 5 Realizations. The Percent of Bridges is the Percent of Total Bridges in Each Category

Overall, it is surprising to see in Figure 6.21 that the average of the likelihood of extensive to complete damage, at most reaches around 40% for any case. This indicates that the majority of bridges have a good likelihood of not experiencing severe damage.

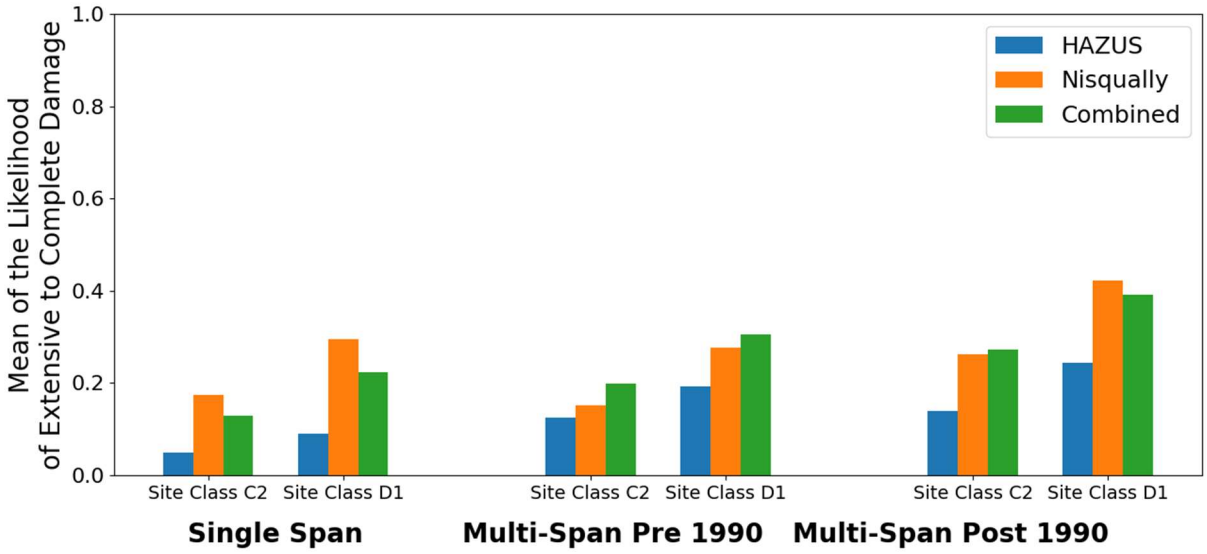

(a) All Realizations

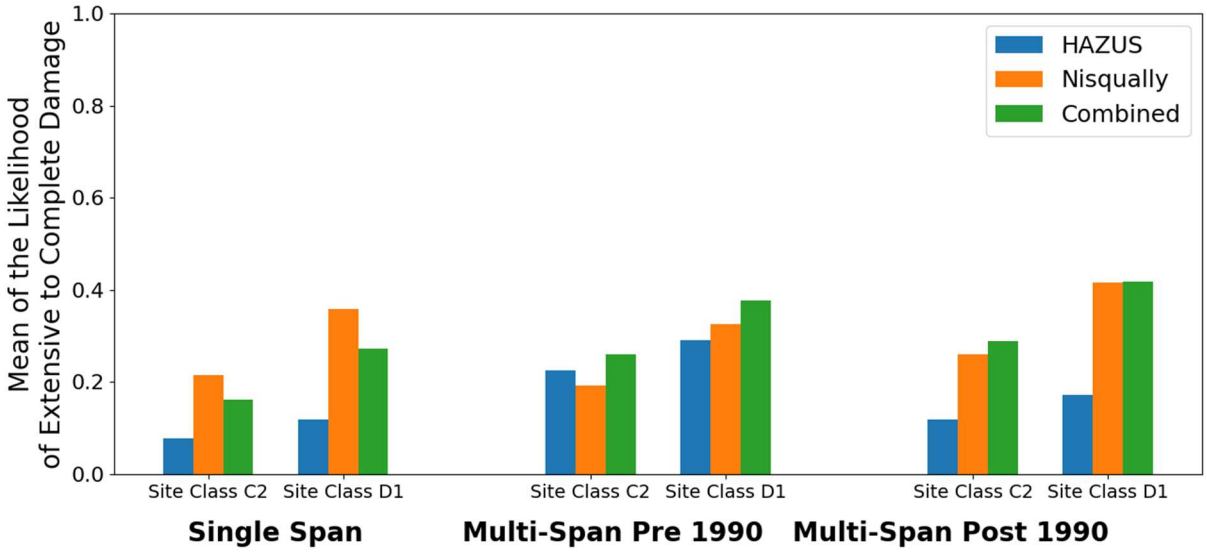

(b) Top 5 Realizations

Figure 6.21 Mean of the Likelihood of Extensive to Complete Damage for All Bridges Combined in Each Category

Chapter 7. SUMMARY AND CONCLUSIONS

This thesis examined the sensitivities of predictions of bridge performance to key assumptions regarding the selection of physics-based ground motions (Chapter 2), local site amplification (Chapter 3) and bridge fragility relationships (Chapter 4). The examination was conducted for individual bridges (Chapter 5) as well for a bridge population consisting of all publicly owned bridges in Gray's Harbor and Pacific counties in Washington State (Chapter 6).

7.1 SENSITIVITY TO SELECTION OF GROUND MOTION REALIZATIONS

The presence of the Cascadia Subduction Zone in the Pacific Northwest and geological evidence of past earthquakes implies that the region will likely experience a magnitude 9 earthquake in the future. Since no historic observations or records of such earthquakes are available in the Pacific Northwest, USGS and University of Washington researchers generated 30 realizations of such events to estimate a wide range of possible ground motion scenarios (Frankel et al. 2018a).

- The intensity of the ground motion at a single location varied greatly among the realizations. For example, at the Reference Point (near Aberdeen, WA), the 30 values of the spectral acceleration at a period of 0.3 seconds, $S_a(0.3)$, ranged from a minimum of 0.65 g to a maximum of 2.55 g, resulting in a maximum variation of 1.9 g.
- Even within the same realization, the intensities of the ground motions varied greatly between two adjacent grid points with a spacing of 20 km. For example, for the realization with a median value of $S_a(0.3)$ = 1.35 g at the Reference Point (Realization

Csz004), the spectral acceleration of the next grid point to the West was 1.58 g, and the spectral acceleration at the next grid point to the East was 1.06 g (same realization).

- Although the intensities of the ground motions varied greatly among the realizations, the same realizations generally produced the higher intensities across the four intensity measure values. The motions that had the highest intensities for one intensity measure, tended to have the highest intensities for the other intensity measures. (Csz029, Figure 2.3)

7.2 SITE CLASS

The baseline M9 ground motions were created without accounting for local site conditions, so it was necessary to consider local site amplification to predict ground motion intensities at the surface. To account for site amplification, site amplification factors for the ground motion intensities were calculated for 10 representative locations in the Pacific Northwest (Grant et al. 2020). At each location, the same 444 soil profiles were divided into seven site classes, which are sub-classes of Site Class C and Site Class D (Grant et al. 2020). Between the soil profiles and ground motion realizations, there is a lot of variability for the amplification factor, however when distilled down to a fitted line at the median, there is not as much difference among the locations for a single site class. To apply the amplification factor to the area of Gray's Harbor and Pacific counties, the median and dispersion between all locations combined was used for each site class at a certain ground motion intensity.

The main conclusion of this work was that, despite the variability in ground motion characteristics at the various locations, the median amplification factor at a certain intensity measure for various locations was similar enough that they can be combined. The results also

showed that site amplification varied more among the sub-site classes in Site Class D than in Site Class C.

7.3 FRAGILITY CURVES

In Gray's Harbor and Pacific counties, the most common bridge type is a prestressed concrete girder bridge. This bridge type was further separated into three more specific subcategories: prestressed simply supported concrete bridges built before 1990, prestressed simply supported bridges built on or after 1990, and prestressed continuous concrete bridges built on or after 1990. A movable bridge was also added as the fourth bridge type to look at in closer detail, because they are known to be highly vulnerable to earthquakes (Ranf et al. 2005). Fragility curves for each bridge category were identified from the literature and compared among each other. The three sources of fragility curves used most in this research are from HAZUS (FEMA 2024), the fragility curves developed from the Nisqually earthquake (Ranf et al. 2005), and the fragility curves derived from the south and central part of the United States (Nielson and DesRoches 2007).

The findings in this chapter include that single span bridges make up 43% of bridges in Gray's Harbor and Pacific counties, only 6.8% of multi-span bridges were built on or after 1990, concrete slab and concrete girder bridges make up the vast majority of bridges across all bridge types, including regular reinforced concrete and pre-stressed concrete. It is difficult to compare fragility relationship sets because many of them have different intensity measures by which they are applied, but for those that were the same, they were fairly different if they came from different authors.

7.4 IMPACTS OF ASSUMPTIONS ON INDIVIDUAL BRIDGE

A series of parametric studies were performed for a single bridge. First, the ground motion realization was varied as the bridge type, fragility curve, and soil amplification was kept the same. Then, the soil amplification was varied as the ground motion realization, bridge type, and fragility curve were kept the same. Lastly, the bridge type and fragility curves were varied as the ground motion realization, and soil amplification were kept the same.

The parameter that caused the greatest variation in the outcome of the damage states for a certain bridge type are the fragility curves used to evaluate it. This shows a lot of uncertainty in this area. When keeping the bridge type and fragility curve the same, the different ground motion realizations and site class amplification did make a difference in the damage state probabilities but not as much when varying the fragility curves. For example, the greatest difference in probabilities at the None Damage State between the 14^{th}, 50^{th}, and 86^{th} percentile realizations is 30%. The greatest difference in probabilities at the None Damage State between the Site Class C2 14^{th} percentile amplification and Site Class D1 86^{th} percentile amplification is 13.8%. The greatest difference in probabilities at the None Damage State for the same bridge but using different fragilities is 90.8% (Newer Continuous Concrete Bridge). In fact, when varying ground motion realization or site amplification, the middle damage states, Slight, Moderate, and Extensive stayed relatively consistent. Perhaps if the realization with the lowest value was compared with the realization with the highest intensity, there would be a more noticeable difference. Likewise, if Site Class C1 amplification was compared against Site Class D3 amplification there would be more of a difference as well.

7.5 IMPACTS OF ASSUMPTIONS ON BRIDGE INVENTORY

Chapter 6 describes a regional case study that was performed on all 483 bridges in Gray's Harbor and Pacific counties using R2D. Twelve cases were analyzed using all combinations of two sets of ground motions, two local soil site classes, and three sets of fragility relationships.

- The two ground motions sets used was one that included all 30 realizations at each location, and another that included just the top 5 realizations at each location.
- The two site classes for amplification that were used are Site Class C2 and Site Class D1.
- The three sets of fragility relationships used were the HAZUS, Nisqually, and a combined set that included the fragility curves for common bridge types in South and Central United States, and the Nisqually fragility curves.

By looking at the maps of the Most Likely Damage State and the Average Damage State, it is clear that no matter the ground motion or fragility relationship set used, the southern portion of the region (mainly Pacific County), tended to have higher damage. Going from Site Class C2 Amplification to Site Class D1 amplification of course increased the likelihood of damage all around, however using the Top 5 Realizations as defined by the chapter, does not universally increase the probability of damage. The Top 5 Realizations were based off of the Reference Point located near Aberdeen, WA, as such bridges around that area show great increases in likely damage, but in other areas it doesn't make as much of an impact. Conversely, in the southern region it even decreases slightly the likelihood of damage for some bridges. This shows that the realizations that produce the highest intensities at one point, might not at another.

There is also a more noticeable impact when using the Top 5 Realizations with the HAZUS fragility curves than using the Top 5 Realizations with other fragility sets. For

example, for a bridge located at (46.97333, -123.81092) near the Reference Point, the average damage state goes from 0.93 to 1.66 when going from using All Realizations – D1 to the Top 5 Realizations – D1 for HAZUS fragility curves. That is a difference of 0.73. When using the Nisqually fragility curves for the same ground motions and site amplification, the same bridge's average damage state only goes from 1.47 to 1.74, which is only a difference of 0.27. Thus, there is a proportionally greater increase of damage using the HAZUS curves than the other curves around the Reference Point. This is because the Top 5 Realizations were chosen using the intensity measure that HAZUS uses ($S_a(1.0)$) and the other fragility sets use a different intensity measure (PGA and $S_a(0.3)$). However, it is still generally seen that certain realizations tend to have higher intensities across all intensity measures because the Top 5 Realizations still showed an impact around the bridges near Aberdeen for fragility sets Nisqually and Combined, despite them using a different intensity measure. Ultimately though, the factor that makes the biggest difference in likelihood of damage across the region is the fragility relationship set used.

7.6 RECOMMENDATIONS FOR FUTURE WORK

This thesis considered three sources of modeling uncertainty in order to identify the main sources of uncertainty. Future work would lead to an increased understanding of these sensitivities.

7.6.1 Updated M9 Ground Motions

For this research, the ground motion grid points were spaced 20 km apart. It would be better if the grid points were spaced closer together, ensuring a better approximation of the ground motions for a bridge that falls between the grid points.

USGS researchers have now generated a new set of M9 ground motions, which includes 36 realizations (Dunham 2025). Other key differences between this set and the old M9 ground motions include:

- Using a finite-element model, rather than a finite-difference model
- Using a wider range of magnitude (M8.7 – M9.2)
- Allowing the rupture to be "buried" or extend to the surface
- Allows for some scenarios where the slip deformation is informed by offshore geophysical measurements

Another analysis of the bridges could be done with this second set of motions to see the difference it would make, and to compare the old M9 ground motions with the new ones.

7.6.2 A Larger Region of Study

In this thesis, Gray's Harbor and Pacific counties was the area of focus. However, more than just those two counties make up the Olympic Peninsula and Washington coastline. Approximately nine counties make up the Olympic Peninsula and Washington coastline region and include Clallam, Jefferson, Mason, Kitsap, Thurston, Lewis and Wahkiakum counties in addition to Gray's Harbor and Pacific counties. In these nine counties there are 1,641 bridges in the NBI database. The region that was analyzed in this study include only 29% (483/1641) of all bridges. It is worth noting however, that the counties where I-5 freeway crosses through might have different levels of damage susceptibility to damage. The bridges along a freeway often have different properties from the bridges along the rural largely rural coastline.

7.6.3 HAZUS Seismic Cut-Off Year

HAZUS (FEMA 2024) considers bridges built past 1990 to be of a seismic design for all states except California. For California that cut-off year is 1975, a few years after the 1971 San Fernando Earthquake. Soon after the San Fernando Earthquake, California started implementing modern seismic design. However, Washington State also started implementing seismic design sooner than 1990. The Nisqually fragility curves which were based specifically on some of the bridges in Washington, separates the bridges by the years pre-1941, 1941 – 1975 and post 1975. A bridge built after 1975 performs better in an earthquake according to the Nisqually fragility curves than a bridge built before 1975, indicating seismic design. The case could be made that Washington state should use the same HAZUS curves as California or perhaps create their own categories (or year ranges) in HAZUS.

7.6.4 More Washington Specific Fragility Curves

The Nisqually fragility curves are one of the few Washington specific bridge fragility curves. They highlight bridge types not commonly analyzed in HAZUS and other fragility research, such as movable and truss bridges. However, for all other bridge types, they are only distinguished by the year built. From the results in Chapter 6 it is clear that single span bridges generally perform much better than multi-span bridges in a seismic event. Future work could be done to create a separate set of fragility curves for single span bridges. In general, more work can be done to develop fragility curves for bridge types in Washington State and its unique seismic challenges. The work done in Liu et al. (2022) is a step forward in this, as well as researcher Andres Sanchez's efforts to take the data from Liu et al. (2022) and create new sets of fragility curves from them.

A bridge type along the Washington coast for which there exists little to no fragility curves for, are timber bridges. While timber bridges don't make up the majority of bridges in Gray's Harbor and Pacific counties, they make up 15% of multi-span bridges built before 1990. More work could be done to understand their seismic vulnerability, especially since they are typically older bridges as well.

7.6.5 Match Soil Site Class to Specific Bridge Location

A major challenge of this thesis was trying to apply the soil site class amplification factors. Those factors were developed for motions from 10 locations within Washington State. The amplification factors for the same site class could also only be applied at each bridge location within Gray's Harbor and Pacific counties. If the soil site class at each bridge location could be approximated, then the amplification factors could be matched more specifically to the bridge rather than applying one site class to an entire region. To improve accuracy, there could also be more locations for which amplification factors are developed for. Instead of taking the average amplification factor across those locations like what was done in this research, with enough locations, the amplification factor for a bridge could come from the nearest city. Or perhaps the amplification factor could be sampled in a nearest neighbor event like what R2D does for the ground motions.

7.6.6 Downstream Impacts

Ultimately, the goal of this thesis is to help people who live along the Washington State coastline be prepared and safe in the event of a magnitude 9 earthquake. There are a lot of factors that go into that beyond whether or not a bridge collapses. Some downstream impacts that can be looked at include whether or not someone could travel from one point to another after the

earthquake, whether rural communities still have access to emergency services given the damage to the transportation network infrastructure, and whether people living right on the coast are still able to evacuate inland before the subsequent tsunami inundates that region.

References

Ahdi, S.K et al. 2017. “Development of VS Profile Database and Proxy-based Models for VS30 Prediction in the Pacific Northwest Region of North America.” Bulletin of the Seismological Society of America 107: 1781-1801.

de Zamacona Cervantes, Gloria E. 2019. Response of Idealized Structural Systems to Simulated M9 Cascadia Subduction Zone Earthquakes Considering Local Soil Conditions. Master’s thesis, University of Washington, Department of Civil and Environmental Engineering.

Dunham, A, 2025. "CSZ Full-Margin Megathrust Earthquake Scenarios", in 3D Broadband Ground Shaking Simulations of Cascadia Subduction Zone Earthquake Scenarios. DesignSafe-CI.

Federal Emergency Management Agency. Hazus Earthquake Model Technical Manual. Version 6.1. 2024.

Federal Highway Administration. 1995. Recording and Coding Guide for the Structure Inventory and Appraisal of the Nation's Bridges. Washington, DC: U.S. Department of Transportation, Office of Engineering, Bridge Division. https://www.fhwa.dot.gov/bridge/mtguide.pdf.

Federal Highway Administration. 2024. National Bridge Inventory ASCII Files 2024. U.S. Department of Transportation. https://www.fhwa.dot.gov/bridge/nbi/ascii2024.cfm.

Frankel, A., N. Marafi, E. Wirth (2018b). The M9 Project Ground Motions. DesignSafe-CI. https://doi.org/10.17603/DS2WM3W

Frankel, A., Wirth, E., Marafi, N., Vidale, J., and Stephenson, W., (2018a). Broadband Synthetic Seismograms for Magnitude 9 Earthquakes on the Cascadia Megathrust Based on 3D Simulations and Stochastic Synthetics, Part 1: Methodology and Overall Results. Bulletin of the Seismological Society of America; 108 (5A): 2347–2369. doi: https://doi.org/10.1785/0120180034

Google. 2024. Google Maps. Accessed June 9, 2025. https://www.google.com/maps

Grant, Alex, E. A. Wirth, Nasser A. Marafi, and Arthur D. Frankel. 2020. "Ensemble ShakeMaps for Magnitude 9 Earthquakes on the Cascadia Subduction Zone." Seismological Research Letters 92: 199–211. https://doi.org/10.1785/0220200240.

Liu, Kan-Jen, Addie Lederman, Zachary Kortum, Marc O. Eberhard, Jeffrey W. Berman, N. Marafi, and Brett Maurer. 2022. Impacts of Cascadia Subduction Zone M9 Earthquakes on Bridges in Washington State: Three-Dimensional Bridge Models. Research Report WA-RD 908.2. Washington State Transportation Center, University of Washington. Sponsored by Washington State Department of Transportation.

Mangalathu, Sujith, 2017. “Performance Based Grouping and Fragility Analysis of Box-Girder Bridges in California” Ph.D. thesis, Georgia Institute of Technology, Georgia.

Marafi, Nasser Abdulazim. 2018. Impacts of Large Magnitude Earthquakes on Structures in Deep Sedimentary Basins. PhD diss., University of Washington, Department of Civil and Environmental Engineering.

Nielson, Bryant G. "Analytical Fragility Curves for Highway Bridges in Moderate Seismic Zones." PhD diss., Georgia Institute of Technology, 2005. https://repository.gatech.edu/handle/1853/10499.

Nielson, Bryant G., and Reginald DesRoches. 2007. "Analytical Seismic Fragility Curves for Typical Bridges in the Central and Southeastern United States." Earthquake Spectra 23 (3): 615–633. https://doi.org/10.1193/1.2753548.

Pacific Northwest Seismic Network. “Cascadia Subduction Zone.” https://pnsn.org/outreach/earthquakesources/csz (May 31, 2021)

Palmer, Stephen P. et al. 2007. “Liquefaction Susceptibility and Site Class Maps of Washington State, By County.” Washington Division of Geology and Earth Resources. Open File Report 2004-20. ftp://ww4.dnr.wa.gov/geology/pubs/ofr04-20/ (June 4, 2019).

Ranf, R.T., M.O. Eberhard, and S. Malone. 2005. Post-Earthquake Prioritization of Bridge Inspections. Department of Civil and Environmental Engineering, University of Washington.

SimCenter. 2024. "R2D Tool." NHERI SimCenter. Accessed May 21, 2025. https://simcenter.designsafe-ci.org/research-tools/r2dtool/.

United States Geological Survey (USGS), 2017, Illustration of Seismic Source Zones in the Pacific Northwest, https://geomaps.wr.usgs.gov/pacnw/pacnweq/pdf/subd_eqpg.pdf

APPENDIX A

Table A.1 M9 Baseline Ground Motion Intensities at the Reference Point for All 30 Realizations

Realizations	**PGA** (g)	**S_a (0.3)** (g)	**S_a (1.0)** (g)	**S_a (2.0)** (g)
Csz002	0.729	1.829	0.474	0.280
Csz003	0.536	1.204	0.362	0.190
Csz004	0.565	1.352	0.784	0.289
Csz005	0.316	0.966	0.253	0.082
Csz006	0.472	1.199	0.552	0.118
Csz007	0.506	1.314	0.433	0.324
Csz008	0.354	0.827	0.512	0.208
Csz009	0.720	2.177	0.614	0.492
Csz010	0.470	1.414	0.433	0.215
Csz011	0.274	0.781	0.255	0.124
Csz012	0.777	1.910	0.469	0.186
Csz013	0.299	0.745	0.208	0.042
Csz014	0.558	1.520	0.624	0.253
Csz017	0.557	1.796	0.552	0.266
Csz018	0.622	1.691	0.511	0.251
Csz019	0.336	1.030	0.219	0.052
Csz020	0.591	1.461	0.711	0.193
Csz021	0.250	0.762	0.238	0.106
Csz022	0.393	1.060	0.335	0.128
Csz023	0.471	1.391	0.280	0.161
Csz024	0.640	1.621	0.619	0.560
Csz025	0.722	1.587	0.814	0.426
Csz026	0.419	1.237	0.266	0.144
Csz027	0.538	1.534	0.373	0.107
Csz028	0.302	0.654	0.384	0.196
Csz029	1.050	2.548	0.940	0.427
Csz030	0.624	1.470	0.407	0.274
Csz031	0.382	1.236	0.279	0.063
Csz032	0.391	1.031	0.242	0.085
Csz033	0.438	1.156	0.417	0.162

Table A.2 M9 Baseline Ground Motion Intensities at the North Point for All 30 Realizations

Realizations	**PGA** (g)	**S_a (0.3)** (g)	**S_a (1.0)** (g)	**S_a (2.0)** (g)
Csz002	0.985	2.000	0.929	0.635
Csz003	0.849	1.448	0.981	0.335
Csz004	0.472	1.264	0.442	0.389
Csz005	0.248	0.737	0.291	0.091
Csz006	0.375	1.028	0.336	0.153
Csz007	0.691	1.481	0.485	0.317
Csz008	0.295	0.611	0.303	0.220
Csz009	0.672	1.732	0.589	0.368
Csz010	0.438	1.249	0.381	0.210
Csz011	0.382	0.806	0.251	0.122
Csz012	0.516	1.253	0.464	0.282
Csz013	0.356	0.962	0.252	0.042
Csz014	0.486	1.084	0.429	0.297
Csz017	0.434	1.062	0.629	0.275
Csz018	0.703	1.709	0.525	0.124
Csz019	0.499	1.310	0.305	0.080
Csz020	0.445	1.164	0.432	0.193
Csz021	0.219	0.673	0.237	0.108
Csz022	0.256	0.810	0.235	0.113
Csz023	0.605	1.412	0.351	0.161
Csz024	0.463	0.890	0.506	0.466
Csz025	0.685	1.372	0.555	0.577
Csz026	0.531	1.383	0.343	0.156
Csz027	0.650	1.729	0.466	0.266
Csz028	0.431	0.934	0.421	0.284
Csz029	0.851	1.942	1.016	0.482
Csz030	0.947	2.125	0.628	0.503
Csz031	0.400	1.188	0.294	0.100
Csz032	0.568	1.278	0.297	0.109
Csz033	0.421	1.419	0.480	0.301

Table A.3 M9 Baseline Ground Motion Intensities at the South Point for All 30 Realizations

Realizations	**PGA** (g)	**S_a (0.3)** (g)	**S_a (1.0)** (g)	**S_a (2.0)** (g)
Csz002	0.667	1.804	0.470	0.157
Csz003	0.433	0.983	0.299	0.096
Csz004	0.775	1.527	0.866	0.484
Csz005	0.508	1.220	0.407	0.171
Csz006	0.635	1.322	0.447	0.164
Csz007	0.510	1.454	0.527	0.274
Csz008	0.368	0.985	0.409	0.190
Csz009	0.701	1.987	0.792	0.400
Csz010	0.596	1.531	0.466	0.256
Csz011	0.209	0.624	0.174	0.105
Csz012	0.811	2.254	0.630	0.166
Csz013	0.230	0.629	0.168	0.029
Csz014	0.760	1.442	0.481	0.347
Csz017	0.611	1.236	0.692	0.356
Csz018	0.390	0.993	0.445	0.187
Csz019	0.315	0.822	0.274	0.043
Csz020	0.769	2.089	0.606	0.241
Csz021	0.327	0.701	0.357	0.127
Csz022	0.418	0.964	0.414	0.228
Csz023	0.401	1.241	0.254	0.148
Csz024	0.650	1.347	0.571	0.514
Csz025	0.781	1.414	0.918	0.670
Csz026	0.383	0.941	0.330	0.098
Csz027	0.508	1.279	0.273	0.083
Csz028	0.291	0.747	0.254	0.108
Csz029	1.091	2.490	0.665	0.574
Csz030	0.445	0.773	0.302	0.177
Csz031	0.350	0.673	0.266	0.065
Csz032	0.305	0.862	0.267	0.077
Csz033	0.496	1.203	0.556	0.335

Table A.4 M9 Baseline Ground Motion Intensities at the West Point for All 30 Realizations

Realizations	**PGA** (g)	**S_a (0.3)** (g)	**S_a (1.0)** (g)	**S_a (2.0)** (g)
Csz002	0.941	2.363	0.945	0.691
Csz003	0.480	1.129	0.367	0.216
Csz004	0.897	1.578	0.928	0.657
Csz005	0.375	1.046	0.294	0.186
Csz006	0.598	1.670	0.563	0.572
Csz007	0.767	2.335	1.125	0.505
Csz008	0.452	1.276	0.513	0.602
Csz009	0.985	1.891	0.832	0.441
Csz010	0.448	1.043	0.674	0.264
Csz011	0.242	0.634	0.308	0.162
Csz012	0.952	2.385	0.546	0.362
Csz013	0.319	0.823	0.189	0.046
Csz014	0.633	1.259	0.763	0.576
Csz017	1.106	1.863	1.615	1.217
Csz018	0.597	1.252	0.529	0.192
Csz019	0.353	0.849	0.218	0.073
Csz020	0.914	2.227	0.761	0.602
Csz021	0.280	0.664	0.503	0.389
Csz022	0.438	0.983	0.520	0.557
Csz023	0.628	1.592	0.405	0.211
Csz024	0.732	1.261	0.843	0.854
Csz025	0.989	2.220	1.101	1.515
Csz026	0.636	1.524	0.353	0.155
Csz027	0.936	2.134	0.595	0.296
Csz028	0.281	0.690	0.343	0.224
Csz029	0.896	2.042	1.049	0.638
Csz030	0.749	2.163	0.509	0.421
Csz031	0.439	0.953	0.331	0.182
Csz032	0.460	1.150	0.278	0.158
Csz033	0.476	1.089	0.829	0.469

Table A.5 M9 Baseline Ground Motion Intensities at the East Point for All 30 Realizations

Realizations	**PGA** (g)	**S_a (0.3)** (g)	**S_a (1.0)** (g)	**S_a (2.0)** (g)
Csz002	0.797	1.510	0.705	0.333
Csz003	0.543	1.551	0.760	0.251
Csz004	0.483	1.061	0.614	0.233
Csz005	0.354	0.832	0.259	0.080
Csz006	0.376	0.944	0.410	0.223
Csz007	0.434	1.208	0.351	0.134
Csz008	0.238	0.549	0.184	0.094
Csz009	0.835	2.020	0.544	0.415
Csz010	0.500	1.225	0.423	0.278
Csz011	0.234	0.524	0.257	0.082
Csz012	0.660	1.637	0.470	0.143
Csz013	0.249	0.646	0.207	0.029
Csz014	0.517	1.218	0.276	0.101
Csz017	0.459	0.862	0.332	0.171
Csz018	0.548	1.053	0.435	0.140
Csz019	0.326	0.813	0.209	0.046
Csz020	0.612	1.425	0.353	0.141
Csz021	0.213	0.681	0.332	0.084
Csz022	0.337	0.866	0.286	0.096
Csz023	0.391	0.877	0.209	0.104
Csz024	0.444	0.987	0.443	0.159
Csz025	0.551	1.443	0.427	0.136
Csz026	0.397	0.855	0.252	0.069
Csz027	0.485	1.055	0.364	0.064
Csz028	0.253	0.817	0.287	0.105
Csz029	1.169	2.385	0.872	0.548
Csz030	0.478	0.734	0.219	0.158
Csz031	0.323	0.987	0.208	0.071
Csz032	0.387	1.033	0.212	0.078
Csz033	0.386	1.007	0.297	0.108

Table A.6 Variability in Ground Motion Intensity Measures Between All 30 Realizations at the North Point

Percentile	**PGA** (g)	**S_a (0.3)** (g)	**S_a (1.0)** (g)	**S_a (2.0)** (g)
14th	0.357	0.815	0.291	0.108
50th	0.479	1.258	0.430	0.243
86th	0.703	1.728	0.626	0.461

Table A.7 Variability in Ground Motion Intensity Measures Between All 30 Realizations at the South Point

Percentile	**PGA** (g)	**S_a (0.3)** (g)	**S_a (1.0)** (g)	**S_a (2.0)** (g)
14th	0.316	0.749	0.266	0.084
50th	0.502	1.228	0.429	0.174
86th	0.768	1.788	0.663	0.397

Table A.8 Variability in Ground Motion Intensity Measures Between All 30 Realizations at the West Point

Percentile	**PGA** (g)	**S_a (0.3)** (g)	**S_a (1.0)** (g)	**S_a (2.0)** (g)
14th	0.355	0.855	0.310	0.163
50th	0.613	1.269	0.538	0.405
86th	0.940	2.217	0.944	0.655

Table A.9 Variability in Ground Motion Intensity Measures Between All 30 Realizations at the East Point

Percentile	**PGA** (g)	**S_a (0.3)** (g)	**S_a (1.0)** (g)	**S_a (2.0)** (g)
14th	0.257	0.739	0.209	0.072
50th	0.439	0.997	0.332	0.121
86th	0.609	1.506	0.539	0.250

APPENDIX B

Table B.1 Values of the Parameters of the 50th Percentile Line When All 10 Locations are Combined

Site Class	PGA		$S_a(0.3)$		$S_a(1.0)$		$S_a(2.0)$	
	A	B	A	B	A	B	A	B
C1	0.04	1.05	0.01	1.08	-0.001	1.01	-0.001	1.00
C2	0.01	1.07	0.02	1.13	0.001	1.02	-0.001	1.01
C3	0.02	1.18	0.02	1.22	0.01	1.05	-0.001	1.02
C4	-0.04	1.34	0.01	1.42	0.02	1.09	0.001	1.04
D1	-0.27	1.56	-0.14	1.74	0.10	1.20	0.05	1.07
D2	-0.66	1.71	-0.34	1.81	0.08	1.33	0.14	1.10
D3	-1.05	1.68	-0.46	1.60	-0.37	1.78	0.27	1.34

Table B.2 Values of the Parameters of the 14th Percentile Line When All 10 Locations are Combined

Site Class	PGA		Sa(0.3)		Sa(1.0)		Sa(2.0)	
	A	B	A	B	A	B	A	B
C1	0.03	1.03	0.01	1.06	-0.001	1.01	-0.001	1.00
C2	-0.05	1.05	-0.01	1.07	-0.01	1.02	-0.001	1.01
C3	-0.04	1.12	-0.01	1.14	0.001	1.03	-0.001	1.01
C4	-0.17	1.24	-0.06	1.25	0.001	1.05	-0.001	1.02
D1	-0.39	1.42	-0.18	1.45	0.03	1.11	0.01	1.04
D2	-0.74	1.54	-0.33	1.49	-0.001	1.18	0.04	1.06
D3	-1.04	1.43	-0.38	1.18	-0.30	1.38	0.04	1.17

Table B.3 Values of the Parameters of the 86th Percentile Line When All 10 Locations are Combined

Site Class	PGA		Sa(0.3)		Sa(1.0)		Sa(2.0)	
	A	B	A	B	A	B	A	B
C1	0.07	1.09	0.02	1.12	-0.001	1.02	-0.001	1.01
C2	0.05	1.11	0.03	1.16	-0.01	1.07	0.01	1.04
C3	0.09	1.25	0.06	1.31	0.03	1.11	0.02	1.04
C4	0.04	1.46	0.07	1.62	0.07	1.19	0.07	1.08
D1	-0.2	1.73	-0.12	2.10	0.20	1.34	0.18	1.12
D2	-0.55	1.89	-0.34	2.23	0.20	1.55	0.33	1.21
D3	-0.96	1.91	-0.53	2.16	-0.39	2.25	0.50	1.65

APPENDIX C

Table C.1 Site Class C2 – 50% Amplification Factors for Reference Point

Realization	PGA Amplification Factor	S_a (0.3) Amplification Factor	S_a (1.0) Amplification Factor	S_a (2.0) Amplification Factor
Csz002	1.077	1.167	1.020	1.010
Csz003	1.075	1.154	1.020	1.010
Csz004	1.076	1.157	1.021	1.010
Csz005	1.073	1.149	1.020	1.010
Csz006	1.075	1.154	1.021	1.010
Csz007	1.075	1.156	1.020	1.010
Csz008	1.074	1.147	1.021	1.010
Csz009	1.077	1.174	1.021	1.010
Csz010	1.075	1.158	1.020	1.010
Csz011	1.073	1.146	1.020	1.010
Csz012	1.078	1.168	1.020	1.010
Csz013	1.073	1.145	1.020	1.010
Csz014	1.076	1.160	1.021	1.010
Csz017	1.076	1.166	1.021	1.010
Csz018	1.076	1.164	1.021	1.010
Csz019	1.073	1.151	1.020	1.010
Csz020	1.076	1.159	1.021	1.010
Csz021	1.073	1.145	1.020	1.010
Csz022	1.074	1.151	1.020	1.010
Csz023	1.075	1.158	1.020	1.010
Csz024	1.076	1.162	1.021	1.009
Csz025	1.077	1.162	1.021	1.010
Csz026	1.074	1.155	1.020	1.010
Csz027	1.075	1.161	1.020	1.010
Csz028	1.073	1.143	1.020	1.010
Csz029	1.081	1.181	1.021	1.010
Csz030	1.076	1.159	1.020	1.010
Csz031	1.074	1.155	1.020	1.010
Csz032	1.074	1.151	1.020	1.010
Csz033	1.074	1.153	1.020	1.010

Table C.2 All 30 Realizations at Reference Point with C2 – 50% Amplification Factors Applied

Realization	**PGA** (g)	**S_a (0.3)** (g)	**S_a (1.0)** (g)	**S_a (2.0)** (g)
Csz002	0.785	2.134	0.483	0.283
Csz003	0.577	1.389	0.370	0.192
Csz004	0.608	1.564	0.800	0.292
Csz005	0.339	1.111	0.259	0.083
Csz006	0.508	1.384	0.563	0.120
Csz007	0.544	1.519	0.441	0.327
Csz008	0.380	0.948	0.522	0.210
Csz009	0.775	2.555	0.626	0.497
Csz010	0.506	1.638	0.441	0.217
Csz011	0.294	0.895	0.260	0.125
Csz012	0.838	2.232	0.479	0.188
Csz013	0.321	0.853	0.212	0.043
Csz014	0.600	1.764	0.637	0.256
Csz017	0.599	2.094	0.564	0.269
Csz018	0.669	1.968	0.522	0.254
Csz019	0.361	1.186	0.223	0.052
Csz020	0.636	1.694	0.725	0.195
Csz021	0.269	0.873	0.243	0.107
Csz022	0.422	1.220	0.342	0.129
Csz023	0.506	1.611	0.285	0.163
Csz024	0.689	1.884	0.632	0.565
Csz025	0.777	1.844	0.831	0.430
Csz026	0.450	1.428	0.271	0.145
Csz027	0.579	1.780	0.381	0.108
Csz028	0.324	0.748	0.392	0.198
Csz029	1.135	3.009	0.959	0.431
Csz030	0.671	1.704	0.415	0.277
Csz031	0.410	1.427	0.284	0.063
Csz032	0.420	1.186	0.247	0.086
Csz033	0.470	1.333	0.425	0.163

Table C.3 Likelihood of Each Damage State Using HWB17 at Reference Point with C2 – 50% Amplification

Realization	Damage State Probability					Most Likely Damage State	Average
	None 0	Slight 1	Moderate 2	Extensive 3	Complete 4		
Csz002	0.136	0.230	0.164	0.261	0.208	3	2.17
Csz003	0.257	0.285	0.158	0.196	0.104	1	1.61
Csz004	0.026	0.092	0.104	0.267	0.511	4	3.15
Csz005	0.478	0.281	0.110	0.100	0.032	0	0.93
Csz006	0.088	0.188	0.154	0.282	0.288	4	2.49
Csz007	0.172	0.253	0.166	0.242	0.167	1	1.98
Csz008	0.110	0.209	0.160	0.274	0.247	3	2.34
Csz009	0.063	0.157	0.142	0.287	0.351	4	2.71
Csz010	0.172	0.253	0.166	0.242	0.167	1	1.98
Csz011	0.473	0.282	0.111	0.101	0.033	0	0.94
Csz012	0.140	0.233	0.165	0.259	0.203	3	2.15
Csz013	0.607	0.241	0.078	0.059	0.014	0	0.63
Csz014	0.059	0.152	0.140	0.287	0.362	4	2.74
Csz017	0.088	0.187	0.154	0.282	0.289	4	2.50
Csz018	0.110	0.210	0.160	0.274	0.246	3	2.34
Csz019	0.576	0.253	0.086	0.068	0.018	0	0.70
Csz020	0.038	0.116	0.120	0.280	0.445	4	2.98
Csz021	0.518	0.271	0.100	0.086	0.025	0	0.83
Csz022	0.301	0.292	0.150	0.174	0.082	0	1.44
Csz023	0.413	0.291	0.126	0.124	0.045	0	1.10
Csz024	0.061	0.154	0.141	0.287	0.357	4	2.73
Csz025	0.023	0.084	0.098	0.260	0.535	4	3.20
Csz026	0.446	0.287	0.188	0.111	0.038	0	1.15
Csz027	0.241	0.281	0.160	0.205	0.113	1	1.67
Csz028	0.227	0.276	0.162	0.212	0.122	1	1.72
Csz029	0.013	0.056	0.075	0.228	0.629	4	3.41
Csz030	0.199	0.266	0.165	0.227	0.143	1	1.85
Csz031	0.415	0.291	0.125	0.123	0.045	0	1.09
Csz032	0.508	0.274	0.103	0.089	0.027	0	0.86
Csz033	0.188	0.261	0.165	0.233	0.152	1	1.90

APPENDIX D

Only the median value for the Slight Damage State and the dispersion was provided by Ranf et al. (2005). In Chapter 4, the median values for the other damage states for Movable, 1941-1954, and Post – 1975 fragility curves were assumed based off the proportions of the corresponding HAZUS fragility curve for that bridge type. For simplicity, those same proportions were used for the regional case study even though these fragility curves will be applied to more than just the bridge types specified in Chapter 4. For the Truss and Pre-1941 fragility curves, the medians for Moderate – Complete were based off of the average proportions of the other curves. All of this is shown in Table D.1

Table D.1 Fragility Function Median and Dispersion Values Derived from Ranf et al. (2005)

Bridge Type	**Intensity Measure**	**Median**				**β**
		Slight	Moderate	Extensive	Complete	
Movable	$S_a(0.3)$	0.60	0.75	0.90	1.28	0.60
Truss	$S_a(0.3)$	0.55	0.73	0.90	1.31	0.60
Pre-1941	$S_a(0.3)$	0.90	1.20	1.48	2.15	0.60
1941-1975	$S_a(0.3)$	1.40	2.21	2.84	4.41	0.60
Post - 1975	$S_a(0.3)$	1.60	1.86	2.28	3.11	0.60

Table D.2 Fragility Function Median and Dispersion Values for Bridge Types in Southern and Central United States (Nielson and DesRoches 2007)

Bridge Type	**Intensity Measure**	**Median**				**β**
		Slight	Moderate	Extensive	Complete	
MSSS Slab	PGA	0.18	0.52	0.94	1.92	0.75
MSSS Concrete	PGA	0.20	0.57	0.83	1.17	0.65
MSC Concrete	PGA	0.15	0.52	0.75	1.03	0.70
MSC Slab	PGA	0.17	0.45	0.78	1.73	0.70
MSC Steel	PGA	0.18	0.31	0.39	0.5	0.55
MSSS Box	PGA	0.21	0.65	1.19	2.92	0.75
MSSS Steel	PGA	0.24	0.44	0.56	0.82	0.5
SSSS Steel	PGA	0.41	1.84	2.62	3.64	0.9
SSSS Concrete	PGA	0.63	1.14	1.52	2.49	0.55

In DesRoches and Padgett (2009), four of the nine bridge types specified in Nielson and DesRoches (2007) are expanded upon and include bridge system fragility curves for a variety of retrofits that can be done to a bridge. There are several retrofit types that include the inclusion of shear keys, however the “Retrofit – Seat Extenders & Shear Keys” is the type technically used below in Table D.3 and in this thesis because it has the greatest impact on the median values. In DesRoches and Padgett (2009) specific dispersion values for each damage state is also specified, however for this study only the average is used to prevent any errant intersection of fragility curves, similar to what occurs in Chapter 5 section 5.6, in R2D. An intersection of the fragility curves in R2D could result in an error and it likely would not be able to complete the analysis. In Table D.3 below, the average dispersion is shown and that is what is inputted into R2D.

Table D.3 Fragility Function Median and Dispersion Values for Bridge Types in Southern and Central United States (DesRoches and Padgett 2009)

Bridge Type	**Intensity Measure**	**Median**				**Average β**
		Slight	Moderate	Extensive	Complete	
MSC Concrete SK	PGA	0.16	0.57	0.84	1.62	0.72
MSC Steel SK	PGA	0.21	0.41	0.51	0.8	0.58
MSSS Concrete SK	PGA	0.22	0.66	0.89	1.6	0.64
MSSS Steel SK	PGA	0.25	0.46	0.6	1.13	0.45